IS-T 1748

A theoretical study of the electronic structure of Invar Fe*3Pt and related materials

by

Zuo, Zhiqi

PHD Thesis submitted to Iowa State University

Ames Laboratory, U.S. DOE
Iowa State University
Ames, Iowa 50011

ph

Date Transmitted: January 10, 1997

PREPARED FOR THE U.S. DEPARTMENT OF ENERGY
UNDER CONTRACT NO. W-7405-Eng-82.

DISCLAIMER

Graduate College
Iowa State University

This is to certify that the Doctoral dissertation of

Zhiqi Zuo

has met the dissertation requirements of Iowa State University

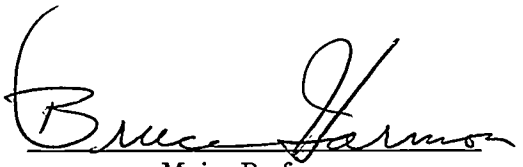

Major Professor

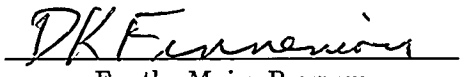

For the Major Program

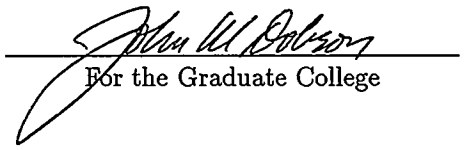

For the Graduate College

TABLE OF CONTENTS

LIST OF TABLES

LIST OF FIGURES

ACKNOWLEDGMENTS

I am very grateful to my advisor Prof. Bruce N. Harmon for his extraordinary patience, constant encouragement and insightful advice for me for the past five years.

I am also indebted to Prof. Kenneth E. Lassila, Prof. Kaiming Ho, Prof. David W. Lynch, Prof. Shashi Gadia, Prof. James P. Vary and Prof. Costas M. Soukoulis for their concerns for me and for their evaluations of my work. I also want to express my special gratitude to Prof. Yiying Ye for her helps during the past ten years.

I especially thank my wife Li Zheng for her continuous caring, understanding, inspiring and helping me in every aspect of my life.

This work was performed at Ames Laboratory under contract W-7405-Eng-82 with the U.S. Department of Energy (DOE), supported by the Division of Materials Sciences, Office of Basci Sciences of DOE.

The United States government has assigned the document number IS-T 1748 to this report.

ABSTRACT

The Full Potential Linear Augmented Plane Wave (FPLAPW or FLAPW) method is used for a spin-polarized band calculation for ordered Fe_3Pt. As major purpose, the momentum distributions of the spin-polarized electrons are calculated and compared with results from a magnetic Compton scattering measurement. To get related information, the electronic behavior is also analyzed by examining the partial densities of states and the spatial electron distributions; the role of alloying effects is then explored by studying the electrons in some related alloys: Fe_3Ni, Fe_3Pd, Ni_3Pt and Co_3Pt.

1 GENERAL INTRODUCTION

Invar has nearly a century old history. Guillaume received the Nobel Prize in 1920 for his discovery of the first Invar material (Guillaume 1897), $Fe_{65}Ni_{35}$. The major feature of Invar materials is a very small or even negative thermal expansion coefficient. The exploration for the microscopic origin of Invar only started to have some success since 1950s. The last two decades have seen resurgent interest in Invar research, and the associated efforts have brought about many new Invar materials. Advances in computing technologies have helped for a better understanding of the Invar origin.

The purpose of this theoretical work is primarily to determine if magnetic Compton scattering might provide some useful information concerning the temperature-dependent magnetic state of a well known Invar alloy Fe_3Pt, by investigating its electronic properties, particularly the momentum distribution of spin electrons of the alloy. A few other related materials are also studied to get some related information. The work is presented in a united frame by a thorough exploration of some important aspects related to the study of Invar.

The next three chapters concern the theoretical foundations. Chapter 2 reviews the electronic band theory. The group theory is studied for the reduction in various later calculations for electrons. Chapter 3 examines the *Local Spin Density Approximation* (LSDA) and also a commonly used calculation approach, the *Full Potential Linear Augmented Plane Wave* (FLAPW) method, for electronic bands. Chapter 4 contains the formalism for Compton scattering calculation under the FLAPW approach for multi-component systems. The results are used to set up a program for *Magnetic Compton Profile* (MCP) calculations.

Chapter 5 reviews experimental and theoretical research of Invar systems to provide a general context for the study of the Invar material Fe_3Pt.

Chapter 6 presents various calculated results and their implications for Fe_3Pt as well as for some other related materials. The calculation results include electronic bands, densities of states, momentum distributions and spin electron and charge distributions. The discussions are specially focused on the calculated MCPs by comparing them with the results from a Compton scattering experiment.

2 ELECTRONIC STATES AND SPACE GROUP THEORY

Introduction

An ideal crystal is constructed by the repetition of identical structural units in space. The structure of all crystals can be described in term of a Bravais lattice composed of mathematical points and with an identical group of atoms being attached to every lattice point. There are fourteen distinct lattice types for seven possible lattice systems which are associated with 32 point symmetry groups. Symmetry studies of a crystal further take into account of the exact detailed arrangement of the atoms within the unit cell of the crystal. Such studies of crystal symmetries can greatly help to simplify many physical problems. There are 230 crystal symmetry groups, or space groups. These space groups have been systematically investigated to some degree (Bell 1954; Kurki-Suonio 1977; Bradley and Cracknell 1972; Inui, Tanabe and Onodera 1990; Ludwig and Falter 1988; Evarestov and Smirnov 1993). This chapter will briefly review the space group theory and its applications specifically to the electronic states in crystals. The study of space groups will be beneficial to the calculations pursued in later chapters.

Irreducible Representations of Space Groups

An operation $R = \{\alpha|\mathbf{t}\}$ of a space group G is defined to have such an effect on a point at $\mathbf{r}$ in the real space that

$$\{\alpha|\mathbf{t}\}\mathbf{r} = \alpha\mathbf{r} + \mathbf{t}, \tag{2.1}$$

where α is a rotation matrix and $\mathbf{t}$ a translation vector. The same operation transforms a function $\Psi(\mathbf{r})$ in the following way:

$$\begin{aligned} \{\alpha|\mathbf{t}\}\Psi(\mathbf{r}) &= \Psi(\{\alpha|\mathbf{t}\}^{-1}\mathbf{r}) \\ &= \Psi(\alpha^{-1}(\mathbf{r}-\mathbf{t})). \end{aligned} \tag{2.2}$$

For the translation group T, an invariant subgroup of the space group G, its irreducible representation corresponding to a particular wave-vector $\mathbf{k}$ is one dimensional and satisfies

$$\begin{aligned} \{\varepsilon|\mathbf{t}\}\Psi_{\mathbf{k}}(\mathbf{r}) &= \Psi_{\mathbf{k}}(\mathbf{r}-\mathbf{t}) \\ &= e^{-i\mathbf{k}\cdot\mathbf{t}}\Psi_{\mathbf{k}}(\mathbf{r}). \end{aligned} \tag{2.3}$$

The Bloch function $\Psi_{\mathbf{k}}(\mathbf{r})$ can be rewritten as

$$\Psi_{\mathbf{k}}(\mathbf{r}) = e^{i\mathbf{k}\cdot\mathbf{r}}u_{\mathbf{k}}(\mathbf{r}), \tag{2.4}$$

with $u_{\mathbf{k}}(\mathbf{r})$ being a function with the lattice periodicity:

$$u_{\mathbf{k}}(\mathbf{r}-\mathbf{t}) = u_{\mathbf{k}}(\mathbf{r}). \tag{2.5}$$

Each wave-vector $\mathbf{k}$ has its "symmetry" group as a very important subgroup $g(\mathbf{k})$ of the space group G. This wave-vector group is defined as

$$g(\mathbf{k}) = \{\{\beta|\mathbf{t}\} : \beta\mathbf{k} \doteq \mathbf{k}, \{\beta|\mathbf{t}\} \in G\}, \tag{2.6}$$

where "$\doteq$" means "equals to when modulo reciprocal lattice vectors". The space group G can then be decomposed in terms of $g(\mathbf{k})$:

$$G = g(\mathbf{k}) + \{\alpha_2|\mathbf{t}_2\}g(\mathbf{k}) + \cdots + \{\alpha_s|\mathbf{t}_s\}g(\mathbf{k}). \tag{2.7}$$

Let $\{\alpha_1|\mathbf{t}_1\}$ be the unit element $\{\epsilon|\mathbf{0}\}$, then

$$\mathbf{k}_j \doteq \alpha_j\mathbf{k} \qquad (j = 1, 2, \cdots, s) \tag{2.8}$$

constitute the star, or orbit, of $\mathbf{k}$. There are many linearly independent Bloch wave-functions $\Psi_{\mathbf{k}}(\mathbf{r})$ that correspond to one wave-vector $\mathbf{k}$. A basis for any irreducible representation can be constructed by selecting a subset of these $\Psi_{\mathbf{k}}(\mathbf{r})$. Let $\{\Psi_{\mathbf{k}\nu} \quad (\nu = 1, 2, \cdots, d)\}$ be such basis functions for a d-dimension small representation $D^{\mathbf{k}}$ of $g(\mathbf{k})$, with each $\Psi_{\mathbf{k}\nu}$ being a basis function for the irreducible representation $\mathbf{k}$ of the translation group T. Define

$$\Psi_{\mathbf{k}_j\nu} \equiv \{\alpha_j|\mathbf{t}_j\}\Psi_{\mathbf{k}\nu}, \quad j = 1, 2, \cdots, s; \nu = 1, 2, \cdots, d. \tag{2.9}$$

It can be proved that the above sd functions form a basis for an irreducible representation I of the space group G. As will be shown, this conclusion is very important in studying electronic states in a crystal.

Group Theory and Electronic States in a Crystal

Electrons moving in a crystal obey a Schrödinger-like equation:

$$H\Psi_{\mathbf{k}}(\mathbf{r}) = \varepsilon(\mathbf{k})\Psi_{\mathbf{k}}(\mathbf{r}). \tag{2.10}$$

The one-electron Hamiltonian $H(\mathbf{r})$ commutes with any symmetry operation R of the space group G:

$$RH = HR \qquad (R \in G). \tag{2.11}$$

It is easy to prove that for any operation R, $R\Psi_{\mathbf{k}}(\mathbf{r})$ is also an eigenfunction of H with the same eigenvalue $\varepsilon(\mathbf{k})$ as that of $\Psi_{\mathbf{k}}(\mathbf{r})$. If

$$H\Psi_{\mathbf{k}\nu} = \varepsilon(\mathbf{k})\Psi_{\mathbf{k}\nu}, \tag{2.12}$$

then

$$H\Psi_{\mathbf{k}_j\nu} = \varepsilon(\mathbf{k})\Psi_{\mathbf{k}_j\nu}, \tag{2.13}$$

which means

$$\varepsilon(\mathbf{k}) = \varepsilon(\mathbf{k}_2) = \cdots = \varepsilon(\mathbf{k}_s). \tag{2.14}$$

Therefore, the energy band ε has the full point–group symmetry in the $\mathbf{k}$ space. The eigenfunctions belonging to a certain eigenvalue of the Hamiltonian can always be chosen in such a way that they form the basis of an irreducible representation I of the space group. Therefore, the eigenstates of H can be classified according to the irreducible representations of the symmetry group G. How this can be done will be shown below.

A consequence of the above conclusion is that each of the *sd* degenerate states has the same probability $W_{\mathbf{k}}^{(I)}$ of being occupied. For this reason, the electron density, which is the most important quantity for the ground state of an electronic system in the density functional theory (see the next chapter), can be expressed as

$$\rho(\mathbf{r}) = \sum_I \sum_{\mathbf{k}} W_{\mathbf{k}}^{(I)} \sum_j \sum_\nu |\Psi_{\mathbf{k}_j\nu}^{(I)}|^2 \qquad (\mathbf{k} \in \textit{irreducible } B.Z.). \tag{2.15}$$

This expression can be simplified by symmetry information of the crystal.

Based on the representation theory of groups, it can be shown that

$$\sum_\nu |\Psi_{\mathbf{k}\nu}|^2 = \frac{d}{g_{\mathbf{k}}} \sum_{\{\beta|\mathbf{t}\}\in g(\mathbf{k})} |\{\beta|\mathbf{t}\}\Psi_{\mathbf{k}\mu}|^2 \tag{2.16}$$

holds for all the basis eigenfunctions $\Psi_{\mathbf{k}\mu}(\mathbf{r})(\mu = 1, \cdots, d)$ of an irreducible representation. Here, $g_{\mathbf{k}}$ is the order of $g(\mathbf{k})$, and d is the dimension of the irreducible representation. Further, it can be demonstrated that

$$\sum_j \sum_\nu |\Psi_{\mathbf{k}_j\nu}|^2 = \frac{d}{g_{\mathbf{k}}} \sum_{\{\alpha|\mathbf{t}\}\in G} |\{\alpha|\mathbf{t}\}\Psi_{\mathbf{k}\mu}|^2 . \tag{2.17}$$

If one decomposes G with respect to its invariant subgroup T:

$$G = T + \{\gamma_2|\mathbf{t}_2\}T + \cdots + \{\gamma_g|\mathbf{t}_g\}T, \tag{2.18}$$

then the previous expression for the density can take a more symmetric form:

$$\rho(\mathbf{r}) = \sum_n \sum_{\mathbf{k}} W_{n\mathbf{k}} P^{\Gamma_1} |\Psi_{n\mathbf{k}}(\mathbf{r})|^2, \tag{2.19}$$

where

$$P^{\Gamma_1} = \frac{1}{g} \sum_{\{\gamma_i|\mathbf{t}_i\}} \tag{2.20}$$

is the effective projection operator for the invariant irreducible representation Γ_1 of the space group G, and the indices I and ν have been jointly denoted as n, the conventional band index. Physically, this implies that the electron density has the Γ_1 symmetry of the space group G. By using the space group theory, all the information about the electronic states can be obtained through the eigenfunctions $\Psi_{n\mathbf{k}}$ of all those k's which are inside the irreducible $B.Z.$. Such a reduction into the considered $B.Z.$, based on the symmetry, greatly simplifies the problem of electrons in crystals. Actually, many band calculation approaches are based on the above equation to extract the electron spatial distributions $\rho(\mathbf{r})$ to determine the ground state. In the actual computational calculations, practical approaches should be used to do the extraction of the invariant components of

$$\rho_{n\mathbf{k}}(\mathbf{r}) = P^{\Gamma_1} |\Psi_{n\mathbf{k}}(\mathbf{r})|^2. \tag{2.21}$$

The next two sections will present two such approaches.

Plane Wave Scheme

Generally, any function having the space group symmetry can be expanded into a series of lattice functions which have the same symmetries. Normally, this can be done by using some commonly used functions, as shown below, for a particular quantity $\rho(\mathbf{r})$ without losing generality. Let $\mathbf{K}_i$ be a reciprocal vector; for notational simplicity, $\mathbf{k} + \mathbf{K}_i$ will be denoted as $\mathbf{q}_i$.

Eigenfunctions can be always expressed in a series of plane waves:

$$\Psi_{n\mathbf{k}}(\mathbf{r}) = \sum_{\mathbf{K}_i} C_{n\mathbf{q}_i} \frac{e^{i\mathbf{q}_i\cdot\mathbf{r}}}{\sqrt{NV}}, \tag{2.22}$$

where N is the number of unit cells of the crystal and V is the volume of a unit cell. Then one gets

$$\rho_{n\mathbf{k}}(\mathbf{r}) = \sum_{\mathbf{K}_{i'}} \left(\sum_{\mathbf{K}_i} \frac{C_{n\mathbf{q}_i} C^*_{n\mathbf{q}_i - \mathbf{K}_{i'}}}{\sqrt{NV}} \right) \frac{1}{g} \sum_{\{\gamma_j|\mathbf{t}_j\}} \{\gamma_j|\mathbf{t}_j\} \frac{e^{i\mathbf{K}_{i'}\cdot\mathbf{r}}}{\sqrt{NV}}. \tag{2.23}$$

All the reciprocal vectors can be classified into stars with the s-th star being

$$\{\mathbf{K}_{si}: \quad \mathbf{K}_{si} = \gamma_{si}\mathbf{K}_{s1} \ (i = 1, \cdots, n_s)\}. \tag{2.24}$$

A symmetrized plane wave function can be defined as

$$\begin{aligned} \Upsilon_{si} &= \frac{1}{g} \sum_j \{\gamma_j|\mathbf{t}_j\} \frac{e^{i\mathbf{K}_{si}\cdot\mathbf{r}}}{\sqrt{NV}} \\ &= e^{i\mathbf{K}_{si}\cdot\mathbf{t}_{si}} \Upsilon_{s1}. \end{aligned} \tag{2.25}$$

So, the symmetrized plane wave-functions Υ_{si} $(i = 1, \cdots, n_s)$ are not linearly independent of each other, but one can select one of them, say Υ_{s1}, to construct a maximal set of independent symmetrized plane waves as a complete basis of a functional space which has the same invariant symmetry. Using these independent functions, one gets

$$\rho_{n\mathbf{k}}(\mathbf{r}) = \sum_s \left(\sum_j \sum_{K_{i'}} \frac{C_{n\mathbf{q}_{i'}} C^*_{n\mathbf{q}_{i'} - \mathbf{K}_{sj}}}{\sqrt{V}} e^{i\mathbf{K}_{sj}\mathbf{t}_{sj}} \right) \Upsilon_{s1}. \tag{2.26}$$

Therefore, $\rho_{n\mathbf{k}}(\mathbf{r})$ has already been explicitly expressed in a series of independent functions which have the space group symmetry.

Lattice Harmonics Scheme

Another important use for applying crystal symmetry is the use of lattice harmonics. First one constructs those invariant lattice harmonics, which are invariant under the transformation of the space group, by using the spherical harmonic functions:

$$W^{\Gamma_1}_{lj} = \sum_m A_{lmj} Y_{lm}. \tag{2.27}$$

For symmorphic space groups, all the coefficients A_{lmj} are independent of $\mathbf{r}$, or, they are just constants. For non-symmorphic groups, however, these coefficients usually depend on $\mathbf{r}$, making the current scheme to get $\rho_{n\mathbf{k}}(\mathbf{r})$ impractical. Therefore, only the symmorphic group case will be considered below. It should

be understood that the above equation only holds for certain selected l's only and the summation is over certain selected m's, for spherical symmetry is broken in the crystal. Projecting $|\Psi_{n\mathbf{k}}|^2$ onto $W_{lj}^{\Gamma_1}$'s leads to

$$\rho_{n\mathbf{k}}(\mathbf{r}) = \sum_{lj} B_{lj}(r) W_{lj}^{\Gamma_1}. \tag{2.28}$$

Alternatively, $\rho_{n\mathbf{k}}(\mathbf{r})$ can be expressed in terms of the spherical harmonics:

$$\rho_{n\mathbf{k}}(\mathbf{r}) = \sum_{lm} C_{lm}(r) Y_{lm}, \tag{2.29}$$

where

$$C_{lm}(r) = \sum_{j} B_{lj}(r) A_{lmj}. \tag{2.30}$$

Applying the spherical Harmonics to $|\Psi_{n\mathbf{k}}|^2$, we get

$$|\Psi_{n\mathbf{k}}|^2 = \sum_{lm} D_{lm}(r) Y_{lm}, \tag{2.31}$$

it can be easily shown that

$$C_{lm}(r) = \sum_{j} A_{lmj} \sum_{m_1} A_{lm_1 j} D_{lm_1}(r). \tag{2.32}$$

Symmetries of Eigenfunctions in Momentum Space

Symmetry properties are also important in momentum space. An example is an application to the most fundamental quantity, the wave function. In momentum space, or k-space, wave-functions can be obtained from a Fourier transformation:

$$\Phi_{n\mathbf{k}_j}(\mathbf{q}) = \int \Psi_{n\mathbf{k}_j}(\mathbf{r}) \frac{e^{-i\mathbf{q}\cdot\mathbf{r}}}{\sqrt{NV}} d^3\mathbf{r} \tag{2.33}$$

After some algebraic calculations, it is not difficult to find out that

$$\begin{aligned} \Phi_{n\mathbf{k}_j}(\mathbf{q}) &= \frac{e^{-i\mathbf{q}\cdot\mathbf{t}_j}}{|D_3(\alpha_j)|} \Phi_{n\mathbf{k}}(\alpha_j^{-1}\mathbf{q}) \\ &= \pm e^{-i\mathbf{q}\cdot\mathbf{t}_j} \Phi_{n\mathbf{k}}(\alpha_j^{-1}\mathbf{q}), \end{aligned} \tag{2.34}$$

where the denominator $D_3(\alpha_j)$ of the rotation α_j is ± 1, depending on whether or not the rotation α_j is a proper rotation. Therefore, a property is

$$|\Phi_{n\mathbf{k}}(\mathbf{q})|^2 = |\Phi_{n\mathbf{k}_j}(\mathbf{q}_j)|^2. \tag{2.35}$$

Similar to symmetry properties in the real space, the above symmetry property is crucial to many calculations in the momentum space as shown in latter calculations.

3 DENSITY FUNCTIONAL THEORY AND THE LOCAL DENSITY APPROXIMATION

Introduction

A solid state system is a many body system of nuclei and electrons. The nuclei oscillate relatively slowly around their equilibrium positions, for the mass of the nucleus is greater, by a factor of about three to four orders of magnitude, than the mass of the electrons around it. At low temperatures, the many body system can be roughly viewed as two nearly inter-independent systems of electrons and nuclei. Such thermal effects, and the phonon-electron interactions as they are usually called, are not to be considered here. In the ground state of this complicated system, the relatively static nuclear configurations mainly provide some potentials for the electron subsystem to be stabilized. The motions of the nuclei thus can often be totally ignored. This is just the Born-Oppenheimer approximation which is to be used throughout this work.

Two Subsystems in a Crystal

For N electrons moving in an "external" (with respect to the electrons) potential $\hat{V}_{ext}$ the Hamiltonian has the form

$$\hat{H} = \hat{T} + \hat{V}_{ext} + \hat{V}_{ee}, \tag{3.1}$$

where $\hat{T}$ is the kinetic operator, and $\hat{V}_{ee}$ is the electron-electron Coulomb interaction operator. The external potential operator is a local operator of the form

$$\hat{V}_{ext} = \sum_{i=1}^{N} v_{ext}(\mathbf{r}_i). \tag{3.2}$$

The "exact" behavior of the electrons is determined by the many body Schrödinger equation:

$$\left[-\frac{1}{2}\sum_i \nabla_i^2 + \sum_i v_{ext}(\mathbf{r}_i) + \hat{V}_{ee} - E\right] \Psi(\mathbf{r}_1, \cdots, \mathbf{r}_N) = 0, \tag{3.3}$$

where E is the total energy of the electron system. Here spin, spin-orbital coupling and other relativistic effects are omitted.

In a solid, the number of electrons N is too large for computers to solve for the above equation. In other words, it is technically impossible to take care of too many microscopic details of the electrons once and for all at this stage of the technique. Alternative approaches have to be found to explain, on a microscopic level, macroscopically observable quantities in a solid system. Such approaches may have to introduce some further approximations in which some minor effects are to be ignored in order to get reliable results without going beyond present computer abilities. As to be shown in this chapter, the *Density Functional Theory* (DFT) effectively provides a way to solve the ground state problem of a solid system. Following the essence of this rigorous functional theory, the *Local Spin Density Approximation* (LSDA) makes practical calculations possible to a great degree.

Density Functional Formalism

This alternative theory was initiated by Hohenberg and Kohn (1964). To avoid any ambiguity, a more recent approach by Levy (1979 and 1982) is to be presented here.

For all "N-representable" densities $\rho(\mathbf{r})$, i.e., for all those electron densities which can be obtained from some antisymmetric wave function $\Psi(\mathbf{r}_1, \mathbf{r}_2, ..., \mathbf{r}_N)$, define a functional

$$F[\rho] = \min_{\Psi \to \rho(\mathbf{r})} \langle \Psi | \hat{T} + \hat{V}_{ee} | \Psi \rangle, \tag{3.4}$$

where the minimum is taken over all antisymmetric N-particle wave functions Ψ that produces a density $\rho(\mathbf{r})$. $F[\rho]$ is universal in the sense that it refers neither to a specific system nor to the external potential $\hat{V}_{ext}$ of which the mean value is

$$V_{ext}[\rho] = \int \rho(\mathbf{r}) v_{ext}(\mathbf{r}) d^3\mathbf{r}. \tag{3.5}$$

By combining the above two functionals, the energy functional can be defined:

$$E[\rho] = F[\rho] + V_{ext}[\rho]. \tag{3.6}$$

Let E_{gs}, $\Psi_{gs}(\mathbf{r})$ and $\rho_{gs}(\mathbf{r})$ be the ground state energy, wave-function and density respectively. From the conventional Rayleigh-Ritz variational principle and the features of the many body Hamiltonian, it is easy to show the following two basic theorems of the density functional theory:

1. The functional $E[\rho]$ reaches its minimum value for the exact electron density of the ground state:

$$E[\rho] = \langle \Psi^{\rho}_{\min} | \hat{T} + \hat{V}_{ee} + \hat{V}_{ext} | \Psi^{\rho}_{\min} \rangle \geq E_{gs}. \tag{3.7}$$

2. The ground state of the electron system is fully determined by the corresponding electron density, and the total energy is given by:

$$E[\rho_{gs}] = \langle \Psi^{\rho_{gs}}_{\min} | \hat{T} + \hat{V}_{ee} + \hat{V}_{ext} | \Psi^{\rho_{gs}}_{\min} \rangle. \tag{3.8}$$

Therefore, of all those antisymmetric functions that yield an electron density $\rho(\mathbf{r})$, the ground state is the one that minimizes the functional $E[\rho]$. and has a density rho_{gs}

It should be noticed that the new variation is on the electron density $\rho(\mathbf{r})$. In spirit, the new variational principle is similar to the original Rayleigh-Ritz variational calculation in quantum mechanics where the variation is on the many body wave-function $\Psi(\mathbf{r}_1, \mathbf{r}_2, ..., \mathbf{r}_N)$. Basically, the above theorems imply that there is a one-to-one correspondence between the many body wave-function and the electron density $\rho(\mathbf{r})$, which is the real reason why the original Rayleigh-Ritz variational principle can be reformulated to the current one. The most important advantage of DFT over the conventional variational principle for the many body system is that it depends only on three spatial variables (and one spin variable if needed), regardless of the number of particles of the physical system.

However, the functional $F[\rho]$ may be nonlocal and is unknown besides the proof of its existence, and has to be decided in order for the DFT to be useful. A lot of studies have been made to use nonlocal density functional (Hu and Langreth 1981; Langreth, D.C., and Mehl 1981; Langreth, D.C., and Mehl 1983; Bagno, Jepsen and Gunnarsson 1989). To find more and more accurate functionals has always been a very challenging work for the past decades. Essentially, all attempts to find any explicit functional form of $F[\rho]$ rely on numerical experience and theoretical methods which lie outside of the formal structure of the DFT methodology.

Kohn-Sham Scheme For the Density Functional Theory

A crucial step to find $F[\rho]$ is to extract the information about the electron-electron interaction. Historically the classical Coulomb potential:

$$V_{Cl}[\rho] = \frac{1}{2} \int \int d^3\mathbf{r} d^3\mathbf{r}' \frac{\rho(\mathbf{r}) n(\mathbf{r}')}{|\mathbf{r} - \mathbf{r}'|} \tag{3.9}$$

is perhaps the most frequently used potential form. Separating $V_{Cl}[\rho]$ from the overall electron-electron potential functional $V_{ee}[\rho]$ leads to:

$$V_{ee}[\rho] = V_{xc}[\rho] + V_{Cl}[\rho], \tag{3.10}$$

where $V_{xc}[\rho]$ is a potential difference term. Then the ground state energy functional can be rewritten as

$$E[\rho] = T[\rho] + V_{xc}[\rho] + V_{Cl}[\rho] + V_{ext}[\rho]. \tag{3.11}$$

It still turns out that directly searching for an explicit form of the kinetic energy functional $T[\rho]$ and the exchange-correlation functional $V_{xc}[\rho]$ with high accuracy is very difficult.

An indirect approach to $T[\rho]$ by Kohn and Sham (1965) transforms the problem into a problem of a fictitious non-interacting system. First $T[\rho]$ is partitioned into two parts:

$$T[\rho] = T_s[\rho] + T_c[\rho], \tag{3.12}$$

then the exchange-correlation energy is defined as

$$E_{xc}[\rho] = V_{xc}[\rho] + T_c[\rho], \tag{3.13}$$

where $T_s[\rho]$ is the kinetic energy of a fictitious non-interacting system and $T_c[\rho]$ is defined to be the correlation part of $T[\rho]$. The above partition is so made that the imaginary non-interacting particles have orbits which obey the Kohn-Sham equations:

$$\left(-\frac{1}{2}\nabla^2 + v_{eff}(\mathbf{r})\right)\psi_i(\mathbf{r}) = \varepsilon_i\psi_i(\mathbf{r}), \tag{3.14}$$

$$\rho(\mathbf{r}) = \sum_{i=1}^{N} f_i|\psi_i(\mathbf{r})|^2, \tag{3.15}$$

with an effective potential

$$v_{eff}(\mathbf{r}) = v_{ext}(\mathbf{r}) + \int d^3\mathbf{r}'\frac{\rho(\mathbf{r}')}{|\mathbf{r}-\mathbf{r}'|} + v_{xc}(\mathbf{r}), \tag{3.16}$$

where the effective exchange-correlation potential is defined as:

$$v_{xc}(\mathbf{r}) = \frac{\delta E_{xc}}{\delta\rho}. \tag{3.17}$$

Let f_i be the occupation number of the orbit corresponding to ε_i, the total energy for the ground state can be found by using

$$E_{gs} = \sum_i f_i\varepsilon_i - \frac{1}{2}\int\int d^3\mathbf{r}d^3\mathbf{r}'\frac{\rho(\mathbf{r})\rho(\mathbf{r}')}{|\mathbf{r}-\mathbf{r}'|} - \int d^3\mathbf{r}\rho(\mathbf{r})v_{xc}(\mathbf{r}) + E_{xc}. \tag{3.18}$$

Here the only two resulting quantities which have a rigorous interpretation are the ground state energy and the electron density. In principle, both of these quantities can be measured experimentally (i.e., they are observable). Therefore, the approach has reduced a many-electron problem, via an intermediary orbital picture, to a one-electron problem where the many-body interactions among electrons are represented by an effective single-electron potential $v_{eff}(\mathbf{r})$.

It should be kept in mind that behind the KS scheme is the equivalent Hohenberg-Kohn variational principle. According to this variational principle, which itself is equivalent to the original Rayleigh-Ritz variational principle, the energy functional:

$$E[\rho] = T_s[\rho] + E_{xc}[\rho] + V_{Cl}[\rho] + V_{ext}[\rho] \tag{3.19}$$

reaches its minimum E_{gs} under the constraint

$$\int d^3\mathbf{r}\rho(\mathbf{r}) = N. \tag{3.20}$$

The corresponding Euler equation states that the chemical potential, as the Lagrange multiplier, is

$$\begin{aligned} \mu &= \frac{\delta E(\rho)}{\delta \rho} \\ &= v_{eff}(\mathbf{r}) + \frac{\delta T_s(\rho)}{\delta \rho}, \end{aligned} \tag{3.21}$$

which can be solved under specified boundary conditions.

A question to a curious mind naturally is why an alternative to the conventional Euler many-body problem is taken here. Among other reasons, the introduction of fictitious orbits draws the system closer to the concept for atoms, where comparisons can lead to clues more intuitive than otherwise. Probably for this reason, DFT calculations have been applied not only to a solid system, but also to molecules, nuclei, clusters and many other less aggregated or less condensed systems. As for what the meaning of these orbits in a solid is, more caution should be taken for a solid system than a simple atom. In a solid, an electron, especially an outer electron from the atomic constituents, is in more intense interactions than in an atom since the interactions now are with more than just one nucleus.

In the equation (3.16), except for the exchange-correlation potential v_{xc}, the other two terms are real potentials and can be easily determined. If the explicit form can be found for the universal functional E_{xc}, or, equivalently for v_{xc}, then all kinds of electronic systems can be solved self-consistently. The KS scheme basically attempts to extract from the original undecided functional $F[\rho]$ some major parts which can be analytically or numerically found, and leave only a relatively small part E_{xc} to be decided.

The electronic exchange-correlation interaction is roughly composed of two contributions. Exchange interaction keeps electrons of the same spin away from each other because of the Pauli exclusion principle. Correlation interaction keeps the electrons of both spins away from each other because of the Coulomb repulsion.

E_{xc} does not have a very clear physical description so far, both for its kinetic part and for its potential part. However, two good features about E_{xc} make it "easy" to evaluate:

- It is short-ranged.
- Because of the isotropic nature of Coulomb interactions, it is relatively insensitive to non-spherical features (Jones and Gunnarson 1989).

Even so, in practice, approximations have to be made to find an accurate E_{xc} which is a decreasing functional with increasing density.

Local Density Approximation

This popular approximation corresponds to the following equation

$$E_{xc}[\rho] = \int d^3\mathbf{r}\rho(\mathbf{r})\epsilon_{xc}(\rho(\mathbf{r})), \tag{3.22}$$

where $\epsilon_{xc}(\rho(\mathbf{r}))$ is the exchange-correlation energy per electron. The exchange-correlation potential then becomes

$$v_{xc}(\mathbf{r}) = \frac{\delta(\rho\epsilon_{xc}(\rho))}{\delta\rho}. \tag{3.23}$$

As mentioned previously, E_{xc} is generally impossible to evaluate because of the complexities involving a solid. Widely used *LocalDensityApproximation* (LDA) or *LocalSpinDensityApproximation* (LSDA) functionals include those proposed by Hedin and Lundqvist (1971), von Barth and Hedin (1972), Gunnarsson and Lundqvist (1976), Rajagopal (1979), Vosko, Wilk and Nusair (1980), and Perdew and Zunger (1981). The exchange and correlation contributions to this potential are derived from the homogeneous electron gas.

Even so implemented, LDA or LSDA has explained many systems in their ground states. The accuracy of LDA possibly lies in the fact that spatial changes are primarily in the valence electron distribution where the gradients of the density are small.

Obviously this approach has its limitations, because, for example, not all forms of electron correlation effects maybe present in a solid also occur in a homogeneous electron gas. An effort to deal with such heterogeneity is by introducing terms containing density gradients into the existing expressions of E_{xc} (Perdew and Yang 1986; Perdew 1986). Although the attempts have some success on some lighter elements up to Si, a problem is that for 3d metals the calculation results are even worse than those without the "correction" (Barbiellini, Moroni and Jarlborg 1990). A few people are still working on improving the approach (Geldcurt 1995; Perdew 1995).

Many calculations in the past decades have demonstrated that LSDA gives a good description of ground state properties of many moderately correlated systems. It is really amazing that the exchange-

correlation potentials extrapolated from uniform electron gases can lead to many reasonable results for the highly nonuniform solids. LDA has actually been the basic tool for the overwhelming majority of the first-principles calculations in solid state physics, and has contributed significantly to the understanding of the macroscopic properties of solids at the microscopic level. As mentioned earlier, LDA often fails because of deficient understandings of the exchange-correlation interactions. Many people are still working to make more corrections to the existing implementations of the DFT theory.

DFT for Complex Systems

To this point, discussions have been limited to non-relativistic, one-component and spinless systems. The Kohn-Sham equations are also generalized to the magnetic systems in which the fundamental quantity ρ is extended to contain two parts, $\rho_\uparrow$ and $\rho_\downarrow$, the spin-up and spin-down densities in a spin-polarized system (Von Barth and Hedin 1972; Rajagopal and Callaway 1973). This generalization gives different effective one-particle potentials for the two spin states in the self-consistent Kohn-Sham equations. The driving force producing the magnetism is the Coulomb energy lowering due to exchange interaction. Actually, the HK theorems and Kohn-Sham scheme were also generalized to multi-component systems (Sander, Shore and Sham 1973; Kalia and Vashishta 1978), and relativistic systems (Rajagopal and Callaway 1973; Ramana and Rajagopal 1983; Rajagopal 1978; MacDonald and Vosko 1979). General reviews about more developments of the density functional theory are included in many other works (Rajagopal 1979; Barth 1982; Kohn and Vashishta 1983; Dreizler and Providẽncia 1985; Andersen, Jepsen and Glötzel 1985; Kohn 1985; Levy 1985; Jones and Gunnarsson 1989; Kryachko and Ludẽna 1990; Mahan and Subbaswamy 1990; Gross and Kurth 1994; Salahub, Castro and Proynov 1994; Geldcurt 1995; Kohn 1995; Levy 1995; Perdew 1995).

Ground State of a Crystal

Only the electronic system is considered so far. The energy functional $E[\rho]$ does not include the electrostatic energy between the nuclei. However, in practice, the electrostatic energy is usually calculated and added to the total energy of the electrons, to get the total energy E_{tot} of the overall crystal system composed of both the electrons and the nuclei.

A condensed matter system can be usually described by some state variables: volume, magnetization, pressure, magnetic field and others that are not closely related to the Invar.

Band calculations can determine the total energy as a function of the volume V to give the binding

curve $E_{tot}(V)$ of the system. This total energy dependency on the volume is found from the band calculations based on some fixed crystal structures, because technically it is still impossible to take into consideration all feasible geometrical configurations of the constituent atoms. The actual ground state of the system appears at the energy minimum where the pressure $dE/dV = 0$, corresponding to an equilibrium volume V_0. Similarly, whether or not spontaneous magnetization occurs can also be derived from the band calculations: Spontaneous magnetization occurs only if the equilibrium magnetization is non-zero. More about this will be discussed later when magnetism is particularly addressed.

4 COMPTON PROFILE CALCULATION FORMALISM

Introduction

Conventional measurements of the Doppler broadening of inelastically scattered X-radiation and γ-radiation, the Compton profile, provide information about the momentum distribution of the scattering electrons. Electron momentum distributions thus obtained are complementary to what is found about the spatial electron distribution and also orbital moments from other standard techniques, such as X-ray and neutron diffraction.

The magnetic scattering of photons was considered from a theoretical standpoint as early as 1954, and its use in condensed matter research emerged in 1970s with the availability of intense synchrotron beams. The latter are demanded simply because the involved magnetic interaction, as a relativistic correction, is considerably smaller than non-magnetic interactions, or, the charge scattering.

Conventional Compton Scattering

Colliding with a stationary free electron, a photon will have its wavelength shifted by

$$\Delta\lambda = \frac{2h}{mc}\sin^2\frac{\theta}{2}, \tag{4.1}$$

where m is the rest mass of electron, and θ the scattering angle.

The maximum shift for a stationary electron thus is

$$\begin{aligned}(\Delta\lambda)_{max} &= \frac{2h}{mc} \\ &= 0.049\mathring{A}, \end{aligned} \tag{4.2}$$

which is independent of the incident photon wavelength λ_0. For the wavelength shift $\frac{\Delta\lambda}{\lambda}$ to be large enough for detection, X-ray or γ-ray (with λ around 1 $\mathring{A}$) is normally chosen as the incident beam in a Compton scattering experiment.

Since Compton scattering is an incoherent process, the structures of the study samples are not important. This means that Compton scattering experiments can be done on solid, amorphous, liquid

or gaseous materials. Since in the materials there are loosely bound electrons as the scatterers of the inelastic process (elastic process can happen between the incident photons and tightly bound electrons or the whole system essentially, causing X-ray diffraction which can be utilized to probe spatial electron distribution).

To make the Compton scattering effect sufficiently visible, the energy transfer, $h\nu = h(\nu_0 - \nu)$, greatly should exceed the outer-electron binding energy, as if the interaction between scattering photons and scattered electrons takes place in such a short duration that the scattering interaction is approximately over before the electron has had a chance to move in the potential well and change its potential energy. This is just called **impulse approximation**, which is equivalently stating that electrons can be treated as free electrons when the scattering occurs.

Magnetic Compton Scattering

Conventional Compton scattering studies did not involve magnetic quantities of the scatterers. A term depending on the electron spin in scattering cross section for free electrons was first derived by Lipps and Tolhoek (1954). An extension to electrons in molecules and solids was done by Platzman and Tzoar (1970). Many theoretical studies have been done ever since (Wakoh and Kubo 1977; Williams 1977; Landau and Lifshitz 1982; Sakai, Tersahima and Sekizawa 1984; Mills 1987; Sakai, Shiotani, Ito, Itoh, Kawata, Amemiya, Ando, Yamamoto and Kitamura 1989; Balcar and Lovesey 1989; Kubo and Asano 1990; Collins, Cooper, Lovesey and Laundy 1990; Cooper, Zukowski, Collins, Timms, Itoh and Sakurai 1992; Tanaka, Skai, Kubo and Kawata 1993; Zukowski, Collins, Cooper, Timms, Sakurai, Kawata, Tanaka and Malinowski 1993; Cooper, Zukowski, Timms, Armstrong, Itoh, Tanaka, Ito, Kawata and Bateson 1993; Timms, Zukowski, Cooper, Laundy, Collins, Itoh, Sakurai, Iwazumi, Kawata, Ito, Sakai and Tanaka 1993).

Let the angle θ be the scattering angle of the photon, ψ the angle between the direction of the incident photon $\mathbf{k}_0$ and that of the electron spin σ_0, ϕ the angle between the $(\mathbf{k}_0, \sigma_0)$-plane and the $(\mathbf{k}_0, \mathbf{k})$-plane, P_l is the linear polarization, and P_c is the circular polarization, $\mathbf{p}$ and p_z the electron momentum and its component along the scattering vector $\mathbf{q} = \mathbf{k} - \mathbf{k}_0$, E_0 and E the energies of the incident and outgoing photons respectively, and mc^2 is the rest mass energy of the electron. Under the impulse approximation, the Compton cross section can be written as

$$\begin{aligned} \frac{d^2\sigma}{d\Omega dE} &= \frac{r_0^2}{2}\left(\frac{E}{E_0}\right)^2 \{(\Phi_0 + P_1\Phi_1) \times \\ &\quad \int\int \left[n^{\uparrow}(\mathbf{p}) + n_{\downarrow}(\mathbf{p})\right] dp_x\, dp_y + \end{aligned}$$

$$P_c\Phi_{spin}\int\int\left[[n^{\uparrow}(\mathbf{p})-n_{\downarrow}(\mathbf{p})\right]\,dp_x\,dp_y\},\tag{4.3}$$

where

$$\Phi_0 = 1+\cos^2\theta+\frac{E_0-E}{mc^2}(1-\cos\theta),\tag{4.4}$$

$$\Phi_1 = \sin^2\theta,\tag{4.5}$$

$$\tag{4.6}$$

and

$$\Phi_{spin} = -(1-\cos\theta)\times \left\{\frac{E_0+E}{mc^2}\cos\theta\cos\psi+\frac{E}{mc^2}\sin\theta\sin\psi\cos\phi\right\}.\tag{4.7}$$

Since only the third function Φ_{spin} changes its sign when the direction of the electron spin is reversed, the following expression is obtained,

$$\left(\frac{d^2\sigma}{d\Omega dE}\right)_{up}-\left(\frac{d^2\sigma}{d\Omega dE}\right)_{down}=r_0^2\left(\frac{E}{E_0}\right)^2P_c\Phi_{spin}J_{mag},\tag{4.8}$$

where

$$J_{mag}(p_z)=\int\int\left\{n^{\uparrow}(\mathbf{p})-n_{\downarrow}(\mathbf{p})\right\}\,dp_x\,dp_y.\tag{4.9}$$

This expression indicates that the difference between the two momentum spectra, one measured with the scatterers magnetized in one direction and the other with the same scatterers magnetized in the opposite direction, gives the magnetic Compton profile J_{mag}.

This magnetic contribution is smaller than pure charge scattering by a factor of E_0/mc^2. For X-rays of about 50 kev, it is about 10% of the total intensity. At normal X-ray energies the magnetic scattering is therefore weak. The effect is observable when circularly polarized photon beams are utilized, and it can only be used to study ferromagnets or ferrimagnets. It is the advent of synchrotron radiation sources, which provide monochromatic beams with 10^{20} photons/s, that make it feasible to exploit magnetic photon scattering as a technique in condensed matter research (Platzman and Tzoar 1970; Blume 1985; Cooper, Laundy, Cardwell, Timms, Holt and Clark 1986; Cooper, Collins, Timms, Brahmia, KaneHolt and Laundy 1988; der Bergevin and Brunel 1986). The experiments are being realized by the application of an external magnetic field where the spin dependent component is isolated by reversing the direction of the magnetization and subtracting the spin-up and spin-down signals.

Therefore, the above theoretical results based on the impulse approximation, which ignores the motion of electrons during the scattering, is valid for the theoretical comparisons of the experimental data.

Compton Profile Calculation Using FLAPW Method

Let $\mathbf{r}$ be a position in a unit cell centered at $\mathbf{R}_\mu$, and ρ_α be the position of the α-th atom relative to the center, then $\mathbf{r}_{\mu\alpha} = \mathbf{r} - \mathbf{R}_\mu - \rho_\alpha$ is the relative position of $\mathbf{r}$ to the atom. Denote the radius of the muffin-tin sphere surrounding the α-th atom as $r_{mt}^{(\alpha)}$, and $\mathbf{k} + \mathbf{K}_i$ as $\mathbf{q}_i$, the eigenfunction can then be expressed as

$$\begin{aligned}\Psi_{n\mathbf{k}}(\mathbf{r}) &= \sum_{\mathbf{K}_i} C_{\mathbf{q}_i}\{\frac{e^{i\mathbf{q}_i\cdot\mathbf{r}}}{\sqrt{NV}}\prod_{\mathbf{R}_\mu}\prod_{\rho_\alpha}\theta(r_{\mu\alpha} - r_{mt}^{(\alpha)}) + \\ &\quad \sum_{\mathbf{R}_\mu}\sum_{\rho_\alpha}\theta(r_{mt}^{(\alpha)} - r_{\mu\alpha})\frac{e^{i\mathbf{q}_i\cdot(\mathbf{R}_\mu+\rho_\alpha)}}{\sqrt{NV}}\cdot \\ &\quad \sum_{lm} R_{lm\alpha\mathbf{q}_i}(r_{\mu\alpha})Y_{lm}(\hat{r}_{\mu\alpha})\}, \end{aligned} \tag{4.10}$$

or ,

$$\begin{aligned}\Psi_{n\mathbf{k}}(\mathbf{r}) &= \sum_{\mathbf{K}_i} C_{\mathbf{q}_i}\{\frac{e^{i\mathbf{q}_i\cdot\mathbf{r}}}{\sqrt{NV}} + \sum_{\mathbf{R}_\mu}\sum_{\rho_\alpha}\theta(r_{mt}^{(\alpha)} - r_{\mu\alpha})\frac{e^{i\mathbf{q}_i\cdot(\mathbf{R}_\mu+\rho_\alpha)}}{\sqrt{NV}}\cdot \\ &\quad (\sum_{lm} R_{lm\alpha\mathbf{q}_i}(r_{\mu\alpha})Y_{lm}(\hat{r}_{\mu\alpha}) - e^{i\mathbf{q}_i\cdot\mathbf{r}_{\mu\alpha}})\}. \end{aligned} \tag{4.11}$$

Electronic waves do not behave like plane waves near the atomic cores, hence it is more efficient to use near-atomic waves inside an atomic muffin-tin (MT) in the solid. For the mostly localized d electrons with both atomic-like character and extended plane-wave-like character, as well as for almost totally localized f electrons, this is really important.

For the LAPW method (Afagada 1972; Koelling and Arbman 1975; Koelling and Harmon 1977; MacDonald, Pickett and Koelling 1980; Weinert 1981; Weinert, Wimmer and Freeman 1982; Jansen and Freeman 1984; Mattheiss and Hamann 1986; Blaha, Schwarz, Sorantin and Trickey 1990),

$$R_{lm\alpha\mathbf{q}_i}(r_{\mu\alpha}) = A_{lm\alpha\mathbf{q}_i}u_{l\alpha}(r_{\mu\alpha}) + B_{lm\alpha\mathbf{q}_i}\dot{u}_{l\alpha}(r_{\mu\alpha}), \tag{4.12}$$

where $\dot{u}_{l\alpha}(r_{\mu\alpha})$ is the energy derivative of $u_{l\alpha}(r_{\mu\alpha})$ with respect to a certain chosen energy value. At MT boundaries, the continuity of $\Psi_{n\mathbf{k}}(\mathbf{r})$ and the radial derivatives can lead us to solve for the $A_{lm\alpha\mathbf{q}_i}$'s and $B_{lm\alpha\mathbf{q}_i}$'s. Since

$$e^{i\mathbf{q}_i\cdot\mathbf{r}_{\mu\alpha}} = 4\pi\sum_{lm} i^l j_l(q_i r_{\mu\alpha})Y_{lm}^*(\hat{q}_i)Y_{lm}(\hat{r}_{\mu\alpha}), \tag{4.13}$$

it is easy to get

$$A_{lm\alpha\mathbf{q}_i} = 4\pi i^l Y_{lm}^*(\hat{q}_i)\cdot\frac{j_l'(q_i r_{mt}^{(\alpha)})\dot{u}_{l\alpha}(r_{mt}^{(\alpha)}) - j_l(q_i r_{mt}^{(\alpha)})\dot{u}_{l\alpha}(r_{mt}^{(\alpha)})}{\dot{u}_{l\alpha}(r_{mt}^{(\alpha)})u_{l\alpha}'(r_{mt}^{(\alpha)}) - u_{l\alpha}(r_{mt}^{(\alpha)})\dot{u}_{l\alpha}'(r_{mt}^{(\alpha)})}, \tag{4.14}$$

and

$$B_{lm\alpha\mathbf{q}_i} = 4\pi i^l Y^*_{lm}(\hat{q}_i) \cdot \frac{j_l(q_i r^{(\alpha)}_{mt}) U'_{l\alpha}(r^{(\alpha)}_{mt}) - j'_l(q_i r^{(\alpha)}_{mt}) u_{l\alpha}(r^{(\alpha)}_{mt})}{\dot{u}_{l\alpha}(r^{(\alpha)}_{mt}) \dot{u}'_{l\alpha}(r^{(\alpha)}_{mt}) - u_{l\alpha}(r^{(\alpha)}_{mt}) \dot{u}'_{l\alpha}(r^{(\alpha)}_{mt})}, \tag{4.15}$$

where j_l is the spherical Bessel function. The momentum wavefunction, the Fourier transform of the real space wave function $\Psi_{n\mathbf{k}}(\mathbf{r})$, is then

$$\begin{aligned}\Phi_{n\mathbf{k}}(\mathbf{q}) = \frac{1}{V} \sum_{\mathbf{K}_j} \delta_{\mathbf{q}_j\mathbf{q}} \{ V_{out} C_{n\mathbf{q}_j} + \sum_{\rho_\alpha} e^{-i\mathbf{K}_j\cdot\rho_\alpha} [4\pi \sum_{lm} (-i)^l \\ \int \sum_{\mathbf{K}_i} C_{n\mathbf{q}_i} e^{i\mathbf{K}_i\cdot\rho_\alpha} R_{lm\alpha\mathbf{q}_i}(r_{\mu\alpha}) j_l(q r_{\mu\alpha}) r^2_{\mu\alpha}\, dr_{\mu\alpha} Y_{lm(\hat{q})} - \\ 3V_\alpha \sum_{\mathbf{K}_i \neq \mathbf{K}_j} C_{n\mathbf{q}_i} e^{i\mathbf{K}_i\cdot\rho_\alpha} \frac{j_l(|\mathbf{K}_i - \mathbf{K}_j| r^{(\alpha)}_{mt})}{|\mathbf{K}_i - \mathbf{K}_j| r^{(\alpha)}_{mt}}] \},\end{aligned} \tag{4.16}$$

where $\mathbf{q}_j$ denotes $\mathbf{k} + \mathbf{K}_j$. Therefore,

$$\begin{aligned}\Phi_{n\mathbf{k}}(\mathbf{q}_j) = \frac{1}{V} V_{out} C_{n\mathbf{q}_j} + \frac{4\pi}{V} \sum_{lm} (-i)^l Y_{lm}(\hat{q}_j) \sum_{\rho_\alpha} e^{-i\mathbf{K}_j\cdot\rho_\alpha} \\ \sum_{\mathbf{K}_i} C_{n\mathbf{q}_i} e^{i\mathbf{K}_i\cdot\rho_\alpha} \int R_{lm\alpha\mathbf{q}_i}(r_{\mu\alpha}) j_l(q_j r_{\mu\alpha}) r^2_{\mu\alpha}\, dr_{\mu\alpha} \cdot \\ 3 \sum_{\mathbf{r}_\alpha} V_\alpha \sum_{\mathbf{K}_i \neq \mathbf{K}_j} C_{n\mathbf{q}_i} e^{i(\mathbf{K}_i - \mathbf{K}_j)\cdot\rho_\alpha} \frac{j_l(|\mathbf{K}_i - \mathbf{K}_j| r^{(\alpha)}_{mt})}{|\mathbf{K}_i - \mathbf{K}_j| r^{(\alpha)}_{mt}}\end{aligned} \tag{4.17}$$

where $\hat{q}_j$ is a unit vector along $\mathbf{q}_j$, V_{out} is the volume outside the MT's in a unit cell, and V_α is the volume for the α-th MT. The result here is the extension of a one-atom system (Wakoh and Kubo 1977) to a multiple-atom system.

5 ON INVAR AND INVAR STUDY

Introduction

Invar systems and their current research are briefly reviewed and discussed in this chapter, with a focus on the typical Invar Fe-X (X = Ni, Pd and Pt) systems to be studied here.

Invar Anomalies and Invar Materials

Invar is associated with the thermal expansion property originating from the anharmonic vibrations of the crystal lattice. The linear thermal expansion coefficient of a common metal or alloy is of the order of $10^{-5}K^{-1}$. However, in 1897, Ch. E. Guillaume found that ferromagnetic (FM) *fcc* Fe_xNi_{1-x} alloys, around Fe atom concentration $x = 65\%$ and in a wide thermal range around room temperature, shows an extremely low thermal expansion coefficient which is an order of magnitude smaller than in ordinary materials. Such a sample first shrinks when the temperature is raised from zero temperature, the thermal expansion then remains small until around and above the Curie temperature T_C where the thermal expansion become larger.

Since 1897, many more Invar materials have been found. Invar anomalies are observed in many other ferromagnetic (FM) as well as in anti-ferromagnetic (AF) binary, ternary and also multi-component transition metal alloys and inter-metallic compounds with large spontaneous volume magnetostriction. Moreover, Invar anomalies are observed in rare earth RE-transition metal compounds with Lavesphase structure (e.g. $RECo_2$, $REMn_2$) or compounds like the hard ferromagnet $Fe_{14}Nd_2B$. The lattice structure is of no influence to the occurrences of Invar, since there are Invar systems having *fcc*, *bcc*, *hexagonal* and other structures like *fct* or even amorphous forms. There are no pure 4f, 5f nor insulating Invar alloys or compounds, and the Invar systems are rich in at least one 3d-transition element, which may imply that the Invar effect is a phenomena associated with 3d magnetic electrons.

An Invar material gives rise to a small or even negative thermal expansion coefficient over a wide temperature range below the Curie or Néel temperature. There are also other anomalies accompanying

the thermal anomaly: large forced volume magnetostriction dV/dH, large negative pressure effect on magnetization dM/dP, large negative pressure effect on Curie temperature dT_C/dP, spontaneous volume magnetostriction for both low and high temperatures, thermal variation of high field susceptibility and of elastic constants, as well as of Young's and bulk moduli. Another characteristic property of Invar alloys is their unusual temperature dependence of the magnetization in comparison to "ordinary" ferromagnets: the magnetization decreases with temperature more abruptly in Invar materials. More details can be found in some general reviews on the study of Invar (Wassermann 1989; Wassermann 1990; Wijn 1994; Shiga 1994).

Magnetic Fluctuations from Thermal Effects

Since Invar appears only in magnetic materials , the relationship between magnetic and thermal effects is very important. A paramagnetic neutron scattering experiment using polarized neutrons and polarization analysis to obtain an unambiguous measure of the magnetic scattering above the Curie point (Ziebeck et al 1983) for Fe_3Pt shows considerable magnetic scattering, which is peaked in the forward direction and implies the presence of spatial correlations which are ferromagnetic in nature extending over 12-16 Å. The correlations persist to at least 2.65 T_C. The iron moment falls from 2.18 μ_B at 1.33 T_C to 1.73 μ_B at 2.65 T_C. This suggests that the local "band" splitting does not collapse at T_C. Yet the importance of such spatial fluctuations to Invar characteristics has still to be explored.

Theoretical Studies of Invar Origins at the Microscopic Level

Efforts to fully understand the microscopic origin of the Invar effect have lasted for decades by now. Many early theories focused on inhomogeneity and the deviations of magnetic moments from the Slater-Pauling curve which seemed to show up in the old Invar materials. However, with the detection of the Invar effect on ordered Fe_3Pt, a system which is a relatively strong itinerant ferromagnet and shows no deviation of the average moment from the Slater-Pauling curve, many of those models put forward before the late 1970s are being questioned.

Magnetostriction Effect

To understand the Invar effect and magnetoelastic properties, electronic and phononic contributions are both important. Typically for an itinerant ferromagnet, there are short–ranged magnetic correlations, longitudinal or transverse spin fluctuations in the temperature range around and above T_C. The

questions are: what is the reason for all the differences observed between the physical behavior of Invar and ordinary ferromagnets? How lattice vibrations and spin disorder will change the total energy with the temperature? Furthermore, anti-ferromagnetism related to Invar should also be equally understood. Understanding these problems is the key to solving the Invar problem.

Since Invar only appears in magnetic (both anti-ferromagnetic and ferromagnetic) materials, naturally one approach to look into the Invar is by studying the relationship of the magnetism and the volume. In 3d metals, spin magnetism accounts for most of the magnetism, so it is possible that the Invar systems are mainly related to spin magnetism when they are chemically dominated by their 3d constituents. Magnetization in itinerant magnets incurs a kinetic-energy price because the electrons must be transferred from minority spin states to majority spin states of higher kinetic energy. Invar systems are itinerant magnetic materials, therefore they expand in the ground state to minimize the kinetic-energy cost of the magnetization (Janak 1976; Andersen, Madsen, Poulsen, Jepsen and Kellar 1977). Comparing the thermal expansion behavior of Invar materials with those of normal metals, which is caused by anharmonic lattice vibrations, it may be true that the volume of the sample expands with the occurrence of spontaneous magnetization. This expansion of volume is called *spontaneous volume magnetostriction.* Since the spontaneous magnetization decreases with temperature, an Invar alloy obviously has a spontaneous volume magnetostriction large enough to compensate the normal thermal expansion caused by lattice vibrations. The linear thermal expansion coefficient curves for ferromagnetic alloys always show positive magneto-volume effects, regardless of the temperature; ferromagnetic alloys also have substantial magneto-volume effects above their Curie temperatures in the paramagnetic range which vanish gradually at very high temperatures. Anti-ferromagnetic Invar alloys, in principle, show the same behavior, although less in absolute values as compared to FM Invar materials below and around T_N. In the case of the cancellation of the anharmonic effect by the spontaneous volume magnetostriction, the thermal expansion coefficient can become very small or even negative.

Theoretical approaches in Magnetism Study

For the description of the nature of the magnetic moments in ferromagnetic metals and alloys, especially for those containing elements from the late 3d series, several models have been proposed. These models are based on either of the two rival pictures, namely the Heisenberg localized spin model and the Stoner model for the description of itinerant or band magnetism.

In the localized model each electron is assumed to remain localized on an atom and, in this way, well localized moments result owing to large intra-atomic electron correlations. The inter-atomic exchange

interactions are much smaller and compete with thermal fluctuations to maintain long range order. The magnetic interactions can be described by the familiar Heisenberg spin Hamiltonian.

In the Stoner or band model the carriers, either electrons or holes responsible for magnetism, are itinerant and the interactions between the carriers are described in the mean-field approximation. The electron densities can be viewed as the thermally averaged values if a Fermi distribution function is introduced to describe the electron behaviors at finite temperature. The exchange splitting of spin-up and spin-down bands leads to the ferromagnetic properties.

Both approaches have their own limitations. In the Stoner model no easy description can be given of the temperature dependent magnetic properties. For an example, the highest temperature for which the self-consistent solution for the total magnetization to be nonvanishing is about a few times higher than the Curie temperature. For Fe_3Pt, the Curie temperature is found to be about 2580K (Kashyap, Solanki, Nautiyal and Auluck 1995), in contrast with its experimental value is just about 450K. Above the vanishing temperature, there is no exchange splitting, and there should be no magnetic moments; but this can not correspond to the Curie temperature T_C since polarized photo-emission experiments shows that there is exchange splitting above T_C (Moriya and Kawabata 1973), and paramagnetic experiments exhibit spin-wave like behavior in Ni though there is no long range magnetic order (Uemura, Sirane, Steinsvoll and Wicksted 1983; Shirane, Born and Wicksted 1986). A major problem of the Heisenberg model is not possible to take into account the dependence of the magnitude of the magnetic moment on temperature, chemical environment, and magnetic ordering. Likewise the coupling parameters between spins should have a temperature dependence which does not appear in the Heisenberg model.

2γ State Model

Important within the group of local models is a historically, widely debated phenomenological "2γ-state model" by Weiss (1963). Weiss claimed that γ-Fe (the fcc phase) can exist in two different magnetic states, the AF low-spin (LS) state γ_1 with a small magnetic moment ($\mu = 0.5\mu_B$) and small volume ($a = 3.57$Å), and the FM high-spin (HS) state γ_2 with large moment ($\mu = 2.87\mu_B$) and large volume ($a = 3.64$Å). The Invar effect is driven by a thermal depopulation of the HS state and the subsequent population of the LS state. The energy difference between the HS state and the LS state is in the thermal range. This model has a great influence on many later studies, and its validity will be addressed more later.

Band Calculations Related to Invar

All transition metals have $E(V, M)$ curves with stable solutions of $M = 0$ for low volumes, and with stable solutions of finite M values at larger volumes. Thus, all transition metals are non-magnetic at sufficiently small volumes. This general result is not surprising when it is considered that, at low volumes the transition-metal d bands are spread over a large energy range and are incapable of supporting magnetic behavior, while at large volumes or the free-atom limit moments are consistent with Hund's rule and the atomic ground-state configuration must be approached.

Band calculations within the local spin density approximation (LSDA) since 1970s predicted the existence of two ferromagnetic states for *fcc* Fe and its crystal alloys, a high-spin state with large moment and large volume and a low-spin state with low moment and volume. The idea is essentially parallel to the 2γ state model. The *ab initio* band calculations can explain many of the essential features of the ground-state properties of Invar alloys.

It has never been clear why the stabilization of competing magnetic states should happen at the magic occupation number of 8.6 electrons per atom in ferromagnetic and at 7.7 electrons per atom in anti–ferromagnetic Invar alloys (Wassermann 1990 and 1991; Moruzzi 1989). In a series of *fcc* 3d alloys, Wassermann (Wassermann 1990 and 1991; Moruzzi 1989) showed that the calculated energy difference between HS and LS becomes very small at the threshold values 7.7 and 8.6 in their band-structure calculations (Krasko 1987; Moruzzi 1989; Moruzzi, Marcus and Kübler 1989). For most calculations, the HS state is normally ferromagnetic state with magnetic moments around 2.8 μ_B per Fe atom, while the LS can be either paramagnetic or antiferromagnetic.

The origin of Invar effects has been debated for a couple of decades, and there is still a lot to be explored about this problem. The difficulty in solving this problem may be ascribed to the difficulty of understanding the magnetism of transition metals. The valence electrons in the solid have a strong tendency to hop from atom to atom because this process will lower the kinetic energy due to the decreased spatial localization of the wave function. These kind of itinerant states are well described by the band picture. However, the Coulomb repulsion between electrons will oppose the hoping of the electrons between atoms. When the cost in potential energy arising from hopping outweighs the saving in kinetic energy, the electron becomes localized.

Experimental Studies of Invar Origins at the Microscopic Level

Corresponding to the theoretical studies, parallel attempts have been made in experiments to explore magnetism generally and Invar theories particularly.

Experimental Aspects in Studies of Magnetism

Although the two extreme models are oversimplifications of the real situation and the d valence electrons have both features, the interpretations of the data from experiments have been purely in terms of localized or itinerant models in the past. As a result, the type of behavior that is obtained is strongly dependent on how the experiment performed is explained conveniently. Experiments that probe the regions close to the nucleus such as nuclear magnetic resonance, neutron scattering, etc. are sensitive to the more local, atomic-like character of the electrons while other techniques, measuring more macroscopic properties such as the specific heat, transport properties, de Hass-van Alphen effect that probe mainly more global or extended aspects of the wavefunctions, are sensitive to the nonlocal or itinerant character. Neutron scattering techniques allowed the measurements of the form factors, magnetization distributions, and the magnon relations. The development of angle-resolved photoemission spectroscopy allowed the direct measurement of the excited-state exchange splitting and band mapping studies.

Explaining the HS and LS States

A photoemission experiment has provided the evidence of the existence of HS and LS states when the calculated densities of states for fcc Fe is fitted qualitatively well with the experimental data for Fe_3Pt (Kisker, Wassermann and Carbone 1987). However, the occurrence of two competing magnetic states (with different volumes) at finite temperatures has not yet been experimentally confirmed. What has been observed by Mössbauer measurements on $Fe_{68.5}Ni_{31.5}$ and $Fe_{72}Pt_{28}$ is a gradual transition from the HM to the LM state at low temperatures under high enough pressure (Abd-Elmeguid 1989). The high temperature specific heats of $Fe_{45}Ni_{55}$ and $Fe_{72}Pt_{28}$ Invar alloys have been measured from room temperature up to 850K. Besides the peak due to spin disordering, no evidence of other excess effects such as a Schottky-type anomaly has been found neither for the Fe-Ni alloy nor for the Fe-Pt alloy. These results thus do not support the 2γ-states type models proposed for Invar (Hausch 1990). There might be some magnetic states between the two special magnetic states which have a total energy very close to both. The reasoning is that the closeness of the HS state to the LS state may just imply that the total energy of an Invar system is insensitive to the spin orientations, implying a high degree

of spin fluctuations are excitable within a thermal energy range. This will be further discussed in the next chapter.

6 ELECTRONIC BEHAVIOR IN Fe_3Pt AND SOME RELATED ALLOYS

Introduction

The concentration of this chapter is to center around the Invar Fe_3Pt alloy. Since Fe is its dominant constituent, we will first explore some experimental and theoretical aspects of bcc Fe, which is the ground state of Fe from low temperature to a very high temperature, and then fcc γ-Fe, which is the structural and compositional reference to the alloy. After some of the experimental results related to Fe_3Pt are looked into, the results from our electronic band calculation based on the FLAPW method are investigated concerning the following electronic features in Fe_3Pt: energy band structures, the densities of states, atomic basis functions, spatial distributions for charges and spins, momentum distributions for charges and spins (or Compton profiles). Chemically and structurally related materials Fe_3Ni and Fe_3Pd from the Fe-Ni and Fe-Pt Invar systems, Co_3Pt and Ni_3Pt are also to be probed for comparisons with Fe_3Pt.

On Fe

In the periodic table, Fe is followed immediately by Co and Ni which both normally have close-packed fcc phases. Although Fe usually has the bcc structure, a fcc structure is favorable under certain conditions.

γ-Fe

At normal pressure, between 1183K and 1663K Fe has a fcc structure called γ-Fe, and the structure has no long range magnetic order; at higher temperatures but below the melting point of 1807K Fe is in the bcc phase which is a ferromagnet below its Curie temperature 1043K. The high temperature fcc structure has a paramagnetic susceptibility following the Curie-Weiss law with a negative Curie temperature, indicating anti-ferromagnetic coupling (Gradmann 1993).

Unstable at low temperature, a fcc γ-Fe structure can be stabilized either as coherent precipitates

in other fcc metal matrices or as ultra-thin epitaxial films on Cu, as shown by antiferromagnetic γ-Fe precipitates in Cu and Cu-Al (Keune 1989) and by γ-Fe thin films on Cu_3Au (Carbone 1988). Experimentally both antiferromagnetic and ferromagnetic orderings are found on precipitates in Cu (Kaufman, Coulgherty and Weiss 1961; Abrahams, Guttman and Kasper 1962; Wright 1971; Gradmann 1976; Keune, Halbauer, Gonser, Lauer and Williamson 1977; Gradmann and Isbert 1980), and ferromagnetic order in Cu-Au alloys (Berghout 1961; Window 1972; Williamson, Bukshpan and Ingalls 1972; Gonser, Krischel and Nasu 1980) by techniques such as Mössbauer measurement and susceptibility measurement. Furthermore, neutron diffraction measurements for γ Fe alloy precipitates with a small amount of Co showed that the fcc Fe precipitates have a spiral-spin-density-wave (SSDW) structure (Tsunoda 1988; Onodera, Tsunoda, Kunitomi, Pringle, Nicklow, and Moon 1994). These results seem to indicate that γ-Fe has very subtle energy differences between its various magnetic states to allow the presence of the complex electronic magnetism. The close-packed fcc structure over the bcc one (with nearly the same volume) through the alloying manipulations at low temperatures might also suggest a relative energy insensitivity of the crystal to volume.

The interest, in the nature of 3d metallic magnetism and in fcc Fe based Invar alloys, has made the fcc Fe a traditional subject in theoretical studies as well.

About Band Calculations of Fe

A major difficulty with band calculations for Fe is to deal with the rather small energy associated with magnetic ordering which is of the order of $k_B T_C$ per electron. This amount of energy is comparable to the presently achievable precision of electronic band theories. Computationally, numerical noises can also be a very serious problem as noticed a long time ago by Wigner and Seitz (1934) when they found out that compensating errors could even produce better results. Consequently calculations for Fe, bcc or fcc, have not always been in agreement. The results are dependent on methods applied to some degree (Jansen, Hathaway and Freeman 1979; Wang, Klein and Krakauer 1985; Hathaway, Jansen and Freeman 1985; Moruzzi and Marcus 1988; Moruzzi, Marcus and Pattnaik 1988; Moruzzi and Marcus 1993). For some of the calculations, Fe can be in any of various paramagnetic, ferromagnetic and antiferromagnetic ground states in a limited lattice constant range, and the states can also coexist (as an example, see Morruzi 1989), while other calculations give more or less different results concerning the existence and conditions of the magnetic or nonmagnetic states. Furthermore, in many of the calculations, even the ground state is not found to be bcc ferromagnetic (for a very detailed review see Morruzi 1993). This difficult situation can be resolved by introducing some additional exchange-correlation potential term

as mentioned in chapter 3 (Leung, Chan and Harmon 1991). However, the latter approach generally gets poorer results for some metals beyond the 3d transitional elements, and further investigations are apparently needed.

Invar Fe-Pt System and Fe_3Pt

The first Invar Fe-Pt alloy was found by Kussman (1937). Many intensive investigations about the magnetic and structural properties of the Fe-Pt system have a more recent history (Ito, Sasaki and Mizoguchi 1974; Hausch 1974; Nakamura, Sumiyama and Shiga 1978; Sumiyama, Shiga, Kobayashi, Nishi, and Nakamura 1978; Caporaletti, Graham, and Sumiyama 1979; Sumiyama, Viard and Gavoille 1979; Shiga, Morioka and Nakamura 1979; Caporaletti, 1980; Sumiyama, Emoto, Shiga, and Nakamura 1980; Sumiyama, Emoto, Shiga and Nakamura 1981; Oomi and Araki 1995). The Fe-Pt alloys show Invar properties not only in their chemically disordered states but also in their ordered ferromagnetic state; on approach to the γ-α transition typical for Fe-rich alloys, there is no deviation of the Fe moment from the Slater-Pauling curve (Kussman and Von Rittberg 1950). For a long time, the above features gave the system an unique position in discussions about the origin of the Invar effect. It is thus believed that possibly as a consequence of the moment-volume instability, both structural disorder and magnetic inhomogeneity are not necessarily the reasons for the Invar. Investigations show that ordered Fe_3Pt materials can be remarkably different from disordered ones magnetically. For ordered alloys around composition Fe_3Pt, the Curie temperature is about 435K but only 280K for the disordered alloys, in contrast with 500K for the most traditional Invar $Fe_{65}Ni_{35}$ (Suzuki, Miyajima, Kido, Miura and Chikazumi 1981; Ishikawa, Onodera and Tajima 1979) which is disordered. Moreover, the disordered Fe-Pt alloys are magnetically more unstable, with their Curie temperatures being about 150K lower systematically, while they have more pronounced anomalies than their correspondingly ordered counterparts; specific heat from electrons is larger for ordered material than the disordered one (Sumiyama, Shiga and Nakamura 1976). The above properties are typical for electrons in a disordered phase (Callaway 1991): the more an alloy is ordered, the less its resistivity is, and the larger its electronic specific heat is. However, it is not quite clear why the disordered material has a more pronounced Invar property than the ordered one.

In the Invar region, the thermal expansion coefficient of the Fe-Pt system can be as low as $-0.3 \cdot 10^{-6}/K$, showing a strong anomaly (Miodownik 1979; Nakamura, Sumiyama and Shiga 1979; Chikazumi 1980). Like other Invar materials, the Fe-Pt Invar materials have their thermal expansion anomaly depending not only on the composition but also on mechanical and thermal treatments. The strongest

thermal anomaly occurs most around 23 at% Pt, and around this composition there are martensitic transformations similar to $\gamma - \alpha$ transformation in Fe-Ni Invar alloys, whereas the shear and the bulk moduli display a dramatic softening (Hausch 1974; Kawald 1989). The martensensitic transformation takes place for ordered alloys with less than 25% Pt, but for the disordered with 28% Pt. The martensitic temperature decreases with increasing degree of order. Above 32% Pt the Fe-Pt alloy has its cubic structure tetragonally distorted, where a martensitic transition takes place.

For the ordered alloys around the above concentration regions and at low temperatures, the magnetic moment per atom is about $2.1\mu_B$, with the local moment at the Fe site being around $2.7\mu_B$ and at the Pt site about $0.4\mu_B$ (Hesse, Nülle and Körner 1983). A recent magnetic circular X-ray dichroism (MCXD) experiment estimates (Maruyama, Matsuoka, Kobayashi and Yamazaki 1995) the orbital moment m_L is about $0.07\mu_B$ for Pt in Fe_3Pt. Since for the 3d electrons the orbital moment in metals and alloys usually is even smaller, their orbital magnetism normally can be ignored.

The Invar Fe-Pt system has a more pronounced thermal expansion anomaly than the Fe-Ni system even in its ordered state (Sumiyama, Shiga and Nakamura 1976). Traditionally, the Fe-Ni system had been a focus theoretically and experimentally because of the long history of the Fe-Ni system as a noted Invar system. Yet the Fe-Ni system is chemically disordered, structurally mixed and magnetically inhomogeneous, and since there are no easy ways to theoretically dealt with the complexities so involved, most theoretical calculations of its ground state and thermal properties assume an ordered structure (for examples: Williams 1983; Podgórny 1989; Moroni, E. G. and Jarlborg 1990; Moruzzi 1990; Podgórny, Thon and Wagner 1992; Entel, Hoffmann, Mohn, Schwarz and Moruzzi 1993). So, the Fe-Pt system should be a better subject of Invar study, and can be better deal with (Hasegawa 1985; Podgórny 1992; Podgórny, Thon and Wagner 1992). If there is no fundamental difference in the origin of the Invar effects in typical Invar Fe-Ni, Fe-Pd and Fe-Pt systems, then such a study may provide insights for the Invar phenomenon.

Among three simple kinds of ordered Fe-Pt structures, Fe_3Pt, Fe-Pt and $FePt_3$, only Fe_3Pt shows the Invar thermal expansion anomaly: the replacement of an Fe atom in a simple cubic unit cell of γ-Fe with a Pt atom makes Invar observable. Naturally Fe_3Pt makes a very good sample for the Invar Fe-Pt system. The thermal expansion coefficients of the Fe_3Pt alloy are negative around T_C.

Method of Calculation for Fe_3Pt

We use the FLAPW method to do a self-consistent, spin-polarized, scalar relativistic band calculation. The method eliminates the spin-orbit interaction term from the Hamiltonian, so that the spin

remains a good quantum number and double group theory treatments are not needed. The exchange and correlation interaction potential being used is by Janak (1976).

Ordered ferromagnetic Fe_3Pt has a simple cubic lattice. Its space group is O_h^1. The average magnetization per atom is $1.94\mu_B$ at 4.2K, and the lattice constant at 290 K is 7.06 a.u. (Sumiyama 1981). In its unit cell, a Pt atom occupies the corners of the cube while three equivalent Fe atoms occupy the face centers. The two kinds of atomic muffin-tin spheres are so chosen that the nearest neighboring muffin-tin spheres nearly contact but do not overlap; the ratio of the two kinds of atomic spheres is taken to be 1.09, which is close to the ratio of their corresponding atomic radii. Thus, the muffin-tin radii are 2.62 a.u. and 2.39 a.u. for Pt and Fe, respectively. The MT spheres account for 69.6% of the volume, comparable to 74%, the maximum possible value of the ideal close-packed structures (hcp or fcc). The replacement of a Fe atom by a Pt atom increases the lattice constant, and with the presence of different sized atoms there is more fractional space between the atomic spheres. To do radial integrals inside the Pt and Fe muffin-tins, logarithmic radial meshes of 381 divisions each are used, and the nearest mesh points to the origin are taken to be 8.12×10^{-5} a.u. and 5.35×10^{-5} a.u. respectively for Pt and Fe, the same order of magnitude as their corresponding nuclei radii; the largest mesh points are taken to be the muffin-tin sphere radii. All these parameters are also fixed throughout our calculations.

Noticing the sensitivity of the magnetic Compton profile calculations to the band occupation of electrons, along each dimension we cut the first reciprocal $B.Z.$ into 32 divisions to generate two fine meshes, an odd mesh of 120 inequivalent points and an even mesh of 165 inequivalent $\mathbf{k}$. An odd mesh point can form an irreducible cube with its eight nearest neighbors. We cut each of the 120 irreducible cubes into twelve tetrahedra of equal volumes to calculate the density of electronic states and, thereafter, the Fermi level. To do other $\mathbf{k}$ integrals, the 120 odd mesh points are assigned weights proportional to the electron occupations of their cubes and their symmetric equivalents. We are not using a Gaussian filling of the energy bands around the Fermi level which can both compensate numerical noise and prevent a discontinuous jump in the assigned weight for an irreducible point when a tentative Fermi energy level crosses the energy value of this point. For each of the irreducible $\mathbf{k}$ mesh points, a set of 256 to 280 basis plane waves are used for the interstitial region. The 120 basis function sets are collectively chosen for all the 120 irreducible $\mathbf{k}$ points to take into account all plane waves giving a significant contribution for the band calculations in order to guarantee valid calculational convergence. In the selection two conditions are satisfied: a plane wave and all its symmetrically related plane waves are taken or not taken all at the same time; the range of the number of plane waves for the 120 irreducible $\mathbf{k}$ points is taken to be the smallest. The basis functions inside the muffin-tins are expanded up to

$l = 6$. Self-consistency of the band calculation is assumed when the differences in the muffin-tin and interstitial partial charges between the input and the output are lowered to the order of 10^{-3} electrons per unit cell.

Once the self consistent potential is obtained, to avoid increasing the costs of other calculations, separate programs are written for determining spatial electron distributions and also for the MCP calculation. For the latter, the above meshes are extended to the "whole space" of a radius whose product with the muffin-tin radius of Fe is 15. Since the calculation demands either a lot of computer memory or a lot of disk space or both, a balance is carefully sought to make the calculation possible for our available computer facility.

Electronic States in Fe_3Pt

When atoms form condensed materials, their atomic energy levels are broadened into bands because of the overlap of the atomic orbitals. The outer electrons of the atoms are now shared by the nuclei in the materials, so hybridization effects become important. The more condensed the materials are, or the less localized the valent electrons in the materials are, the wider the common bands of the electrons are. Atomic configurations for the two constituents of Fe_3Pt are Fe ($3d^6\ 4s^2$) and Pt ($5d^9\ 6s^1$). At low temperature the replacement of a Fe atom by a Pt atom in the fcc Fe unit cell stabilizes the otherwise unstable close-packed fcc structure, and the material becomes ferromagnetic but not anti-ferromagnetic as in fcc Fe. The larger lattice constant, due to the introduction of the larger Pt atoms, has the magnetic Fe atoms more separated from each other, thus ferromagnetism becomes more favorable than antiferromagnetism. On one hand, we expect some electronic behavior in the less close-packed Fe_3Pt crystal different from those in the fcc Fe crystal. On the other hand, the Fe dominant crystal should still bear some features close to those in fcc Fe, such as the weak dependence of total energy on the magnetic states.

Energy Band Structures

The band structures are close to earlier calculations (Hasegawa 1985; Podgórny 1991). Electronic spin-polarized energy band structures along various symmetry axes are shown in Figure 6.1. The correspondences between the energy bands of both spins are quite noticeable, especially for the lowest bands which clearly resemble each other. The majority spin bands have a general downward shift relative to their corresponding minority spin bands by some amount at each point in the reciprocal space. Around the Fermi level, most of the majority spin bands are occupied while nearly all of the

minority spin bands are all partly occupied. Therefore, the system is strongly polarized, leading to a ferromagnetic ground state.

Densities of States and Hybridization

From Figure 6.2 to Figure 6.4, the total density of states (DOS), the partial DOS (orbital decomposed), and the interstitial region DOS contributions are shown. To see the hybridization of atomic electron states of the constituent atoms, the orbital decomposed probability amplitudes of the Bloch states at the 120 representative irreducible k points, which are used for various k-space integrations in our FLAPW calculations, are also plotted in the same graphs for the partial densities of states.

Almost all the majority bands crossing the Fermi level ($E_F = 0.782$ Ryd) are nearly totally occupied. The Fermi level is thus situated just outside the first sharp peak at E_F of the majority spin DOS. The minority spin bands around the Fermi level are all partly filled with the Fermi level being at the middle of the minority band range which is wider than the majority bands. As a result, the density of states for the minority spin bands at E_F is much larger. Our calculated γ coefficient for the electronic specific heat is about 11.5 mJ/K^2/mole, while the experimental one is 9.6 mJ/K^2/mole (Sumiyama, Shiga and Nakamura 1976). The discrepancy between them may be attributed to some of the following factors beside some other theoretical inaccuracies: the chemical compositions for the experimental samples are not exactly the same as Fe_3Pt; the experimental samples were not completely ordered.

Naturally the dominant contributions to the total density of states are from the d states of both Pt and Fe atoms. The majority spin bands mostly with d character are lower in energy than their corresponding minority spin bands. The degrees of the ferromagnetic polarization are different for Fe and Pt atoms though. The Fe spin bands are strongly polarized when the majority bands are almost totally occupied and a large portion of the minority bands are not; the Pt bands are nearly all filled but there are still a noticeable part of the minority bands unoccupied, hence the Pt sites also have significant but smaller spin moments. In addition to the fact that Fe crystals are spontaneously magnetic while Pt crystals are not, it can be concluded that the large exchange splitting of the 3d levels at Fe sites is spontaneous and the relatively small splitting of the 5d levels at Pt sites is of an induced nature. The Fe d states in the minority spin bands make the largest contribution to the total density of states at the Fermi energy, E_F, which approximately lies in the middle of the Fe d bands in the minority spin state and consequently a Pt muffin-tin sphere has nearly twice as many minority spin d electrons in it as an Fe muffin-tin sphere has, as shown in Table 6.1 where some information about the spin polarization and magnetic moments is listed (a few other alloys listed in the same table will be discussed at a later

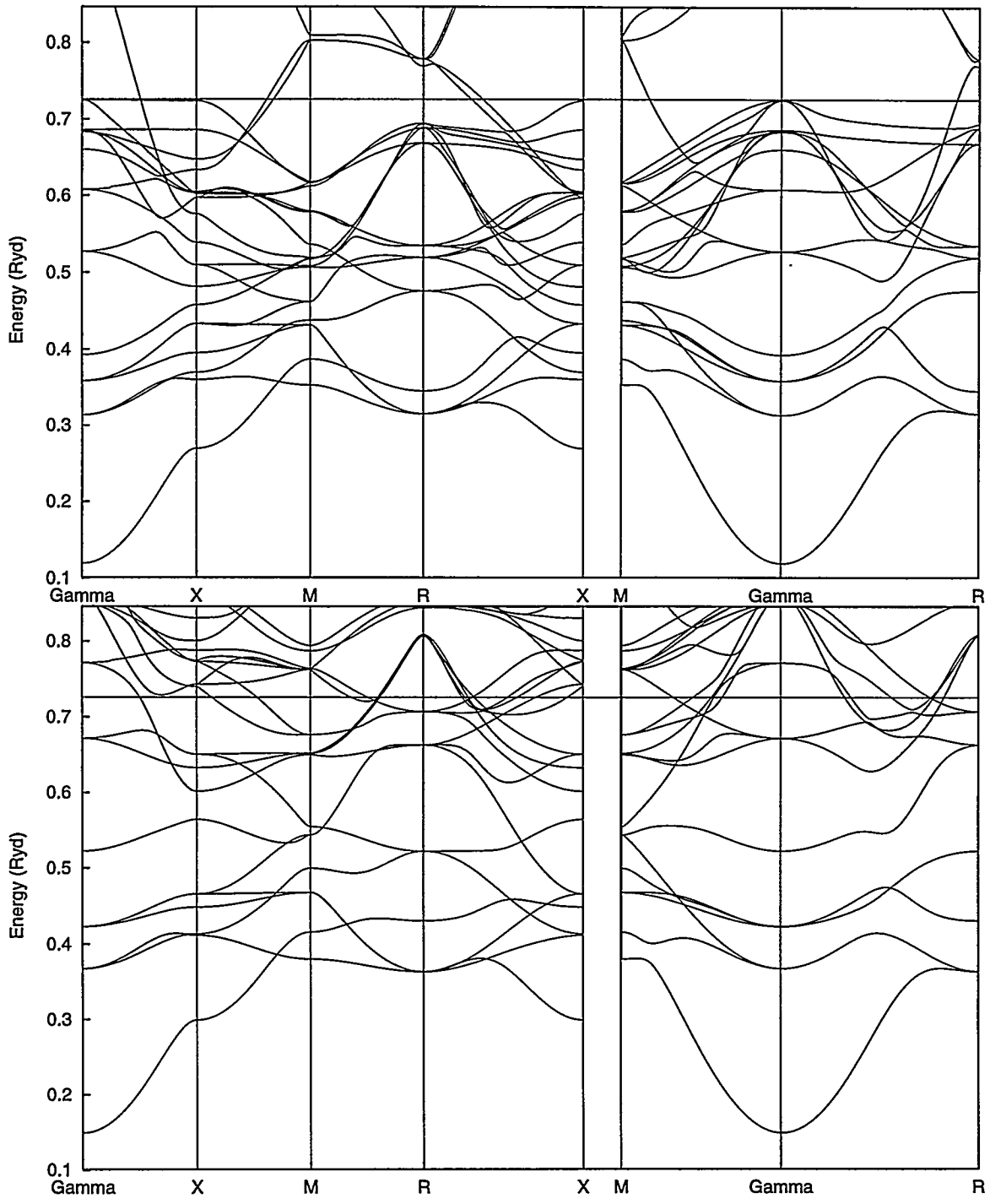

Figure 6.1 Spin-polarized band structures for ferromagnetic Fe_3Pt along some symmetry lines. The Fermi level is shown at 0.726 Ryd. (A) Upper curves for majority spin electrons; (B) lower curves for minority spin electrons.

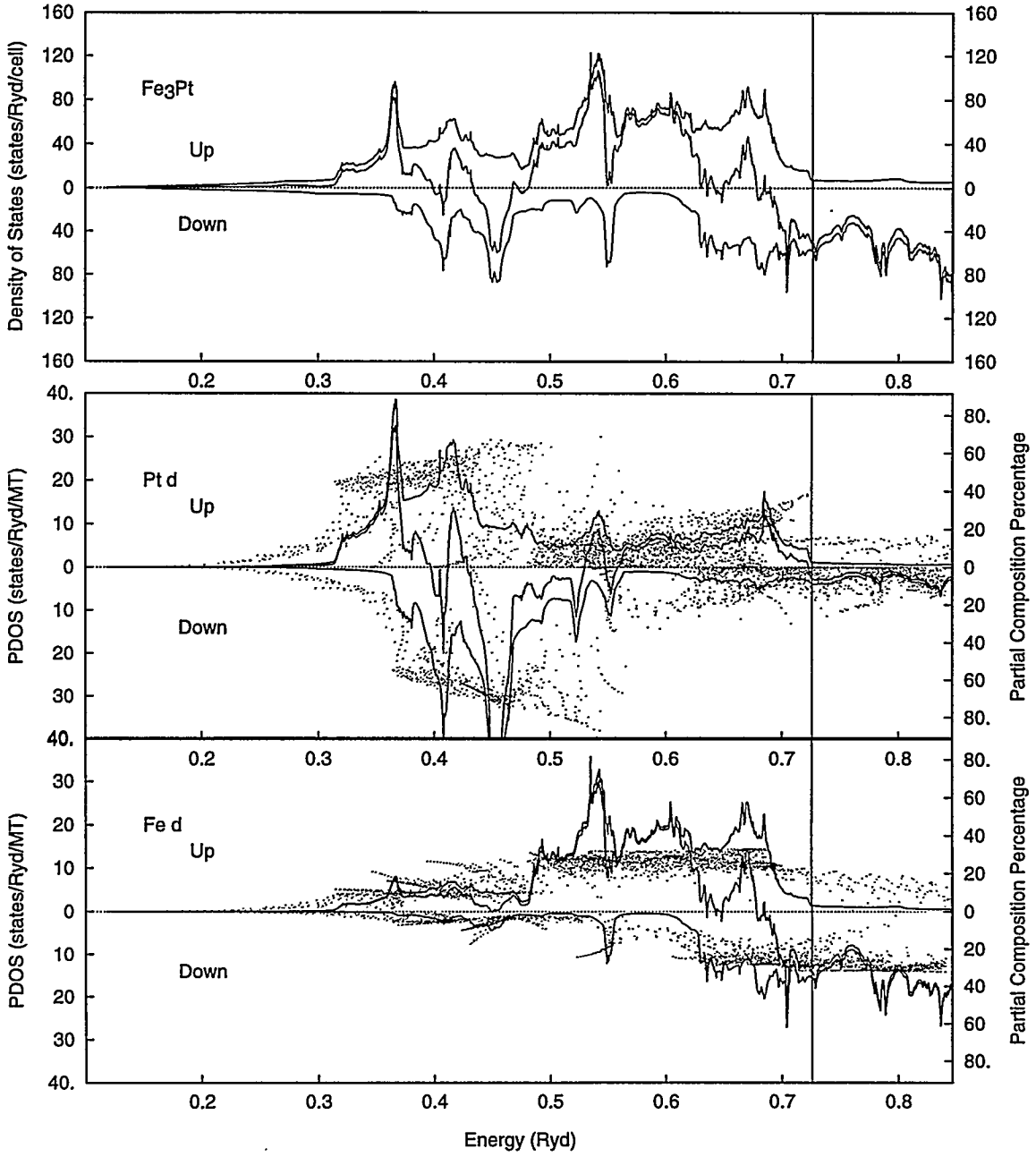

Figure 6.2 Total density of states per unit cell, partial densities of d states within muffin-tin spheres, and the percentages of mixing (dots) between the d electronic states in forming the eigenstates at our 120 representative irreducible k points for Fe_3Pt. The Fermi level E_F = 0.726 Ryd is shown by the vertical line.

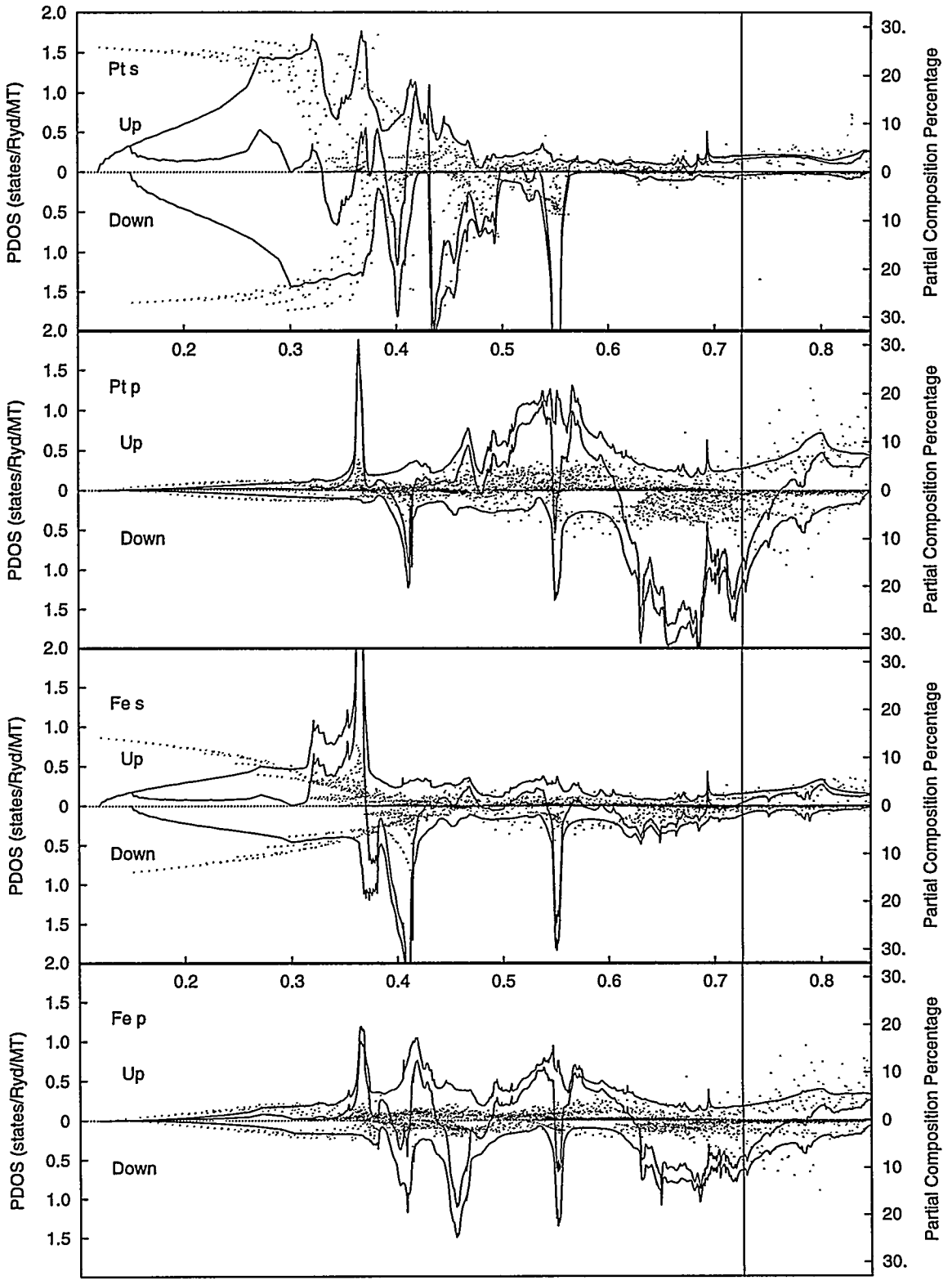

Figure 6.3 Partial densities for s and p states in Fe_3Pt.

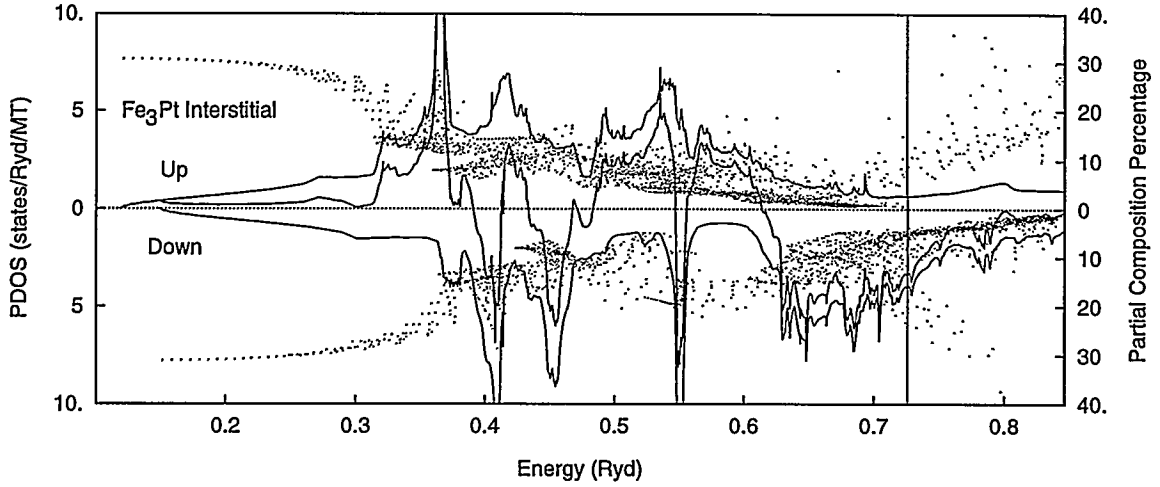

Figure 6.4 Partial densities for states from the interstitial region of Fe_3Pt.

time).

The range of bands mainly with Pt d character is considerably more narrow and lower than the range of bands mostly with Fe d character. If the d states were well distributed inside the muffin-tin spheres, each sphere would account for a 25% weight of the mixed states. But such a scenario is not the actual case here: in each of the above two ranges, the partial composition percentages mostly reach to more than 45% for the Pt sites in the first range and in the second range to more than 75% for the three Fe sites of the unit cell. Therefore, the d states of a Fe site tend to mix with the d states of another Fe site more than the d states of a Pt site, in other words, the electrons at the Pt sites are more localized than the electrons at the Fe sites, which lead to a more sharply peaked and narrow structure for the majority spin and at a slightly higher energy for the minority spin. This is understandable for the Pt atoms have a stronger electro-negativeness or stronger binding ability, which draws more electrons to Pt sites. It is obvious that the Pt d and Fe d ranges just meet and slightly overlap on their ends. As a consequence of the meeting and overlapping of the two energy ranges hybridizations occur at each atomic site, which is demonstrated by the DOS tails outside the two ranges. Because of the smaller chemical composition of Pt in the crystal, the tail at the Fe sites induced by Pt atoms is considerably smaller than the tail at the Pt sites induced by Fe atoms. The probability amplitudes of d electrons, at the 120 representative irreducible points, mostly add up to 85% or even about 95% if there is little s or p components involved. The high percentages for the atomic sites simply indicate that the d states in the alloys tend to be more confined to their own kind of muffin-tin sites. One effect of introducing the more binding Pt atoms into the crystal is that the Fe minority spin bands are less occupied. Therefore,

Table 6.1 Spin moments in Fe_3Pt and some related alloys. First number of each pair is the majority electron count.

Fe_3Ni	20.89-13.12				
Interstitial	1.28-1.32				
	$total_{MT}$	s	p	d	f
Ni	5.07-4.51	0.26-0.29	0.22-0.27	4.57-3.93	0.02-0.01
Fe	4.85-2.44	0.22-0.23	0.20-0.21	4.41-1.98	0.02-0.01
Fe_3Pd	21.19-12.81				
Interstitial	1.40-1.45				
	$total_{MT}$	s	p	d	f
Pd	4.88-4.62	0.24-0.28	0.19-0.23	4.42-4.09	0.02-0.02
Fe	4.98-2.26	0.22-0.23	0.17-0.18	4.56-1.83	0.02-0.01
Fe_3Pt	21.11-12.89				
Interstitial	1.59-1.63				
	$total_{MT}$	s	p	d	f
Pt	4.79-4.44	0.33-0.36	0.20-0.25	4.22-3.80	0.03-0.02
Fe	4.92-2.29	0.21-0.21	0.18-0.19	4.51-1.87	70.02-0.01
Co_3Pt	21.11-15.89				
Interstitial	1.60-1.69				
	$total_{MT}$	s	p	d	f
Pt	4.75-4.37	0.32-0.34	0.20-0.24	4.19-3.76	0.03-0.03
Co	4.93-3.29	0.21-0.21	0.17-0.19	4.53-2.87	0.02-0.01
Ni_3Pt	20.883-19.117				
Interstitial	1.603-1.645				
	$total_{MT}$	s	p	d	f
Pt	4.71-4.45	0.33-0.33	0.21-0.22	4.14-3.86	0.03-0.03
Ni	4.86-4.35	0.20-0.20	0.16-0.17	4.48-3.96	0.01-0.01

the spin moments at the Fe sites are increased to have a value of about $2.63\mu_B$ greater than the $2.2\mu_B$ experimental estimation for fcc Fe at a lattice constant of 6.83 a.u. in Cu (Kittel 1996). Even so, our later calculation for Fe will show that the average magnetic moment per atom essentially has not been decreased in Fe_3Pt when compared to the ground state of a magnetic fcc Fe at 6.73 a.u.. The small spin moment of about $0.35\mu_B$ on Pt, on the other hand, is mainly a magnetic polarization of Pt d states induced by the Fe spin through the hybridization.

Usually s and p electrons do not get much attention for they make almost no direct contribution to spontaneous magnetism. However, these electrons help to sustain the mechanical equilibrium inside the crystal in a most important way. With the condensation of the atoms into crystal, the atomic s and p electrons are the most affected. The resulting s- and p-like electrons may also be the most sensitive electrons in the crystal to external mechanical and thermal disturbances, which deserves significant considerations in Invar study.

The lowest bands for both spin states consist preponderantly of the Pt s and Fe s states. Similar to the d electrons, the s electrons are slightly more localized at the Pt sites than the s electrons at the Fe sites. These electrons interact most strongly with each other, hence the hybridization between them is significant and the compositional percentages reach around 25%, the referential value, for the lowest energies with a value less than 0.35 Ryd. The p states, which are not occupied in atoms, now are lowered to be of comparable occupations as the s electrons. In the higher energy ranges with dominant d character, the s states hybridize with the d states, the generally energetically higher p states have mixed almost completely with the d electrons. Therefore, both s and p states have lost much of their identities in these ranges. Near the Fermi level, the partial densities of minority spin p states, especially at the Pt sites, are much larger than those of other s and p states; the minority electrons of p character are the most populous among the most unlocalized electrons. These p electrons could play some significant role when the crystal is subjected to external influences, and might contribute to some physical properties of the alloy. While there are almost equal number of s or p electrons of opposite spins inside each muffin-tin sphere, a Pt muffin-tin sphere noticeably has more conduction s and p electrons inside themselves than a Fe muffin-tin sphere, and the net spin polarization points opposite to the spins of the majority electrons.

In general, the band states of Fe and Pt are much intermingled, so the generally mixed bands can not be simply identified as either Fe or Pt states. But in some energy ranges the distinct features of the atomic-like states can still be observed, when the Pt characteristic bands generally are lower than those of Fe ones. The peaks of the partial densities of states at the two different kinds of muffin-tin

sites have a very strong tendency to occur at the same energies for all the different kinds of s, p and d electrons with the same polarization. The cause for this is the strong hybridization, typical for an alloy, between Fe and Pt states of the same polarizations in the whole occupied energy range. With the hybridization of the Fe states with the Pt states, the electronic bands get wider; also DOS plots are higher peaked around some energy ranges because of the hybridization. The higher peaks around E_F could mean more remarkable instabilities for electrons at E_F, the Fermi level, are responsive to external disturbances.

Spatial Distributions of Charges and Spins

For the hybridizations to occur in the real space, the atomic-like electron states, required to be energetically close to each other, must be spatially overlapped. Figure 6.5 shows the normalized basis radial wavefunctions at the two muffin-tin sites at 0.546 Ryd, an energy dividing the 34 valence electrons into two equal parts according to their energies. Understandably, the wavefunctions at the Pt sites are extended considerably more outward than their corresponding wavefunctions at the Fe sites, with the differences being the most remarkable between the Fe 3d states and the Pt 5 d states. The p states are the most extended, the d states are the most localized but they still have a tendency to be itinerant, and the s states are similar to the p states as for their localization degree. The s electrons are lower in energy than the p electrons overall, because they are closer to the positive nucleus.

It is generally believed that when free atoms form condensed matter, the forms of atomic wavefunctions change little near the nuclei, so the most affected parts of the wavefunctions inside the muffin-tin spheres are near the interstitial region. The effects of hybridizations from the condensation are displayed around the interstitial region where the most sensitive outer electrons lie. From the spatial distribution patterns, it can be imagined that the s and p electrons must be considerably more exposed to external influences, such as thermal or mechanical ones, than the d electrons. A consequence of the condensation is that the angular momentum becomes an almost meaningless quantum number for individual states because the spherical symmetry of atoms have been broken severely. Around the muffin-tin boundaries, Fe 4p and Pt 6p states have the largest amplitudes of all the radial wavefunctions, while Fe 4s and Pt 6s states have amplitudes comparable to the p states. Only the Fe 3d states are spin polarized remarkably as reflected by the majority spin d wavefunction has a amplitude of 2.5 times smaller than the minority spin d states at the muffin-tin sphere boundary. It means that the majority spin d-like electrons at the Fe sites are considerably more localized than the minority spin d-like electrons. For the Pt d states, the amplitudes for both spins are almost the same except for some noticeable difference around the

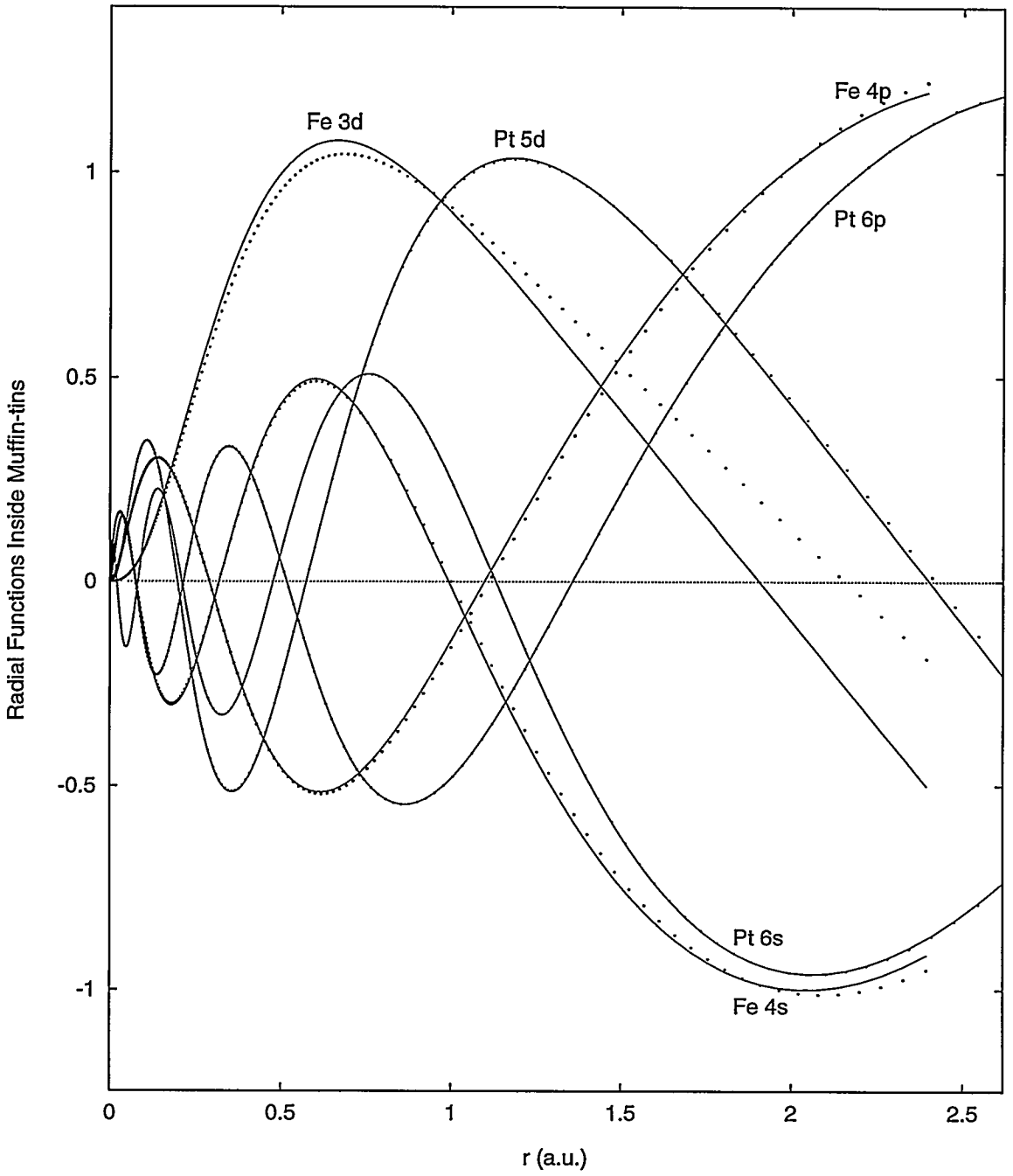

Figure 6.5 Spin-polarized basis radial wavefunctions inside the muffin-tin spheres of Fe_3Pt at E = 0.546 Ryd. The dots are for the majority spin, while the lines are for the minority spin.

muffin-tin sphere boundary, hence they are not much polarized though more extended overall than the Fe d states.

We have plotted charge and spin distributions in Figure 6.6, Figure 6.7 and Figure 6.8. While the charge densities are much extended, the spin densities are mostly localized. Inside the muffin-tin spheres, the angularly averaged charge and spin densities mostly have the features of the d-like electrons except near the MT boundaries where they bear the influences of the s- and p-like electrons and become relatively smooth. The spin distribution is much more localized at the Fe sites than at the Pt sites. Near and inside the Fe muffin-tin spheres, the spin densities are consistently positive, while near the Pt muffin-tin spheres the electrons are all polarized in the opposite direction to the majority spin although the net Pt magnetic moment is parallel to the majority spin. The regional dominance of the minority spin electrons has actually been partly suggested by the larger amplitudes of their radial wavefunction near the Pt muffin-tin boundary shown in the Figure 6.6. Both s-like and p-like states do not contribute significantly to such a slight antiferromagnetic pattern in the this region. Charge densities are generally anisotropic when looked from both atomic sites, and they change very abruptly near and outside of both muffin-tin sphere boundaries. Middle way between the nuclei are the most negatively spin-polarized regions, which is a further indication that the minority spin electrons are more extended. Near the Fermi level, these minority electrons account for a large portion of the occupying electrons which, as we recall, have larger weights over the majority spin electrons in the interstitial region. These highest energetic electrons in the interstitial region are very likely the most sensitive to outside disturbances. Therefore, the minority spin electrons can play a more important role for some Invar complexities of the alloy than the majority electrons. On the other hand, since the spin magnetism of the transitional element dominated materials is mostly of localized nature, external disturbances like thermal effects may be indirectly disruptive to long range static magnetic order but local magnetic moments may still manage to be kept; thus at low temperatures long range spin fluctuations are expected, and at temperatures much higher than Curie or Néel temperatures short range magnetic order can still be observed.

Effects of Inaccurate Information about Exchange-Correlation Interaction on Magnetism of Fe_3Pt

It is known for quite a while that there is inaccuracy in describing the exchange-correlation interaction. In an effort to see how the possible approximation might affect our results for the electronic behavior and magnetism, we have proportionally reduced our exchange-correlation by a factor of from

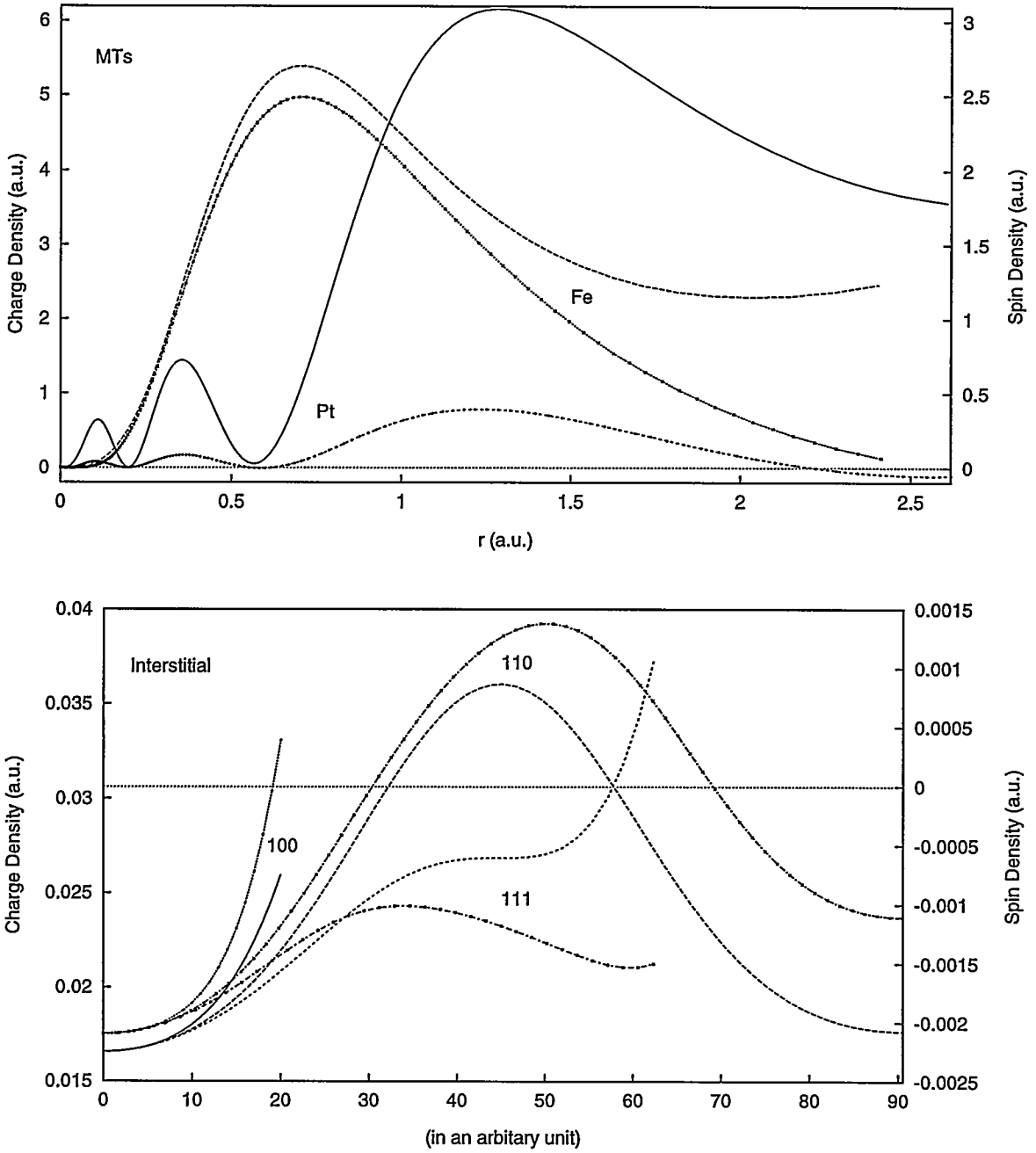

Figure 6.6 Spatial charge and spin distributions in Fe_3Pt. Doted lines are for spins and other curves for charges. (A) The radial densities in the muffin-tins; (B) interstitial densities along some directions starting from the unit cell center.

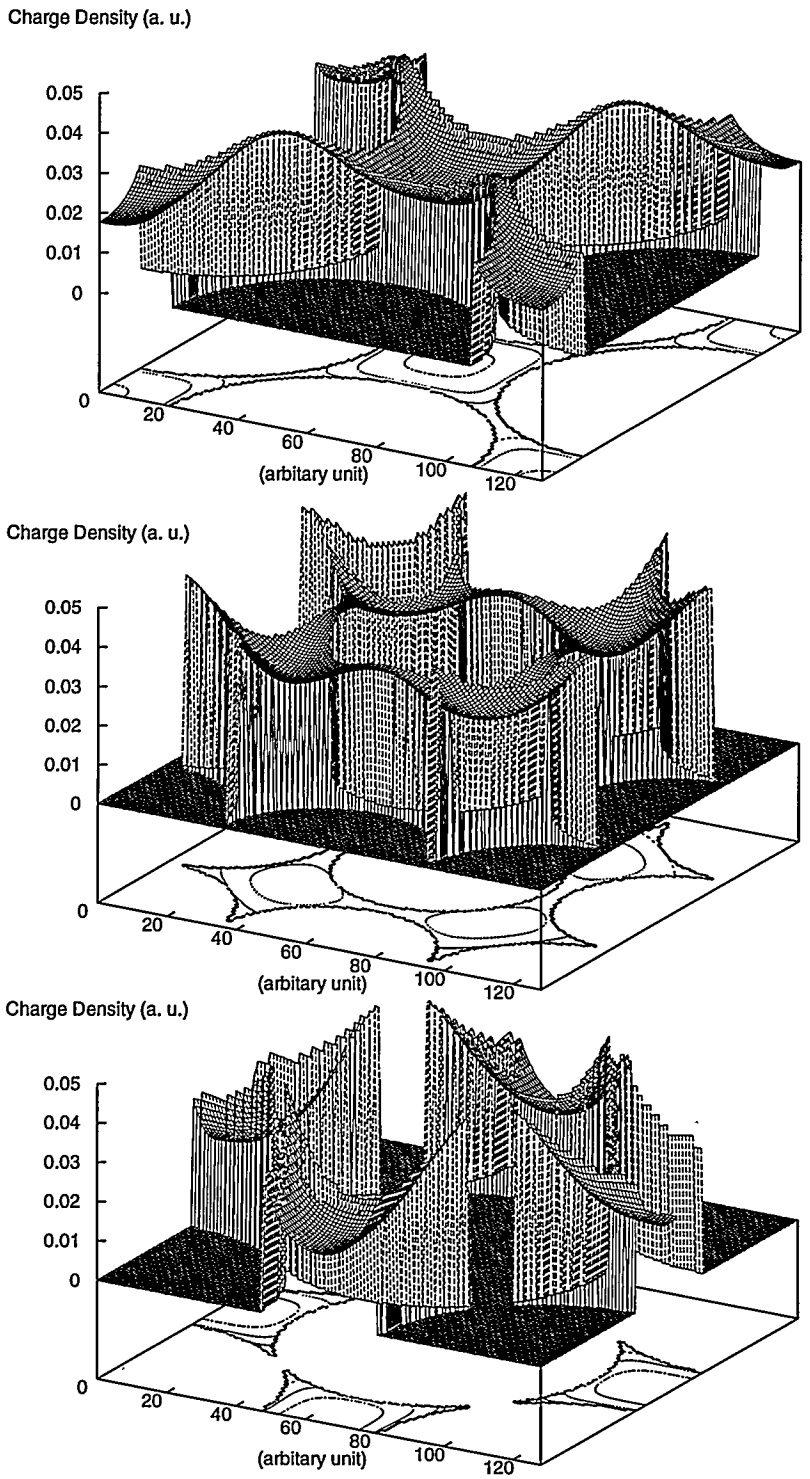

Figure 6.7 Interstitial charge distributions for Fe_3Pt. (A) On a middle plane between the two sides of the unit cell; (B) on a plane between the middle plane and a side of the unit cell; (C) on a side of the unit cell.

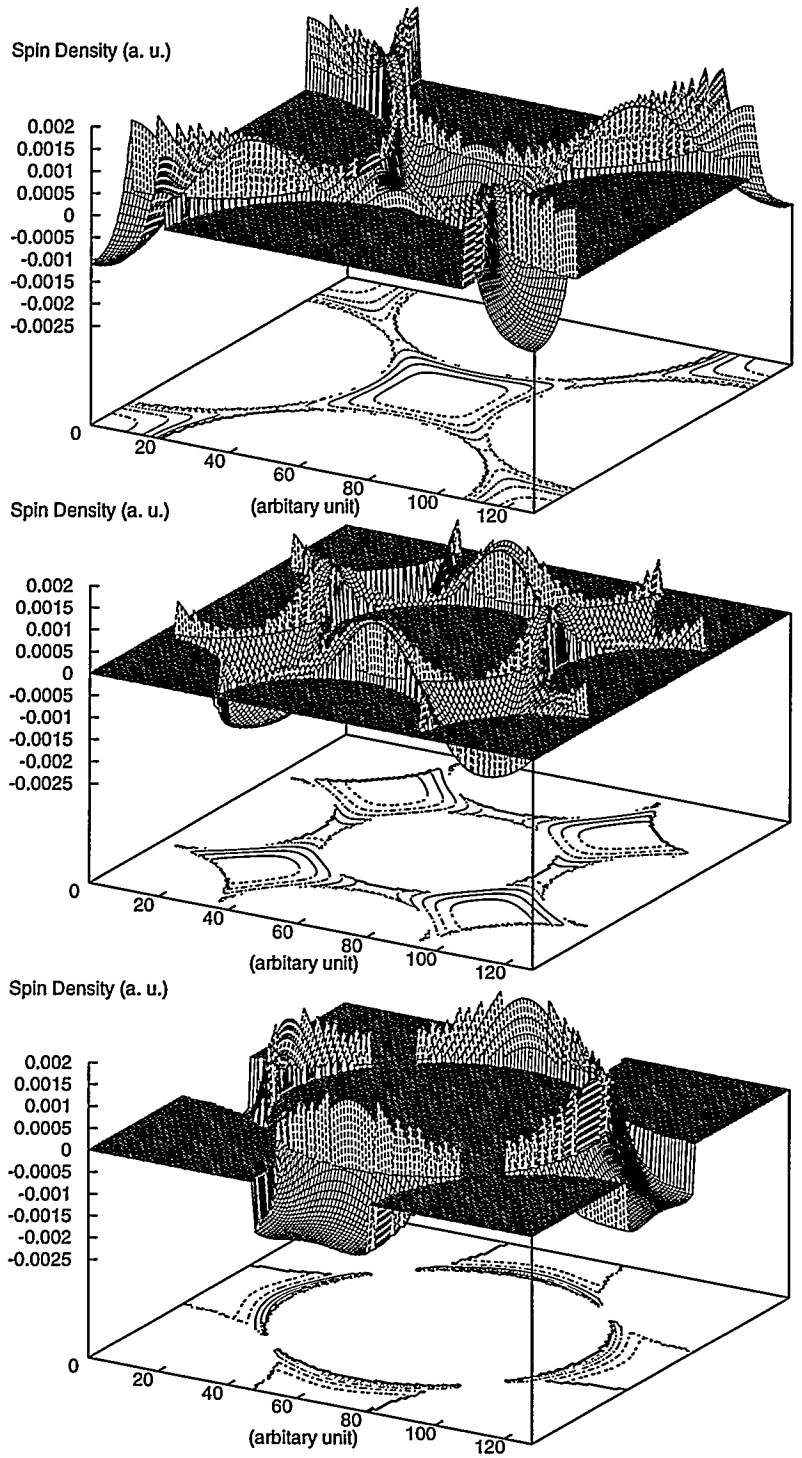

Figure 6.8 Interstitial spin distributions for Fe_3Pt. (A) On a middle plane between the two sides of the unit cell; (B) on a plane between the middle plane and a side of the unit cell; (C) on a side of the unit cell.

Table 6.2 Majority electrons in the MT spheres.

μ per cell	Pt					Fe				
	s	p	d	d-e_g	d-t_{2g}	s	p	d	d-e_g	d-t_{2g}
1.22	0.353	0.272	3.857	1.612	2.245	.212	0.207	3.318	1.430	1.888
1.62	0.352	0.270	3.865	1.617	2.248	.212	0.206	3.386	1.470	1.916
3.12	0.349	0.264	3.903	1.638	2.265	.211	0.205	3.630	1.597	2.033
3.41	0.348	0.262	3.913	1.643	2.270	.211	0.204	3.679	1.618	2.061
3.95	0.347	0.259	3.929	1.650	2.279	.211	0.202	3.769	1.652	2.116
5.78	0.342	0.243	4.006	1.676	2.331	.208	0.194	4.086	1.743	2.343
6.22	0.341	0.240	4.032	1.684	2.348	.208	0.192	4.156	1.758	2.397
7.39	0.339	0.231	4.109	1.702	2.407	.208	0.189	4.342	1.795	2.547

Table 6.3 Minority electrons in the MT spheres.

μ per cell	Pt					Fe				
	s	p	d	d-e_g	d-t_{2g}	s	p	d	d-e_g	d-t_{2g}
1.22	0.358	0.283	3.841	1.594	2.247	.213	0.209	2.906	1.182	1.724
1.62	0.358	0.283	3.841	1.592	2.249	.212	0.208	2.842	1.138	1.704
3.12	0.361	0.286	3.823	1.571	2.252	.212	0.209	2.600	0.962	1.638
3.41	0.361	0.286	3.822	1.569	2.253	.212	0.208	2.555	0.930	1.625
3.95	0.362	0.286	3.820	1.564	2.255	.212	0.207	2.471	0.872	1.599
5.78	0.365	0.282	3.819	1.550	2.269	.211	0.201	2.191	0.715	1.476
6.22	0.366	0.280	3.811	1.543	2.268	.211	0.199	2.128	0.685	1.443
7.39	0.368	0.275	3.784	1.528	2.256	.211	0.196	1.957	0.623	1.334

9% to 15%. The calculated results are listed in the Table 6.2 and Table 6.3. It is clear that the artificially introduced change in the exchange-correlation potential affects s and p electrons very little, but it causes great changes in the distributions of d-like electrons of both spins at the Fe sites as well as some evident alteration of the majority spin electrons at the Pt sites. It is probably true that an inaccurate exchange-correlation potential form is very likely to affect these d electrons at the Fe sites much more than the other electrons. Consequently, the information we get so far for the s, p and minority Pt d electrons should be more reliable than for the others. But we should cautiously add that this conclusion stems from our specific choice for the change in the potential form, and lacking a solid physical interpretation, it may not be a very precise evaluation of the real situation.

Compton Profiles of Fe_3Pt

To investigate the momentum distributions of electrons in Fe_3Pt theoretically, we show the calculated Compton profiles for the majority spin electrons and minority spin electrons respectively in Figure 6.9 and Figure 6.10. The solid lines for the total Compton profile in both figures are normalized to the total charge per unit cell for each spin. Since we have ignored the spin-orbit coupling between the two different kinds of spins, the discussion about both spins can be done separately. We decompose the Compton profiles into three parts: one is from all the orbitally decomposed contributions inside the muffin-tin spheres, another from the interstitial region; and the rest from the coupling or the interference between the two kinds of contributions through their wave behavior. To get first two parts, we take the Fourier transform of the real-space wave function by restricting the integration to over the muffin-tin sphere and to over the interstitial region respectively; the "interference" term arises from cross terms in the square of the above two parts of the total momentum wave function (the momentum wavefunctions squared to obtain the momentum density whose Fourier transform yields the Compton profile). It can be easily shown that such an interference makes no net contribution to the total integral of the overall profile: its negative part and its positive part cancel. The partial contributions from the s, p and d electrons inside the muffin-tin spheres are also shown in the figures. Correspondingly, the two figures show similar patterns. A general rule for the momentum distribution is: the closer an electrons is to a nucleus, the lower its potential becomes, or the larger its kinetic energy gets. Therefore, electrons further away from the cores are moving slower generally. This rule should generally be able to explain the shapes of the curves in both figures, but we will only elaborate on a few. Compared to the d electrons, the s and p electrons are more likely away from the cores, so they are lower in momentum. The s electron are moving slower than the p electrons. Since some d electrons can also penetrate

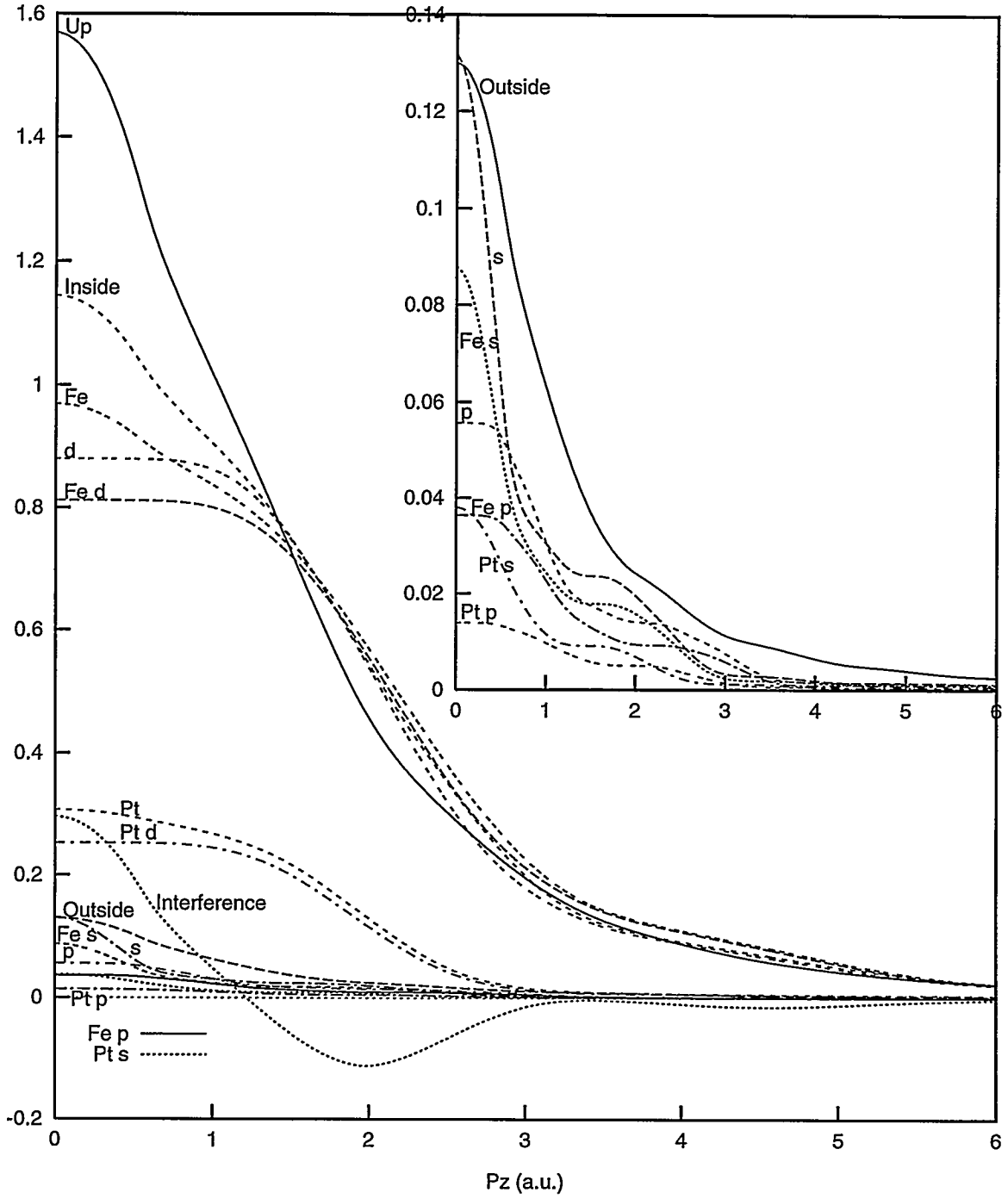

Figure 6.9 Momentum distribution and its partial decompositions for the majority electrons. At the upper right corner an enlarged subgraph is shown for some small partial contributions.

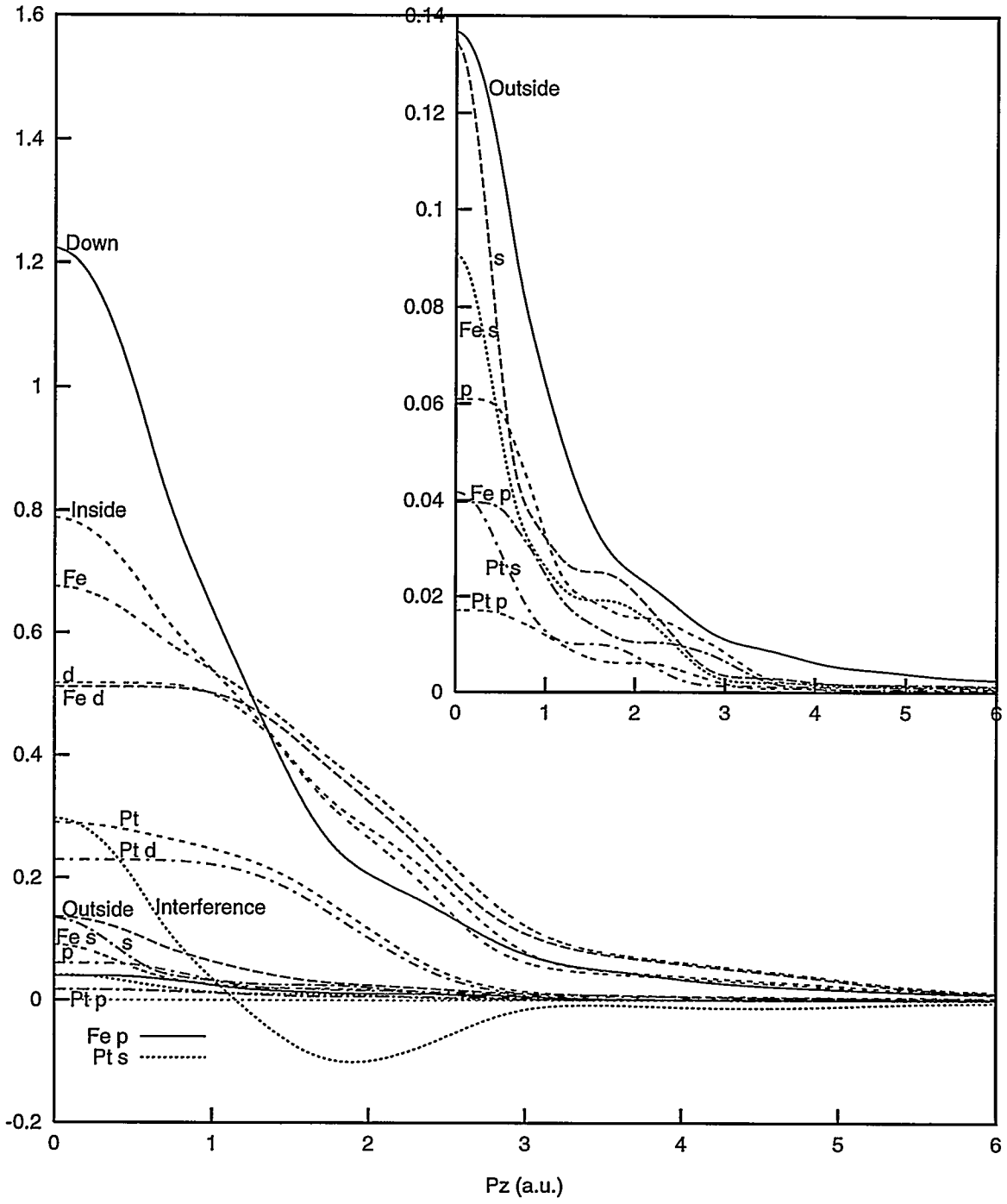

Figure 6.10 Momentum distribution and its partial decompositions for the minority electrons. At the upper right corner an enlarged subgraph is shown for some small partial contributions.

into the interstitial region, the interstitial contribution shows some similarity to the overall profile at large Pz. Proportionally, more of the 6.86 minority spin electrons inside the Fe muffin-tin spheres have smaller momenta than the 4.44 minority spin electrons in the Pt muffin-tins have. So, electrons inside the Pt muffin-tin have more intermediate momenta compared to electrons in the Fe muffin-tins. The contribution in the interstitial region is much associated with the s and p electrons which are rather extended in real space from the muffin-tins into the interstitial region by slowing down to posses small momenta.

Figure 6.11 shows the subtractions of the above two figures to give the magnetic Compton profile (MCP). For comparison, experimental data at 305K from Yahnke (1995) is also shown in the figure. Both calculated and experimental Compton profiles show a dip around Pz = 0. Our previous atomic calculations did not produce such a dip by assuming negative polarized s and p electrons of the amounts from the calculation here for the crystal. The contributions to the magnetic Compton profiles from the s and p electrons are too small to explain the large dip seen experimentally. Although the interstitial region is about 30% of the total volume, its contribution to the total magnetic Compton profile is also too minute to significantly account for the dip. This is because, as we saw before, the interstitial electrons are mainly of s- and p-like characters, and just contribute within a narrow range $Pz \leq 1(a.u.)$. The interference contribution to MCP has an oscillatory character extending to Pz values of about 4.0 a.u., and produces a rise above the d-orbital MCP curve between Pz values of about 0.7 a.u. and 1.8 a.u.. The interference contribution thus accounts for much of the dip. The negatively polarized s- and p-like electrons, possessing small momenta generally, also yield some comparable contributions to the dip. Since the dip appears at the very small momentum region, it is likely that it is due to those electrons with large probability to be in the the interstitial region that are negatively polarized. Accordingly, it can be concluded that the dip near Pz = 0 is partly due to the negative spin distribution from the unpaired s and p electrons at Pt sites and from those negatively polarized conduction electrons in the interstitial regions (a similar explanation to what was given for bcc Fe by Wakoh and Kubo 1977). The interference effect also contributes and demands further explanation.

A Study of Antiferromagnetism

Thermal effects introduce magnetic fluctuations that can not be well taken care of by LSD theories. Associated with the fluctuations in Fe_3Pt are various magnetic states approachable through thermal excitation from the ferromagnetic ground state. We thus have examined some magnetic structures to get a hint of how the antiferromagnetic tendency might influence the electronic behaviors in Fe_3Pt.

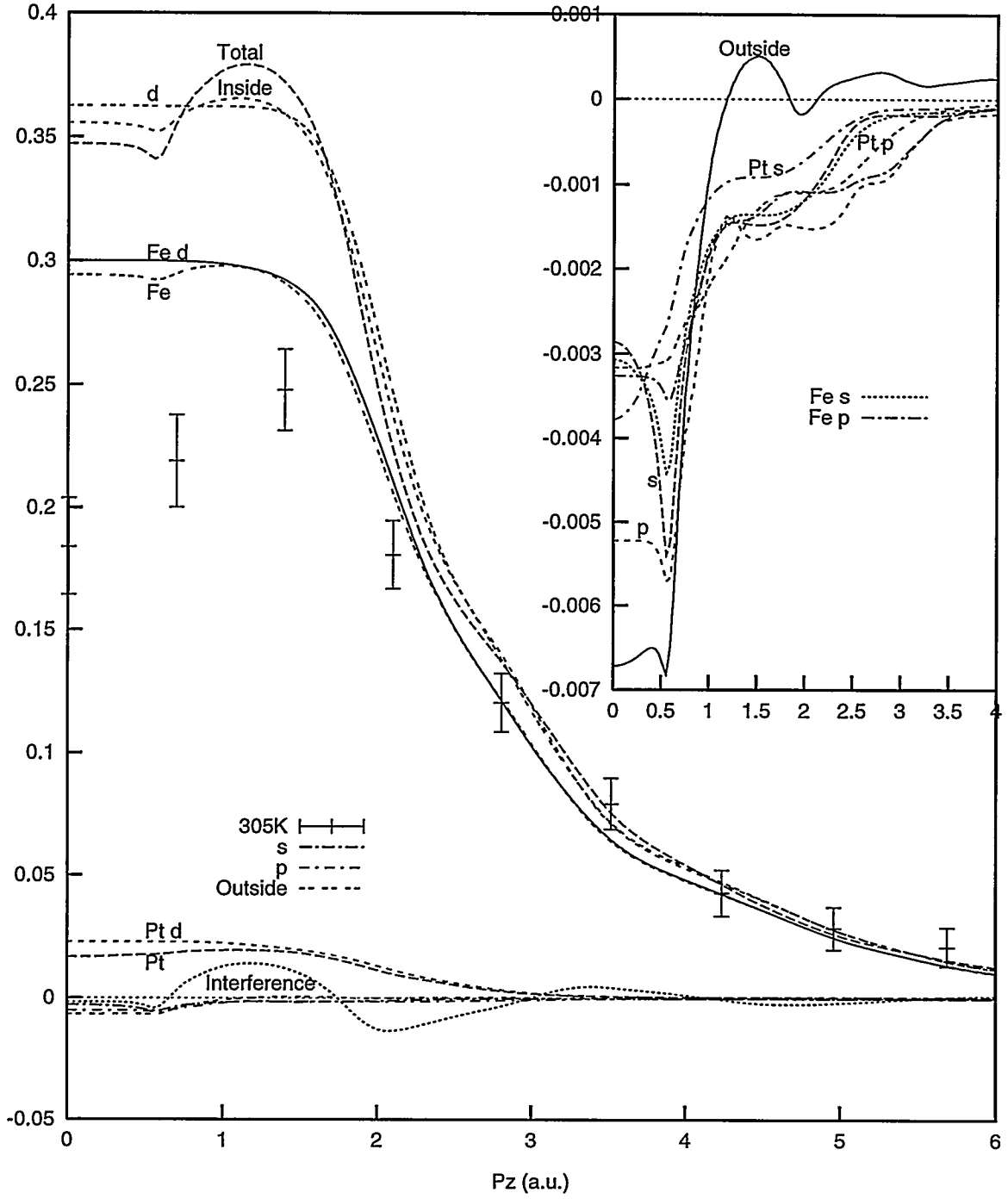

Figure 6.11 Magnetic Compton Profile and its partial decompositions for the electrons. At the upper right corner an enlarged subgraph is shown for some small partial contributions. The experimental data are by Yahnke (1995).

Three Magnetic States of Cubic Fe_3Fe

As a reference to the study of the fcc Fe based Fe_3Pt, a Fe_3Fe structure of a nonprimitive simple cubic unit cell, with one Fe atom of one kind at its corner and three others of the other kind at its face centers, is to be first investigated. We consider the two kinds of Fe atoms to be inequivalent to each other, or the structure would just be a primitive fcc structure otherwise. The lattice constant is chosen to be 6.73 a.u., approximately a value for its ground state in our calculation. The muffin-tin spheres are contacting each other and their radii are chosen to be the same. Since the two kinds of iron atoms are identical, we use a mixing factor of less than 4% between the old and new charges, to avoid too much random flowing of electrons from one atom to the other.

Table 6.4 Spin electron distributions in Fe_3Fe for some magnetic states. The first number in each pair is for the majority electrons.

Total	20.08-11.92				
Interstitial	1.33-1.37				
	total_{MT}	s	p	d	f
Fe	4.69-2.66	0.23-0.24	0.21-0.22	4.22-2.18	0.020-0.01
Fe_3	4.70-2.64	0.23-0.24	0.21-0.22	4.24-2.17	0.020-0.01
Total	16.81-15.19				
Interstitial	1.35-1.37				
	total_{MT}	s	p	d	f
Fe	2.73-4.58	0.22-0.25	0.20-0.24	2.28-4.07	0.02-0.02
Fe_3	4.25-3.09	0.23-0.23	0.22-0.21	3.78-2.63	0.02-0.02
Total	16.26-15.74				
Interstitial	1.36-1.36				
	total_{MT}	s	p	d	f
Fe	3.65-3.69	0.23-0.23	0.21-0.21	3.18-3.22	0.02-0.02
Fe_3	3.76-3.57	0.23-0.23	0.21-0.21	3.29-3.11	0.02-0.02

Since the energy of the structure is relatively insensitive to its magnetic state, we have obtained three converged magnetic states, with moments being 8.16 μ_B, 1.62 μ_B and 0.52 μ_B respectively, as shown in Table 6.4 by trying different starting potentials. The first state is nearly a ferromagnetic state for fcc Fe with a magnetic moment of $8.16\mu_B$, comparable to the value of $8.21\mu_B$ for the ground state of Fe_3Pt. Its densities of states and of partial states are plotted from Figure 6.12 to Figure 6.14. The magnetic moments inside the muffin-tin spheres are about $2.05\mu_B$, in contrast to $2.63\mu_B$ at Fe sites in Fe_3Pt. The s-like and p-like electrons in the muffin-tin spheres and the interstitial electrons have negative polarizations as in Fe_3Pt. From the DOS figures for this state, we can see that the atomic-

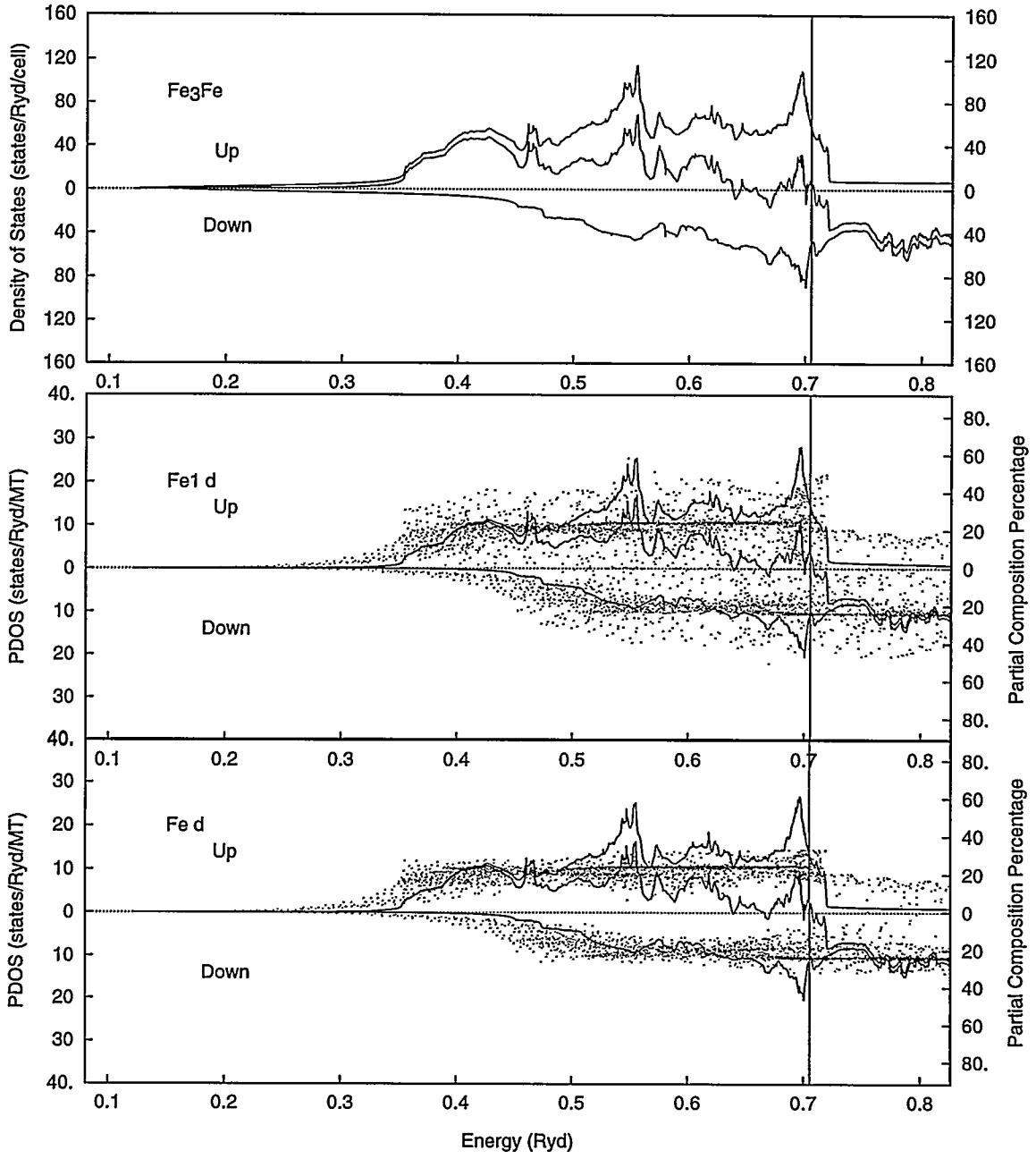

Figure 6.12 Total density of states per unit cell, partial densities of d states at muffin-tin sites, and the percentages of mixing (dots) between the d electronic states in forming the eigenstates at our 120 representative irreducible k points for Fe_3Fe with a total moment of 8.16 μ_B. The Fermi level $E_F = 0.705$ Ryd is shown by the vertical line.

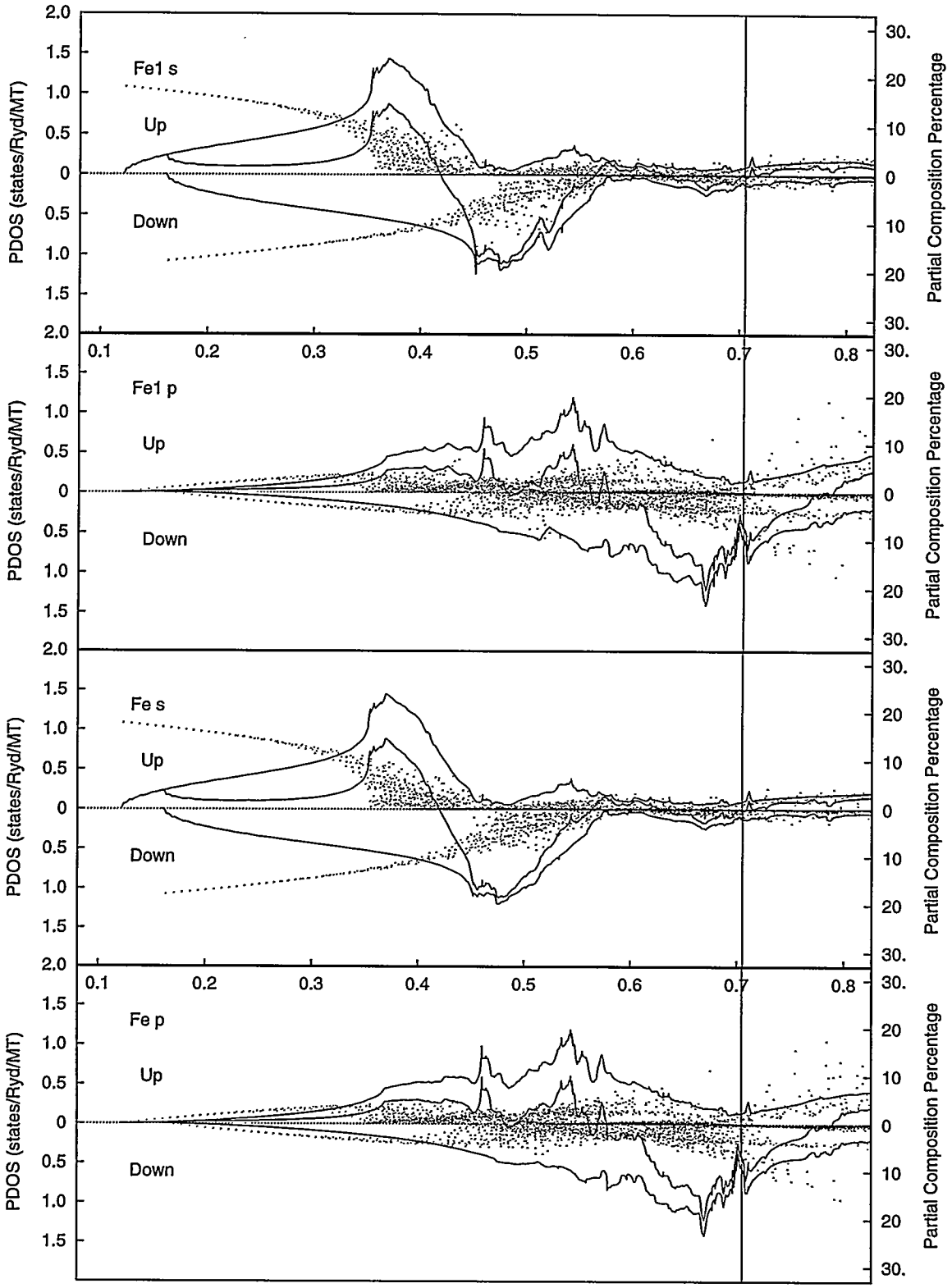

Figure 6.13 Partial densities for s and p states in Fe_3Fe with a total moment of 8.16 μ_B.

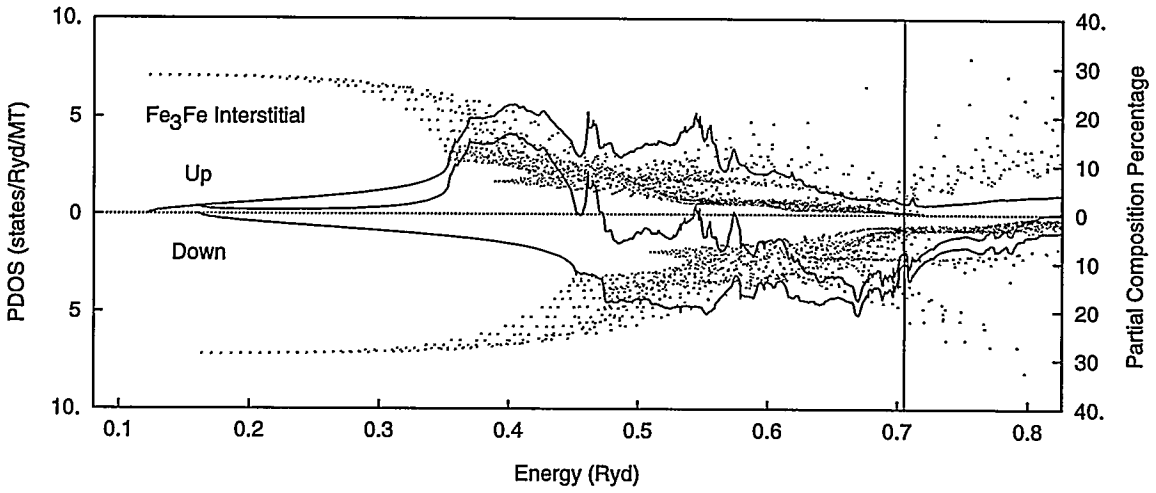

Figure 6.14 Partial densities for states from the interstitial region of Fe_3Fe with a total moment of 8.16 μ_B.

like d states from the Fe sites are nearly uniform with a 25% mixing typical for ferromagnetic fcc Fe. Nevertheless, the corner Fe atom shows some noticeable deviation from the mixing percentage though its net charge and net spin are nearly identical to those of other Fe atoms. Such a distinction of the corner Fe atom is similar to what we have seen for the Pt atom in Fe_3Pt. Like in Fe_3Pt the upper bands are nearly full but with a larger value of DOS at the Fermi level. An observation is that the introduction of Pt atom in Fe_3Pt leads to higher DOS values for s, p and interstitial electrons around E_F.

The second state is a ferrimagnetic state of a magnetization of $1.62\mu_B$ per unit cell. Its densities of states and of partial states are plotted from Figure 6.15 to Figure 6.17. In this state, the corner atom in the unit cell has a moment of $1.86\mu_B$ which is antiparallel to the moments (with a value of $1.16\mu_B$ each) of the other three Fe atoms in the unit cell. It is interesting that s and p electrons now are parallel to the local moments while the interstitial electrons still have a net magnetic moment $0.02\mu_B$ antiparallel to the total magnetization. There are some changes relative to the above ferromagnetic state: the net negative spin polarization in the interstitial region is decreased from about $0.04\mu_B$ to about $0.02\mu_B$; the net spin polarizations of s- and p-like electrons inside muffin-tin spheres, however, are now parallel to their total local moments, while their absolute values for the corner Fe atoms are increased from about $0.01\mu_B$ to about $0.03\mu_B$. These values suggest that the negative spin regions around the interstitial region get smaller with the presence of the antiferromagnetic tendency. For the corner Fe atom, both kinds of spin electrons at the Fermi level have bands that bring about two DOS peaks higher than in

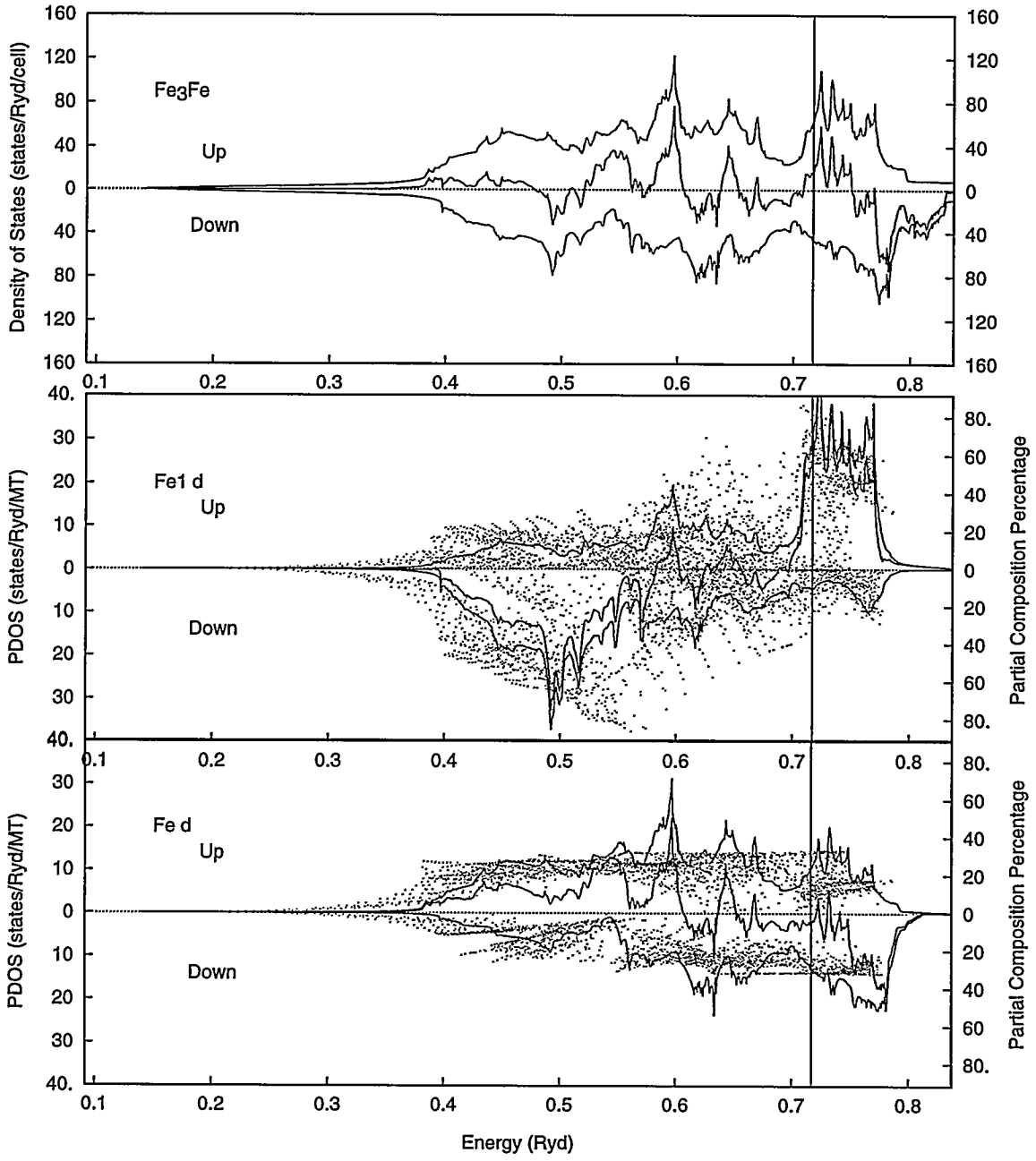

Figure 6.15 Total density of states per unit cell, partial densities of d states at muffin-tin sites, and the percentages of mixing (dots) between the d electronic states in forming the eigenstates at our 120 representative irreducible k points for Fe_3Fe with a total moment of 1.62 μ_B. The Fermi level $E_F = 0.717$ Ryd is shown by the vertical line.

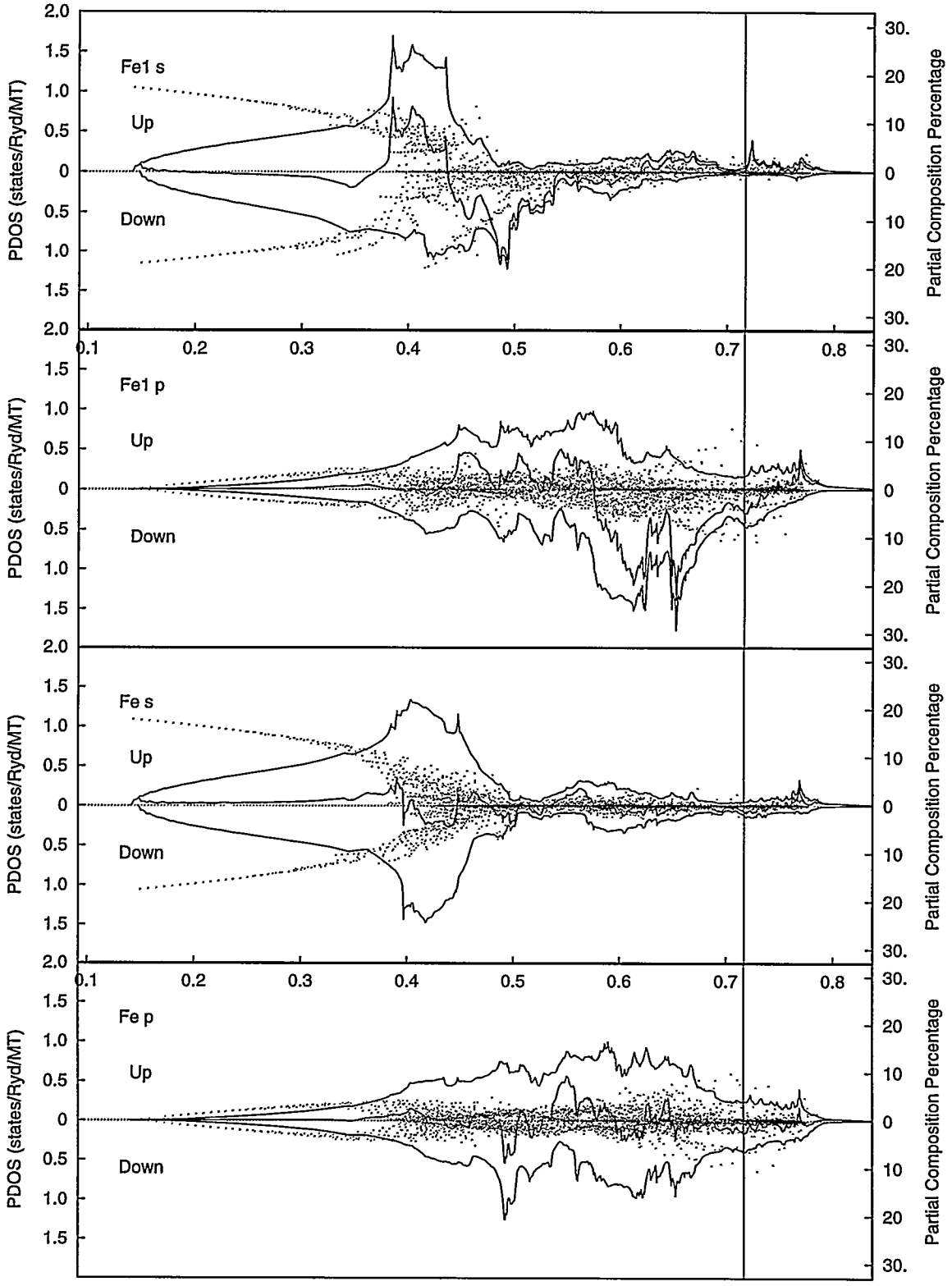

Figure 6.16 Partial densities for s and p states in Fe_3Fe with a total moment of 1.62 μ_B.

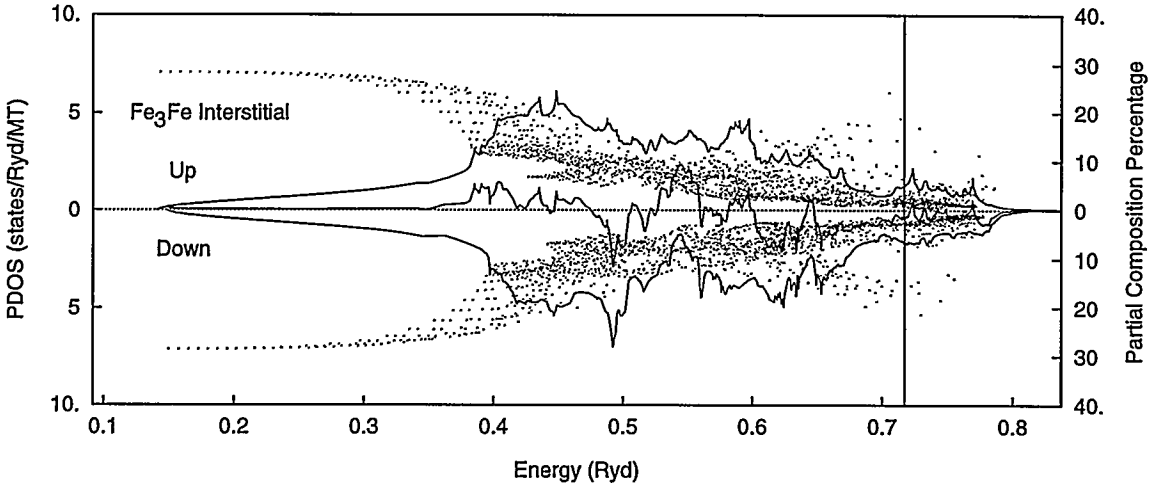

Figure 6.17 Partial densities for states from the interstitial region of Fe_3Fe with a total moment of 1.62 μ_B.

the first state; both DOS peaks are well separated from each other, with a very small portion of the spin up electron peak at E_F being occupied, and with the other peak, well below the Fermi level, being all occupied. Therefore, the electrons in this state are generally more localized because of the reversal of the spin at the corner Fe atom sites. Although the spin up d electrons of the corner Fe atom have a much smaller population than the electrons of the other kind spin, they contribute tremendously to the DOS at E_F. Comparing with the first state, near and above the Fermi level, a smaller population of s, p and interstitial electrons are unoccupied.

The third state is a ferrimagnetic state with a smaller total magnetization of $0.52\mu_B$ per unit cell, and the state has only a very small antiferromagnetic effect: the corner atom has a negative magnetic moment of $0.04\mu_B$, while other three atoms at the face centers each have a magnetic moment of $0.19\mu_B$. Its densities of states and of partial DOSs are plotted from Figure 6.18 to Figure 6.20. The moments of s, p and interstitial electrons are too small to be perceived for our calculation precision. Again, the antiferromagnetic atom has electrons more localized as in the second state.

A Ferrimagnetic State of Fe_2FePt

Similar to the previous calculation for Fe_3Fe, we have approximately reversed the magnetic moment of a Fe atom at a face center of the otherwise Fe_3Pt cubic structure to find a converged ferrimagnetic state at the same lattice constant of Fe_3Pt. The structure has the symmetry of D_{4h}. The figures from Figure 6.21 to Figure 6.24 show the corresponding densities of states for this ferrimagnetic state.

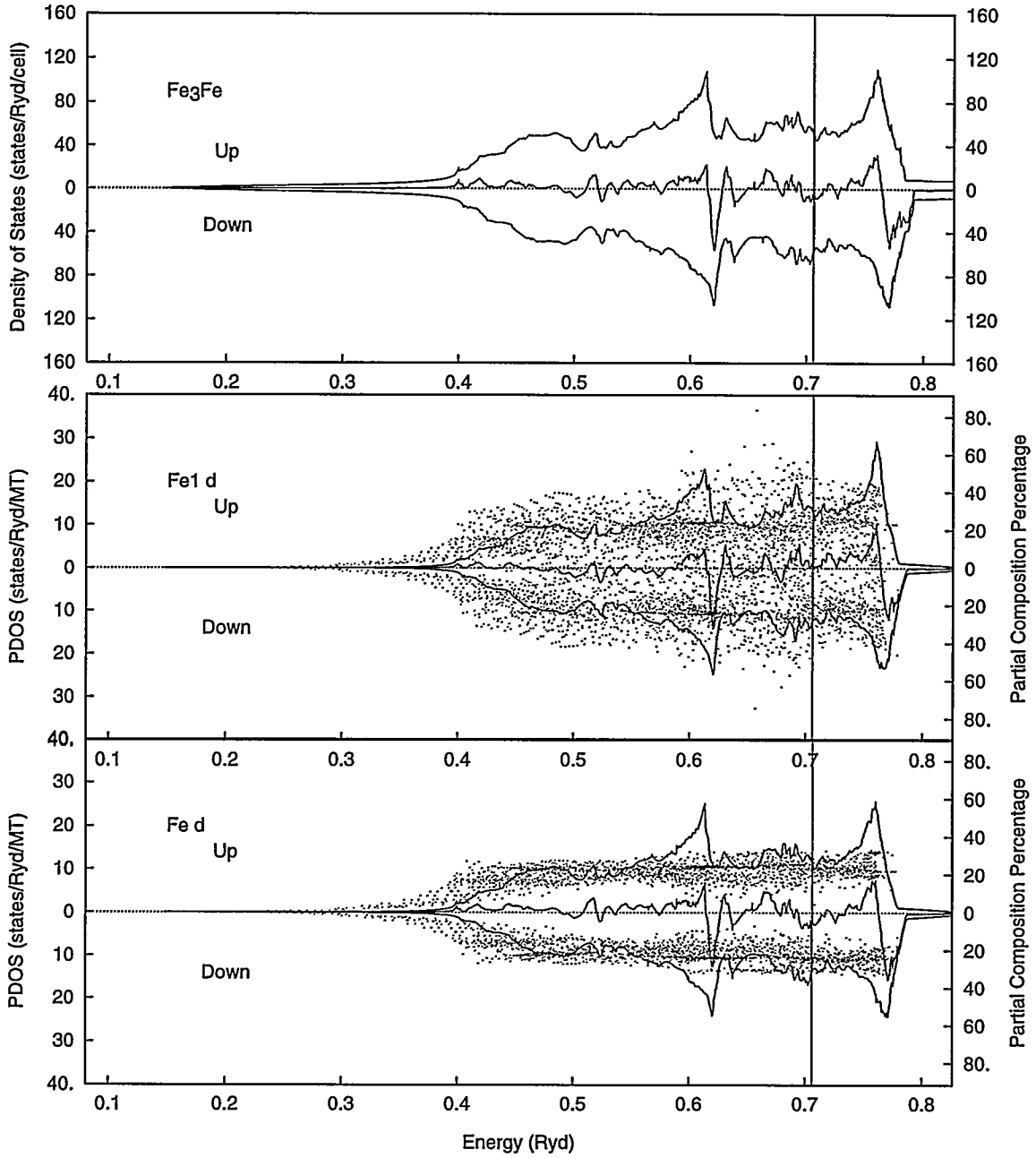

Figure 6.18 Total density of states per unit cell, partial densities of d states at muffin-tin sites, and the percentages of mixing (dots) between the d electronic states in forming the eigenstates at our 120 representative irreducible k points for Fe_3Fe with a total moment of 0.52 μ_B. The Fermi level $E_F = 0.706$ Ryd is shown by the vertical line.

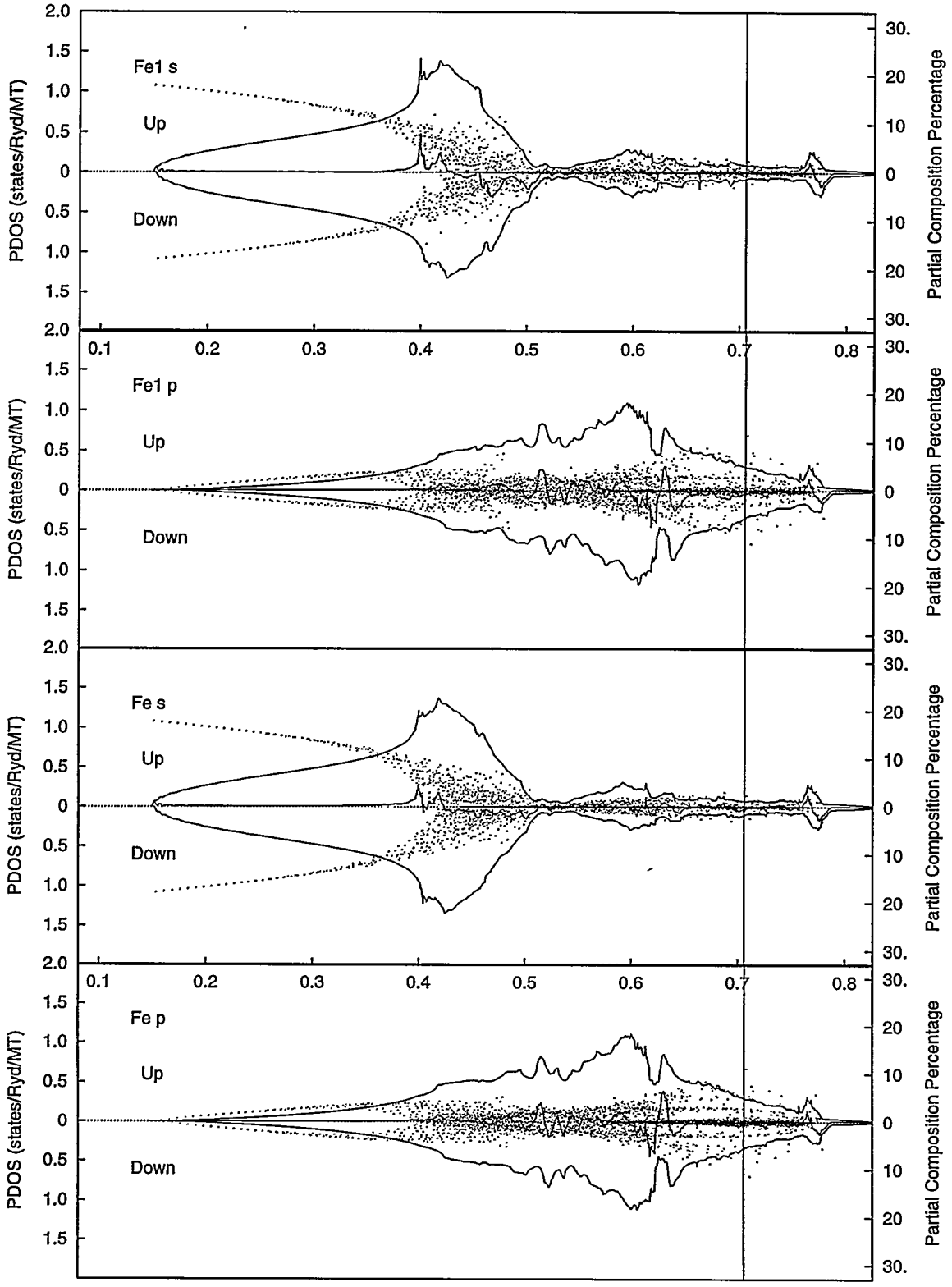

Figure 6.19 Partial densities for s and p states in Fe_3Fe with a total moment of 0.52 μ_B.

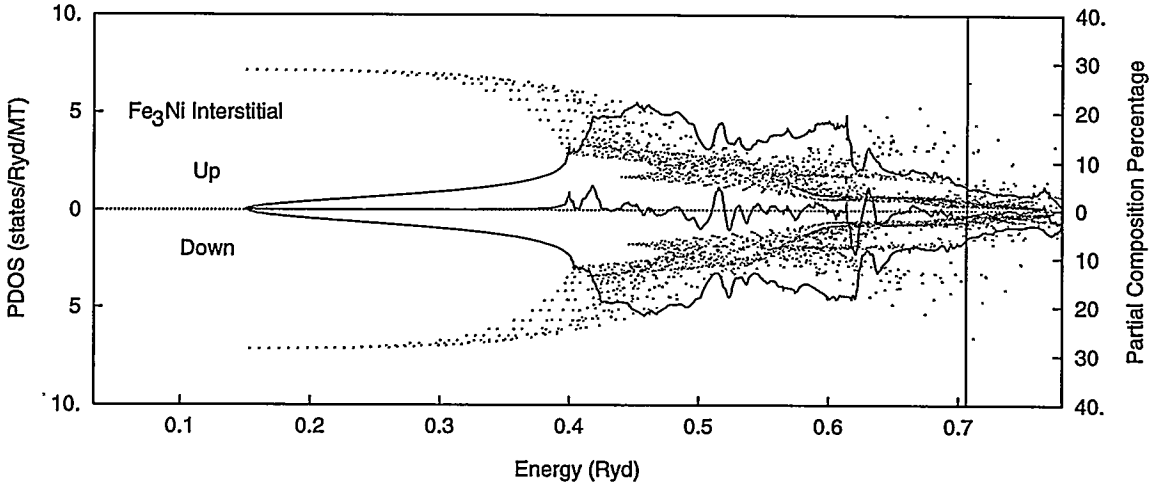

Figure 6.20 Partial densities for states from the interstitial region of Fe_3Fe with a total moment of 0.52 μ_B.

Table 6.5 Spin electron distributions in Fe_2FePt for some magnetic states.

Total	18.12-15.88				
Interstitial	1.60-1.63				
	$total_{MT}$	s	p	d	f
Pt	4.64-4.55	0.34-0.35	0.23-0.25	4.04-3.92	0.03-0.03
Fe	2.38-4.76	0.19-0.22	0.16-0.20	2.01-4.31	0.02-0.01
Fe_2	4.77-2.48	0.22-0.21	0.20-0.19	4.33-2.07	0.02-0.02

Table 6.5 shows some information about the spin distribution. The Fe atoms still have their net magnetic moments of s- and p-like electrons parallel to the direction of their respective total local moments, as in the above antiferromagnetic state for Fe_3Fe. Comparing to the ferromagnetic ground state of Fe_3Pt, there are some significant changes. The interstitial electrons and the s and p electron at the Pt atom sites now have smaller negative spin moments. The local moment at the Pt site is decreased from $0.35\mu_B$ to $0.09\mu_B$. The net negative polarizations are more extended. The two kinds of Fe atoms have nearly equal local magnetic moments, though opposite to each other, that are about 10% smaller than the corresponding ones in the ferromagnetic Fe_3Pt. As some electrons transfer from the corner Fe atoms to the other three Fe atoms when antiferromagnetic order occurs in the Fe_3Fe, the reversal of the local total magnetic moment at the minority Fe site leads to a small amount of electron transfer (0.08 electron per unit cell) from the Fe atom and the Pt atom to the major Fe sites. The bands become narrower, and the DOS peaks are thus higher. The moment-reversed Fe atom has electrons

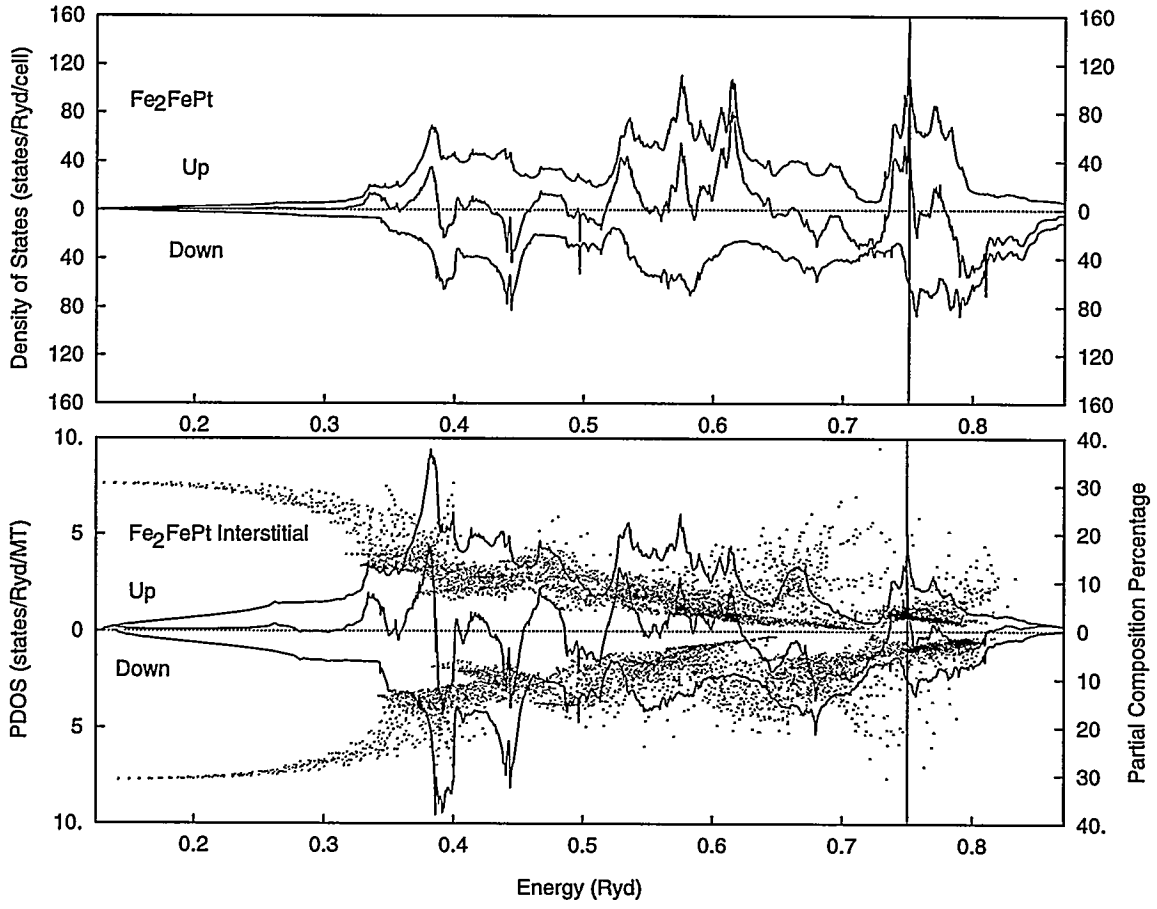

Figure 6.21 Total density of states per unit cell, partial densities of d states at muffin-tin sites, and the composition percentages (dots) in the eigenstates at our 280 representative irreducible k points for Fe_2FePt. The Fermi level $E_F = 0.750$ Ryd is shown by the vertical line.

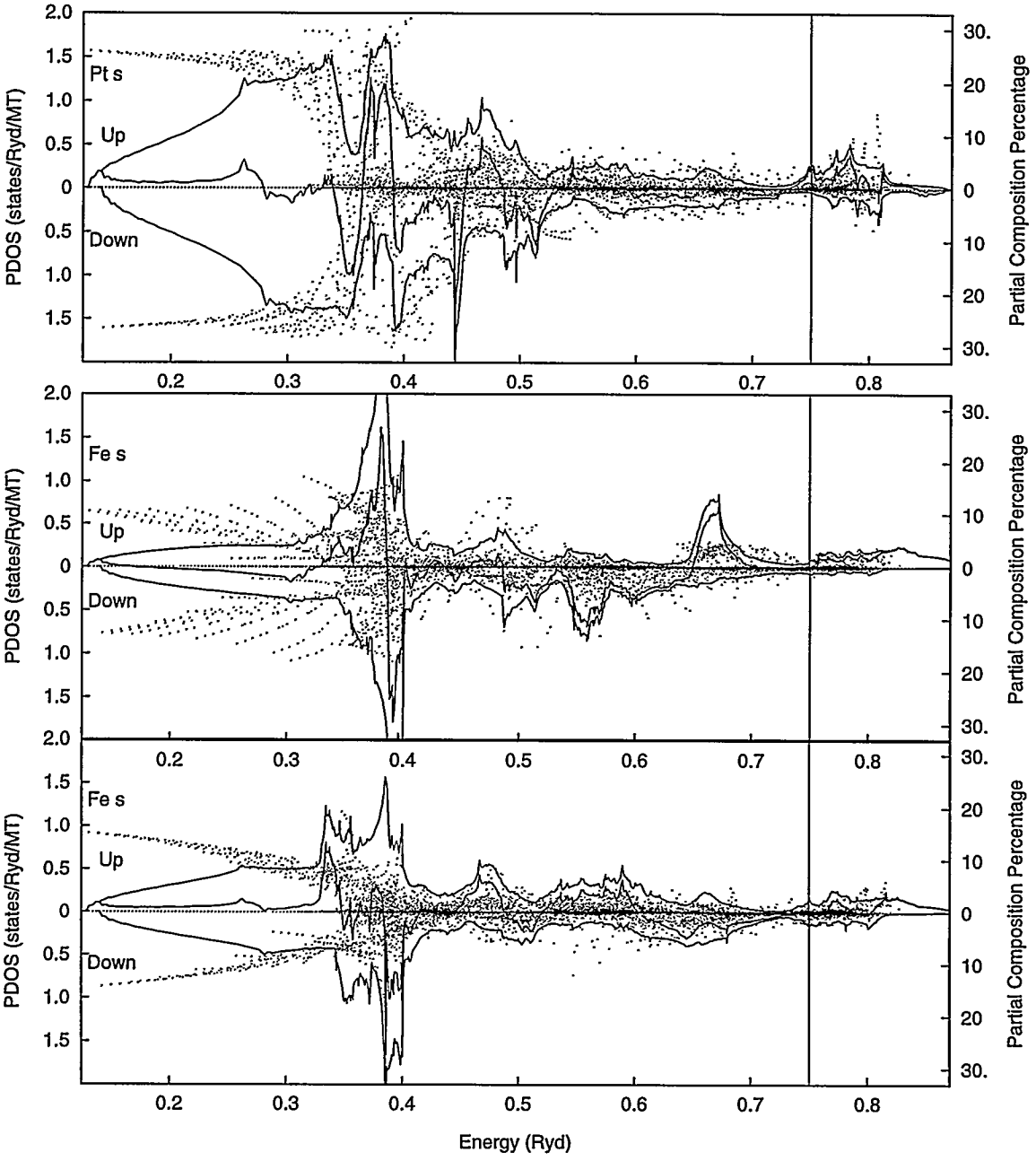

Figure 6.22 Partial densities of s states at muffin-tin sites in Fe_2FePt.

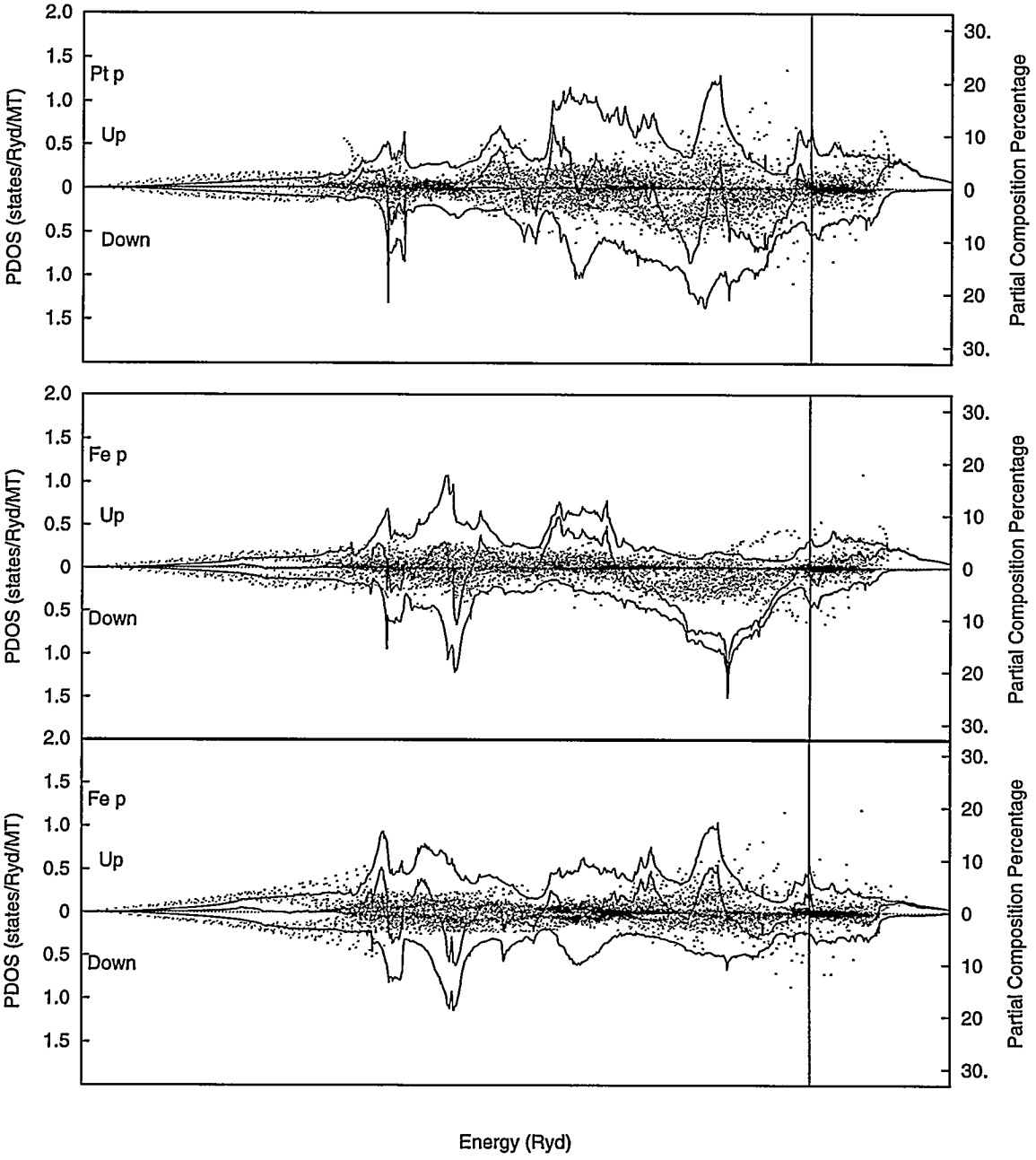

Figure 6.23 Partial densities of p states at muffin-tin sites in Fe_2FePt.

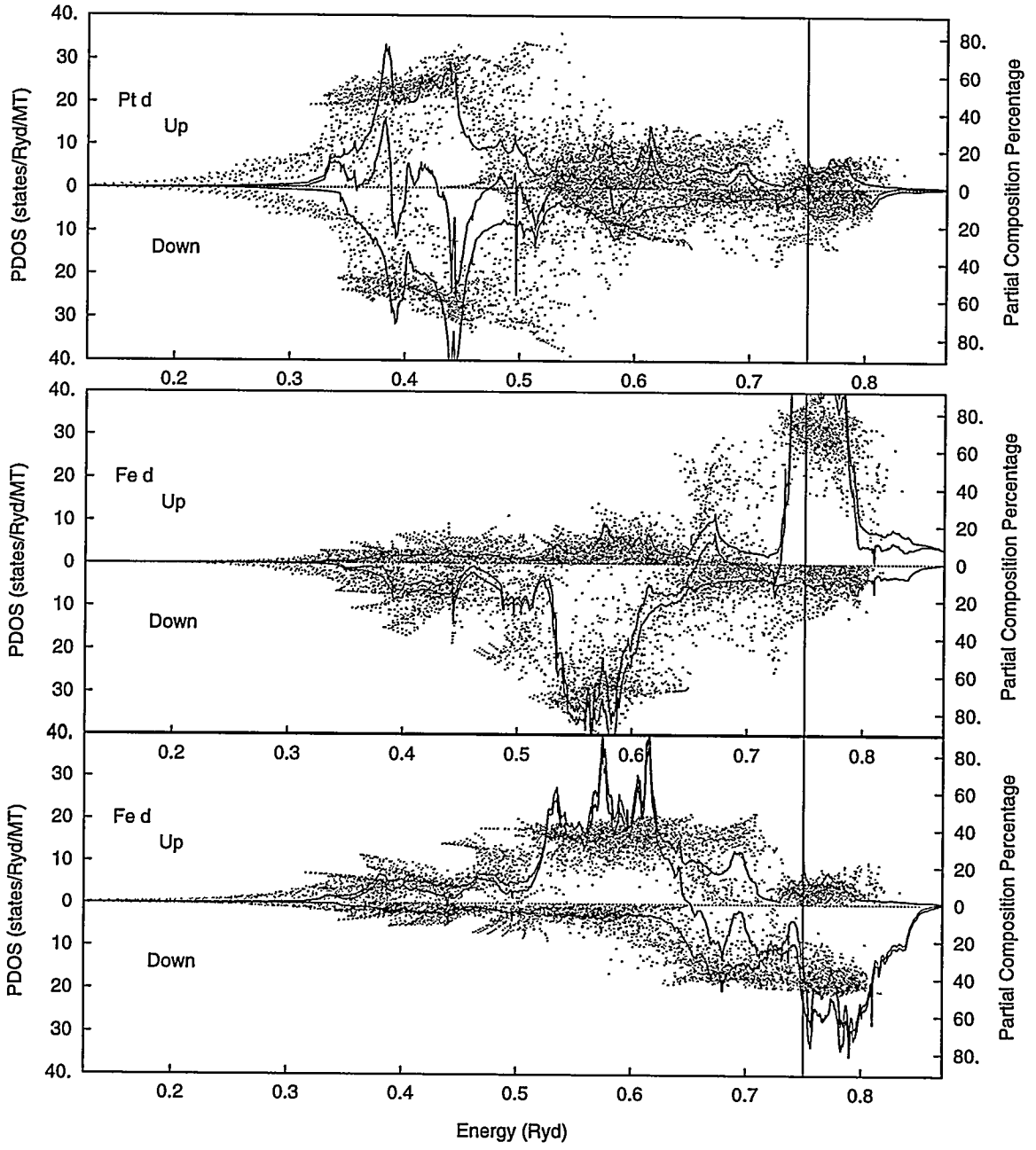

Figure 6.24 Partial densities of d states at muffin-tin sites in Fe_2FePt.

around that are more localized than those in Fe_3Pt.

Magnetic Compton Profiles

Magnetic Compton profiles of all the above states have been calculated and shown in Figure 6.25. Experimental data for ordered Fe_3Pt from Yhanke (1995) are also shown for comparison. Our theoretical curves are all normalized to their corresponding calculated moments within 0.01 electrons per unit cell. The major discrepancies between the experimental data and theoretical ones are for the momentum Pz smaller than 2 a.u.. A major reason is that the experimental profiles have larger oscillating tails for Pz extending beyond 6 a.u. (not shown), which account for some significant weight of the profiles, while our calculated results have little weight beyond Pz = 6 a.u.. This kind of large tails are not found in other MCP measurements. More precise measurements seem needed.

Let us first compare the profile of Fe_3Pt with that of the Fe_3Fe ferromagnetic state. Their generally subtle differences are difficult to observe with the precision of current measurements. For small momenta, particularly those Pz smaller than 1.5 a.u., the theoretical distributions have shown considerable differences that Pt atoms have made in the fcc Fe based structures, but unfortunately its corresponding experimental data have the largest errors. For larger Pz roughly between 1.5 a.u. and 3.5 a.u., the distributions change abruptly while the corresponding experimental errors are generally smaller; because of the poor fitting for the small momentum region, this part of MCP decreases with Pz much faster than the experimental data do. The position for the highest MCP peak of Fe_3Pt is decreased by 0.1 a.u. relative to that of Fe_3Fe, and the MCP of Fe_3Pt in the small momenta region is noticeably higher than that of Fe_3Fe. The MCPs are not very sensitive to the chemical changes from the fcc Fe, thus demanding more precision on MCP experiments for meaningful comparisons.

The discrepancies of the dip between theories and the experiments are not well explained so far, despite the speculation that the negative s- and p-like spin moments are underestimated (Wakoh and Kubo 1977). Further examination of the differences need to be made.

We have calculated a MCP by reducing our exchange-correlation potential by about 8% to study the possible effect of inaccurate descriptions of the interaction on our result. The MCP so derived is almost proportional to the original MCP reduced by the same 8% reduction, while the total magnetic moment is reduced by about 9%. Such a systematic theoretical deviation obviously fails to explain the larger dip around small momentum that experiments imply.

We have also calculated the MCP for the ferrimagnetic states in Fe_3Fe as well as in Fe_2FePt, to examine if the antiferromagnetic ordering can contribute to the dip. The profile of Fe_2FePt shows

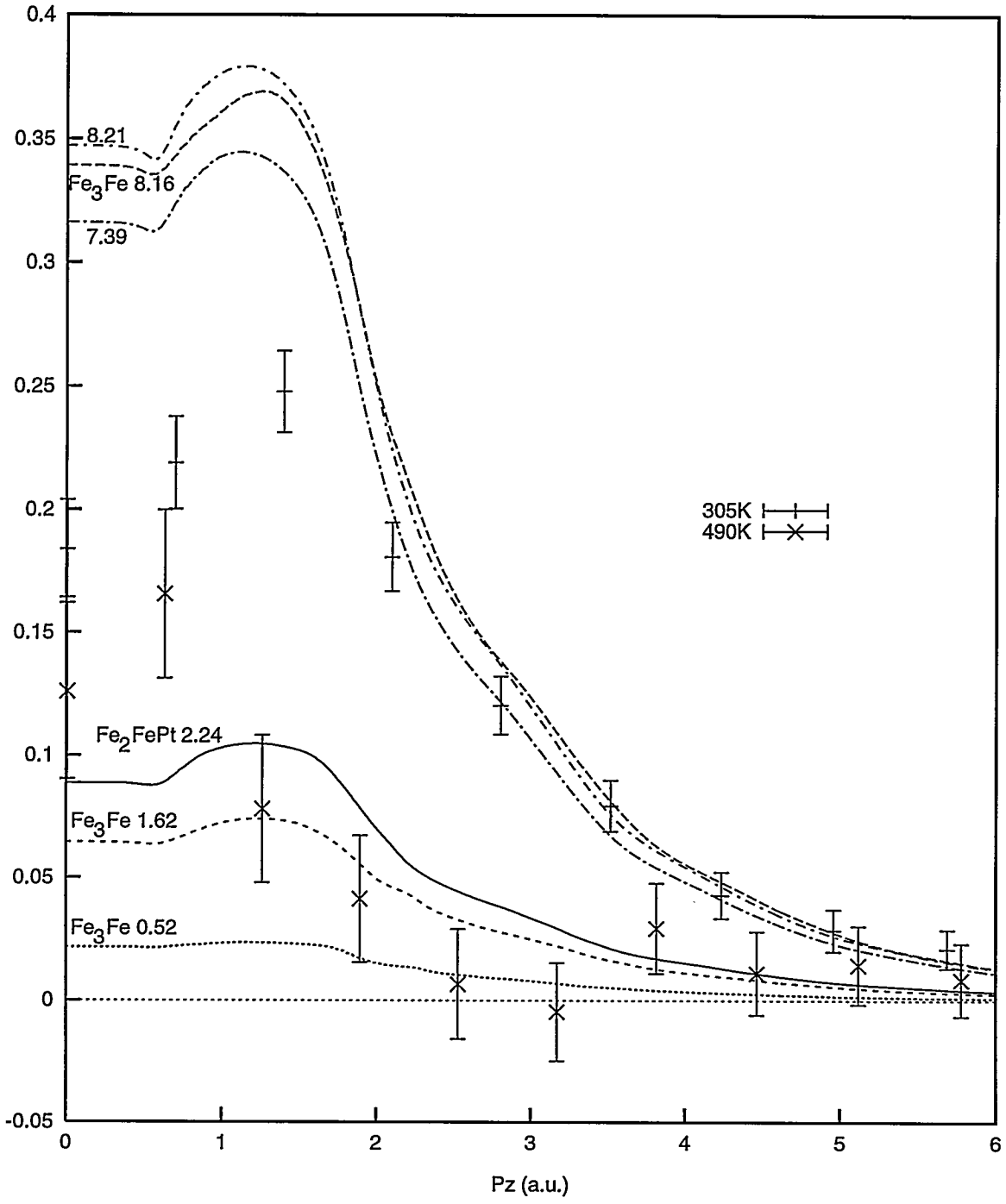

Figure 6.25 Calculated magnetic Compton profiles of various spin moments (the numbers corresponding to the curves are in μ_B) and the experimental data at 350K and 490K.

that the dip is larger than that of Fe_3Pt, if both profiles are scaled to give the same total area for their comparison. A similar scaling is made for the first two fcc Fe magnetic states, and a similarly enlarged dip is found for the ferrimagnetic state relative to the nearly ferromagnetic state. For our second ferrimagnetic state in Fe_3Fe with a very small net spin moment at the minority Fe sites, the dip is almost gone. From this observation, it seems that the dip may have something to do with antiferromagnetic tendency, or even, spin fluctuations which likely show up at the room temperature where nearly all of the MCPs have been measured so far.

Electronic Behavior of Some Related Alloys

Ni, Pd and Pt have the same valent electron occupations. The introductions of a Ni, Pd or Pt atom in a fcc Fe unit cell helps to establish stable Invar materials. How such alloying affects the electrons will be studied here for Fe dominant Invar materials Fe_3X (X = Ni and Pd). As a reference for Fe_3Pt, Co or Ni dominant alloys X_3Pt (X = Co and Ni) are also to be studied.

Invar Fe_3X (X = Ni, Pd and Pt) Systems

Various phases for Fe-Ni, Fe-Pd and Fe-Pt systems have been studied (Madleung 1995). Among the three Invar systems, Fe-Ni can have Invar anomaly over the largest range while Fe-Pt can have the anomaly over the smallest range. On the other hand, the Fe-Ni system can sustain its fcc structure for the largest Fe concentration, while Fe-Pt the smallest.

The existence of antiparallel spins, as well as of the frustrated magnetic moment of Fe atoms in Fe-Ni Invar alloys, are shown by the special experimental method of Mössbauer spectroscopy with polarized γ-radiation in the study by Ullrich and Hesse (1984). But a long range antiferromagnetic order has not been found in Fe-Ni alloys so far.

Polarized Neutron diffraction measurements carried out on Ni and Fe have revealed that the magnetization density localized around each atomic site is greater than the atomic moments given by the magnetization measurements, and in the region between atoms the spin density is essentially opposite to the total magnetization (Brown, Jassim, Neumann and Ziebeck 1989). Measurements for $Fe_{65}Ni_{35}$ at 300K and 77K indicate that the avenge local moment associated with Ni atoms exhibits little temperature dependence below the room temperature (Ito, Akimitsu, Matsui and Chikazumi 1979).

For Fe_3Pd the Curie temperature is 500K, and the local moments for the atoms are $2.7\mu_B$ and $0.36\mu_B$ for Fe atom and Pd atom respectively (Fujimori and Saito 1964; Kimura, Katsuki and Shimizu 1966; Matsui, Shimizu, Yamada and Adachi 1980; Matsui, Shimizu and Adachi 1983). The Fe-Pd has

similar properties as the Fe-Pt system, particularly a minimum thermal expansion around $x = 0.3$ for its high-temperature γ phase, and there is no ordered Fe_3Pd phase at low temperatures when a γ-α transition takes place. Fe_3Pd is metastable (Buschow, van Engen and Jongebreur 1983), alloys with 28-33% Pd transform to fct phase from the fcc phase at low temperature (Sugiyama, Oshima and Fujita 1984 and 1986). In the concentration range between 34.4% and 39.5% Pd a martensitic transformation occurs, it is a mixture of bcc and fct and is very close to fcc (Sohmura, Oshima and Fujita 1980; Matsui, Adachi and Asano1 1981; Predel 1995). The lattice constant of Fe_3Ni is taken as 6.75 a.u. from an experiment at about 200 K (Bonnenberg, Hempel and Wijn 1986). The lattice constant of Fe_3Pd is taken as 7.21 a.u. from an experiment (Madelung 1995).

The γ-α transition occurs for the Fe intermetallic alloys always when the fcc structure is no more able to support the ferromagnetic state. The fcc phase can be sustained for the highest Fe concentrations for Fe-Ni, and Invar concentrations are very close to the γ-α transition line. Further, Pt-Fe confines its Invar anomalies to a very narrow concentration range (22-32% Pt), while the Invar anomalies for Fe-Ni alloy are present in a relatively broad concentration range (25-45% Ni).

For Fe-Pt, its Curie temperature for 50%-75% Fe decreases with increasing iron content. This means that the magnetic contribution to the crystal free energy falls (Menshikov 1989). The concentration dependence of the average magnetic moment for Fe_xPd_{1-x} and Fe_xPt_{1-x} alloys varies linearly with x, while in the Fe_xNi_{1-x} alloys this mixing law exists only up to $x = 0.5$ and then decreases rapidly up to 0.75.

Figure 6.26 to Figure 6.33 show some results from band calculations for Fe_3Ni and Fe_3Pd. Comparing to elemental Fe, the Ni, Pd and Pt dominated bands have more narrow and sharper DOS peaks, similarly the bands dominated by Fe atoms in the alloys. Elemental Ni, Pd, and Pt have the same number of valent electrons and their electro-negativeness increases in the same order. This trend is reflected in their corresponding alloys. For Fe_3Ni, Ni d electron dominated majority bands of Fe_3Ni prove to be enclosed by the majority bands of Fe; for Fe_3Pd, some of the d electrons of Fe are drawn into the Pd dominated bands and lose their original features, but others get more narrow and form sharper DOS peaks. Contrastly, for Fe_3Pt, Pt dominated bands are isolated from Fe bands but the Fe bands become broadened by hybridization and less peaked than in Fe_3Pd. The s states hybridize very well and mostly appear in the states of the lowest energies, s- and p-like states, where Ni, Pd or Pt dominates. The interesting consequence of the above is that the occupied energy range of Fe_3Pd is the smallest among the three alloys. For p electrons in the alloys, the DOS of the minority electrons of Fe at E_F is increased by a few times when comparing to Fe_3Fe. The increase may be attributed to the hybridization between

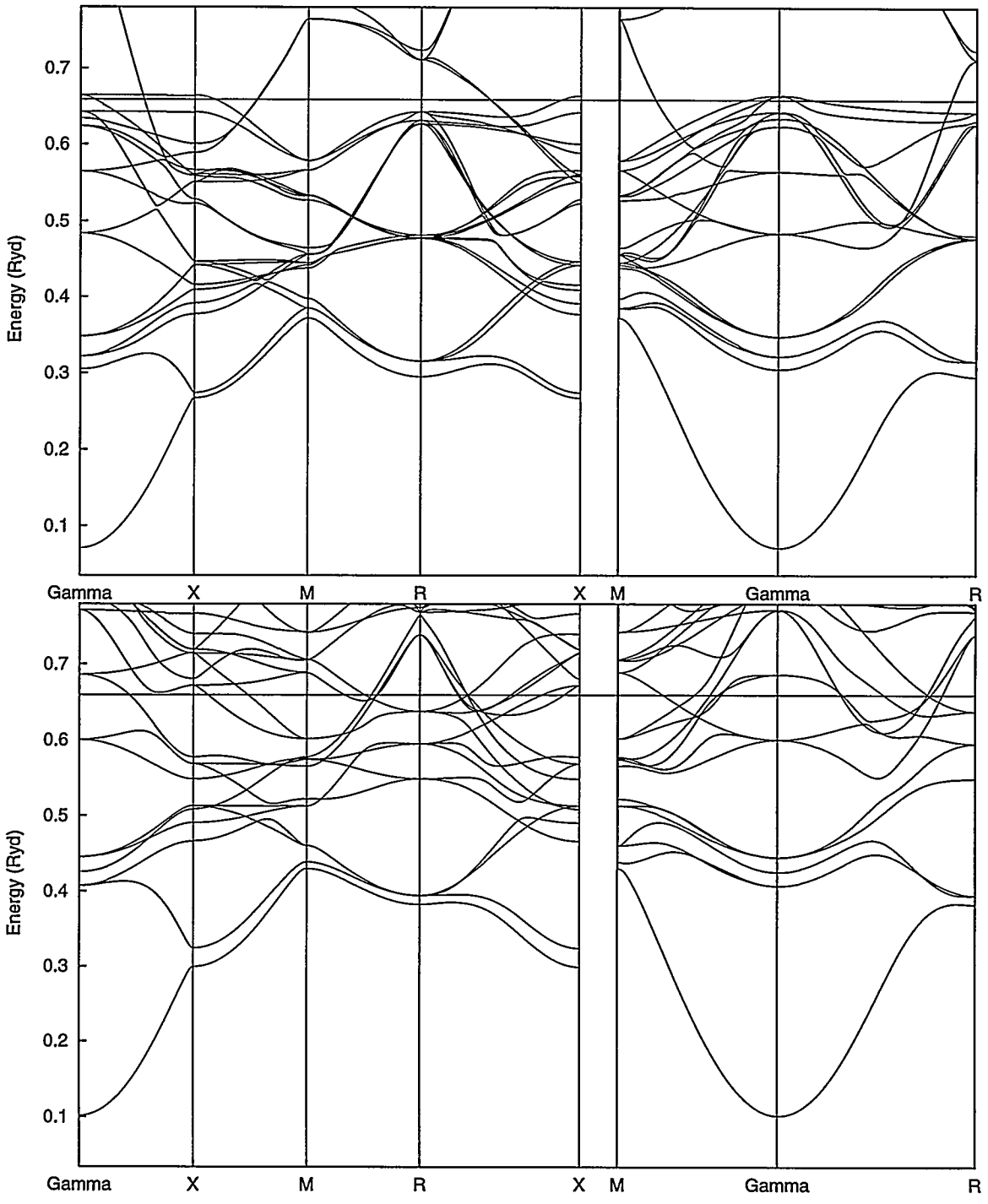

Figure 6.26 Spin-polarized band structures for ferromagnetic Fe_3Ni along some symmetry lines. The Fermi level is shown at 0.660 Ryd. (A) For majority spin electrons; (B) for minority spin electrons.

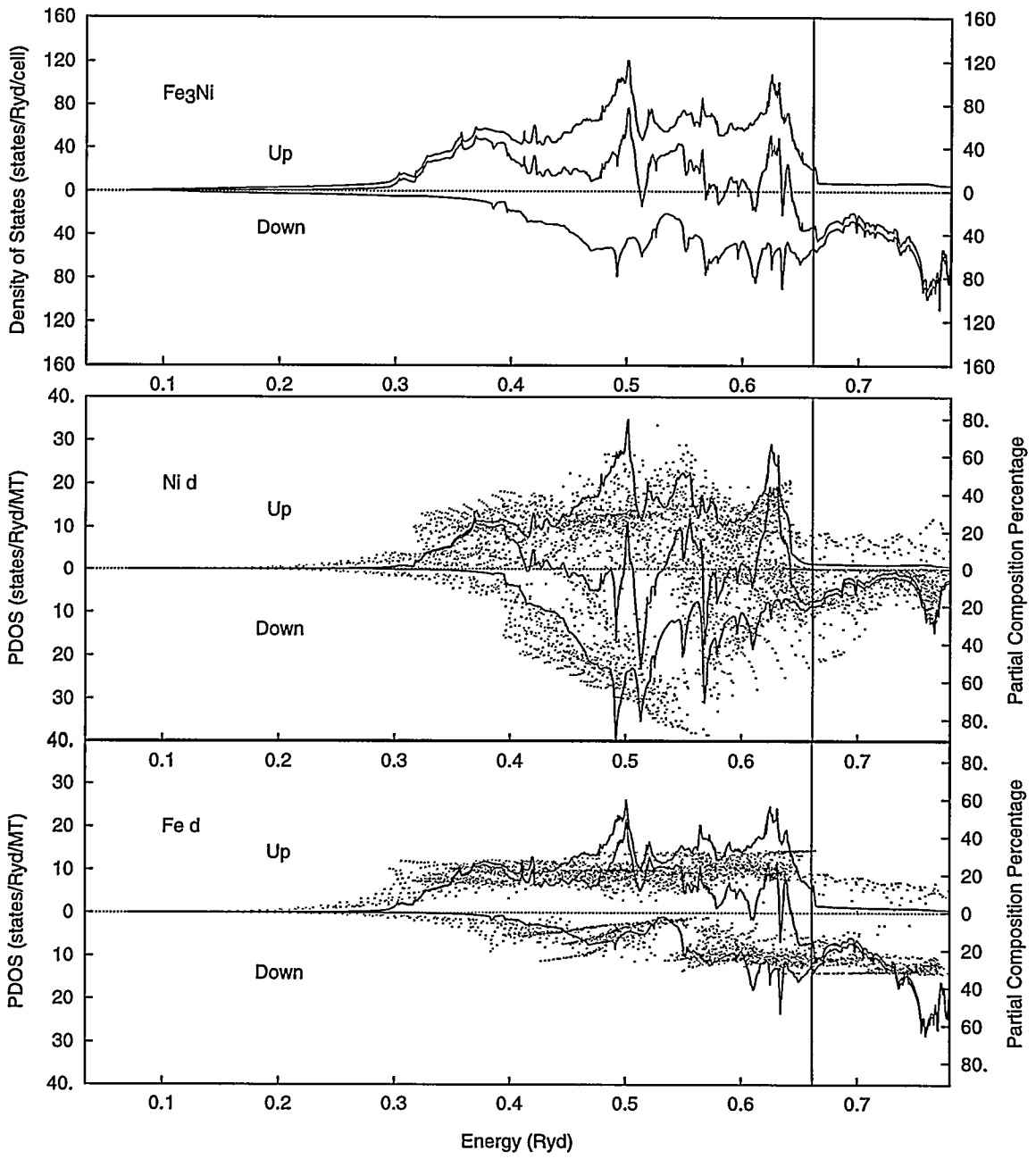

Figure 6.27 Total density of states per unit cell, partial densities of d states at muffin-tin sites, and the percentages of mixing (dots) between the d electronic states in forming the eigenstates at our 120 representative irreducible **k** points for Fe_3Ni. The Fermi level E_F = 0.660 Ryd is shown by the vertical line.

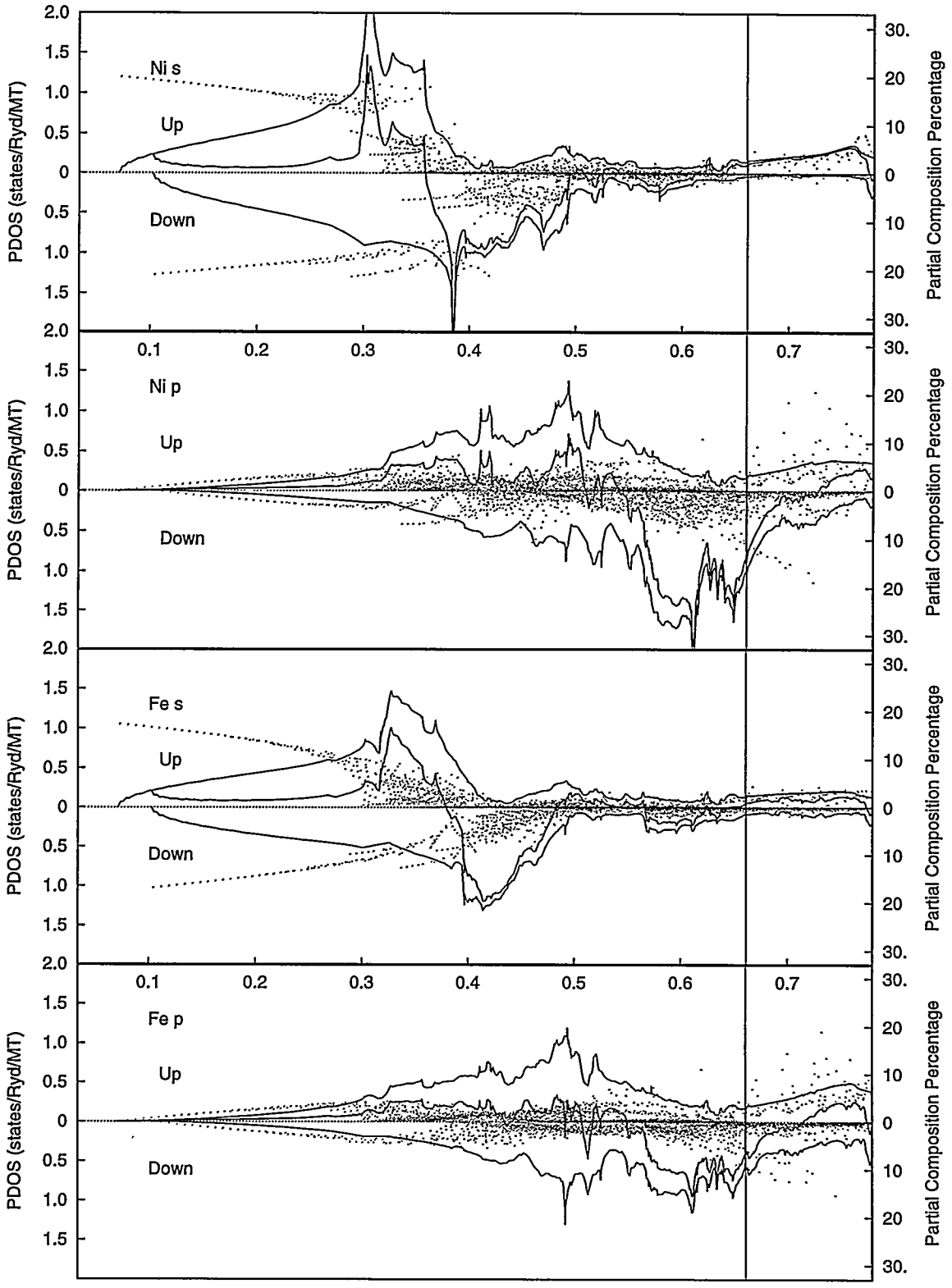

Figure 6.28 Partial densities for s and p states in Fe_3Ni.

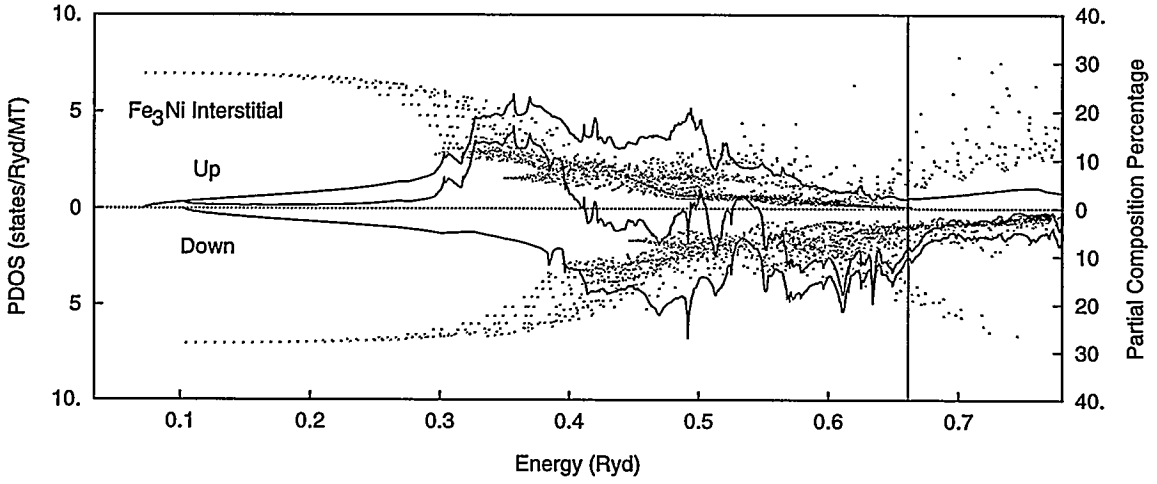

Figure 6.29 Partial densities for states from the interstitial region of Fe_3Ni.

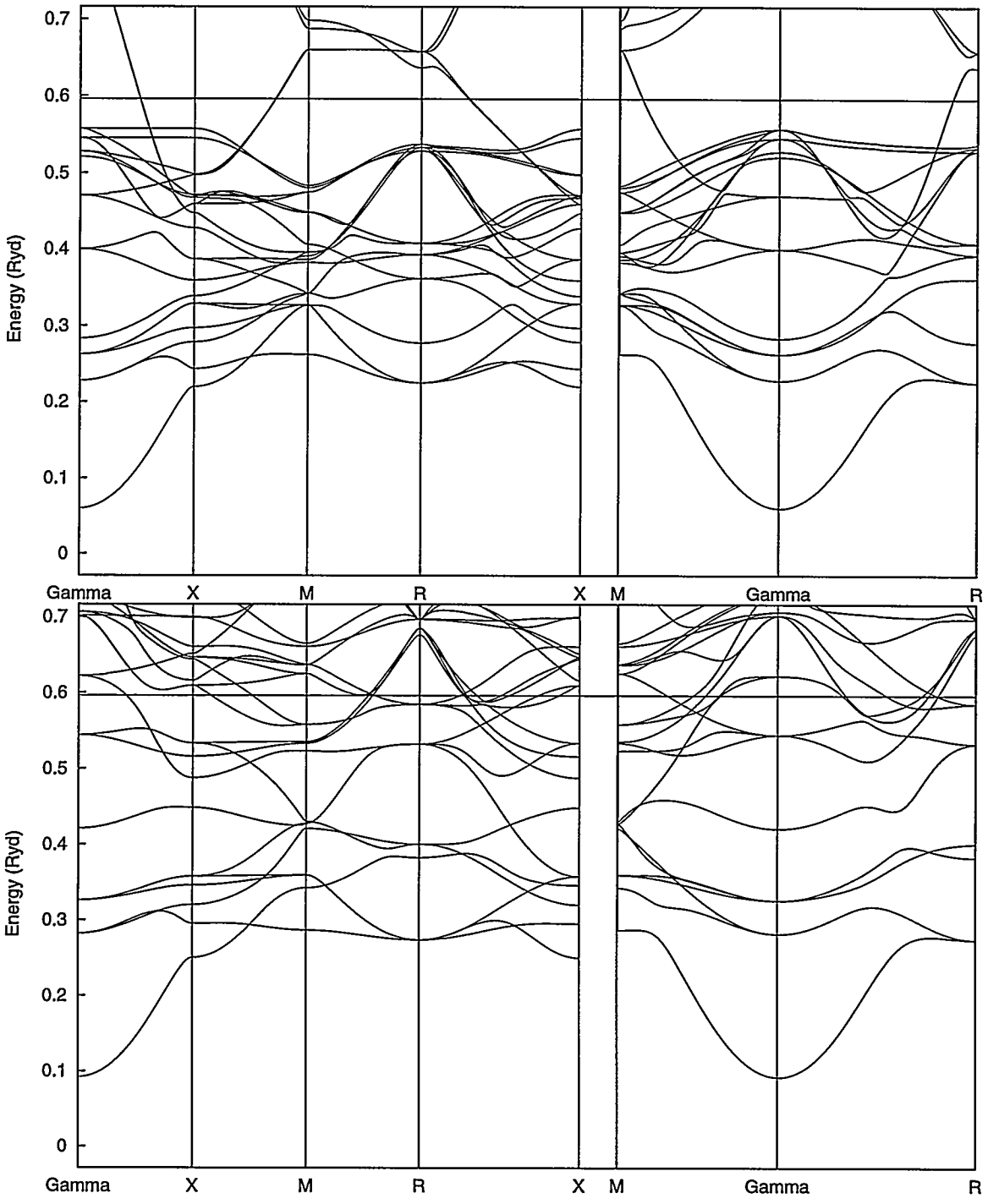

Figure 6.30 Spin-polarized band structures for ferromagnetic Fe_3Pd along some symmetry lines. The Fermi level is shown at 0.597 Ryd. (A) For majority spin electrons; (B) for minority spin electrons.

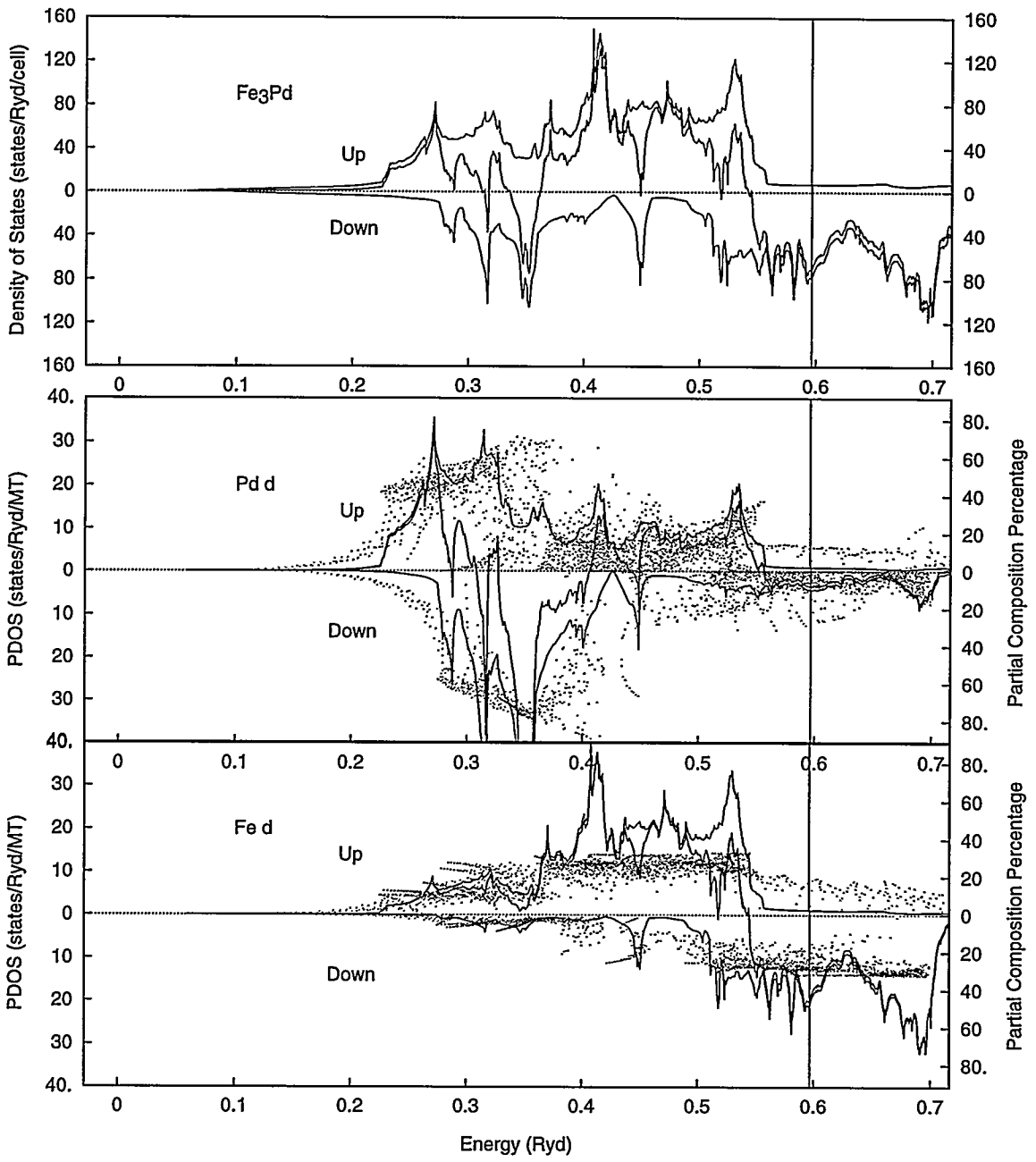

Figure 6.31 Total density of states per unit cell, partial densities of d states at muffin-tin sites, and the percentages of mixing (dots) between the d electronic states in forming the eigenstates at our 120 representative irreducible k points for Fe_3Pd. The Fermi level E_F = 0.597 Ryd is shown by the vertical line.

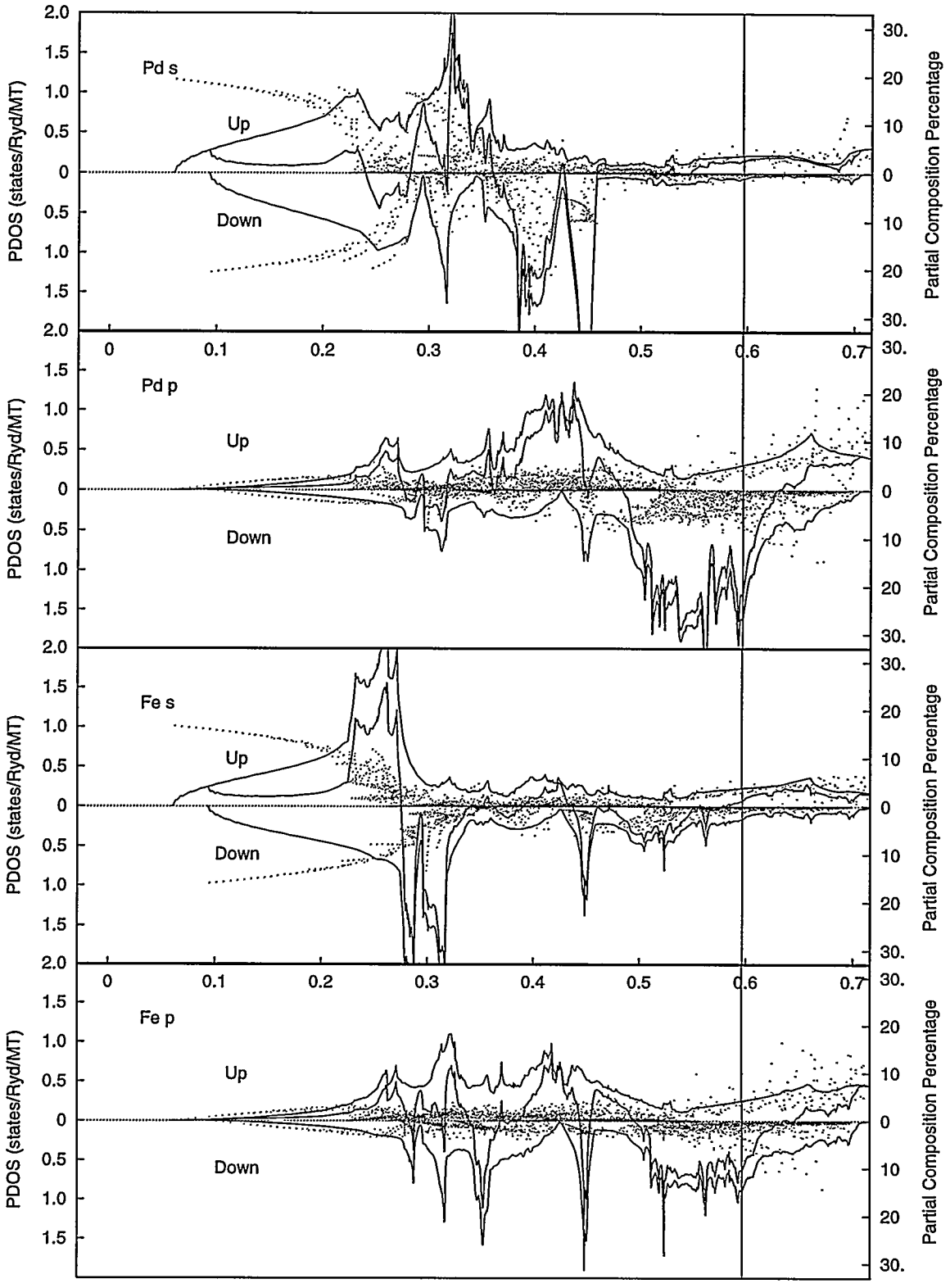

Figure 6.32 Partial densities for s and p states in Fe_3Pd.

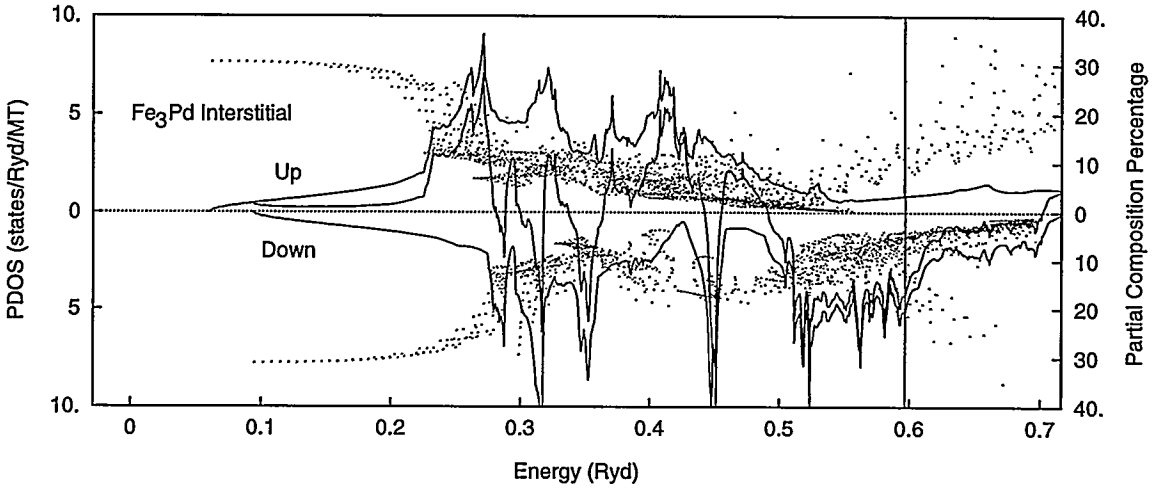

Figure 6.33 Partial densities for states from the interstitial region of Fe_3Pd.

the p electrons from the various atoms. As for the interstitial contributions, Fe_3Pd shows the largest peaks and has the largest DOS value at E_F.

X_3Pt (X = Fe, Co or Ni) Alloys

Co_3Pt can be in chemically ordered states (Inden 1983; Sanchez, Morán-López, Leroux, and Cadeville 1989; Harp, Weller, Rabedeau, Farrow and Toney 1993). The crystal structure of Co_3Pt is described by the space group Pm3m O_h^1 (No. 221 in the international tables). The local moment at the Co site is about $1.7\mu_B$, and at the Pt site is about $0.3\mu_B$ (Cadeville, Dahmani and Kern 1986; Sanchez, Morán-López, Leroux and Cadeville 1989). The lattice constant of Co_3Pt is taken as 6.92 a.u. from an experiment (Kootte, Haas and Groot 1990). The lattice constant of Ni_3Pt is taken as 6.90 a.u. from an experiment (Eckerlin, Kandler and Stegherr 1986).

Nickel and Platinum can be mixed in any proportions to form fcc structures (Cadeville, Dahmani and Kern 1986). Ni_3Pt is a stable Cu_3Au $L1_2$ structure, with a temperature of formation 540°C, and it can be relatively homogeneous (Matveeva 1995). The magnetic moment per atom is about $0.49\mu_B$, while the moment at the Ni site being $0.57\mu_B$ and at the Pt site $0.25\mu_B$, and some slightly negative magnetization in the interstitial region, the negative contribution from the orbital momentum is about $0.056\mu_B$ (Fischer and Besnus 1969; Nakai, Tomenu, Akimitsu and Ito 1979; Parra and Cable 1980; Cadeville and Morán-López 1987).

Figure 6.34 to Figure 6.41 show some results from band calculations for Co_3Pt and Ni_3Pt. Comparing with Fe_3Pt, there are some differences. The lowest energies change little, while the higher energies are

generally changed more and more with the increase in energy. Therefore, DOS changes little of their shapes at the lowest energies, but at the higher energies they change more considerably. The minority bands tend to shift downwards to get more occupied. An interesting fact is that although the total DOS or the PDOSs of the d electrons are increased, the PDOSs from s, p and interstitial regions are increased tremendously. This seems to imply a larger degree of hybridization of d electrons with s and p electrons in Fe_3Pt. This is understandable, for Fe is less localized than Co which in turn is less localized than Ni, so their atomic-like tendencies increase in the same order.

The calculations for the alloys show that the introduction of nonmagnetic but highly polarizable Pd or Pt atoms does not decrease the magnetism very much when the polarizing magnetic Fe atoms have larger moments in the alloys than in fcc Fe.

Partial Pressures and Invar

Electronic pressures have been the subject of some early studies (Janak and Williams 1976; Pettifor 1977; Moruzzi, Janak and Williams 1978) for the 3d, 4d and 5d series, and also to noble metals (Christensen and Heine 1985). There are two kinds of coexisting electronic contributions to the electronic pressures: always existing kinetic energy which yields repulsive pressures; and either antibonding contributions to repulsive pressures or bonding contributions to attractive pressures. Since antibonding bands are generally higher energetically than bonding ones, majority magnetic electrons in ferromagnetic materials are contributing to both positive pressures and negative pressures, unlike the mostly binding minority magnetic electrons which only contribute negative pressures. There are no general signs for the partial electron pressures for s, p and d-like electrons in solids. The s and p electrons are nearly free and less bonding or less antibonding than other electrons, so they usually contribute positive pressures to counterbalance pressures from magnetic electrons if any, or, as predominantly bonding electrons (with hybridizations between all kinds of electrons), they contribute small negative pressures as in noble metals or their nonmagnetic neighbors like Pd or Pt. Podgórny applied the above extended theory to the Fe-Pt ferromagnetic system (1991). The systems are bound together dominantly by the minority d electrons, while the s and p electrons contribute the most to the positive pressure. The majority d electrons compensate each other, for their counterbalancing bonding and anti-bonding tendencies, to give a much smaller net partial pressure. The combination of Pt s and p pressures, both positive, actually is roughly twice as large as that of Fe s and p pressures, also both positive.

A similar study was conducted also by Podgórny (1990) for the ferromagnetic Fe-Ni system. Because Fe and Ni are neighbors in the periodic table, their differences are much more subtle than the difference

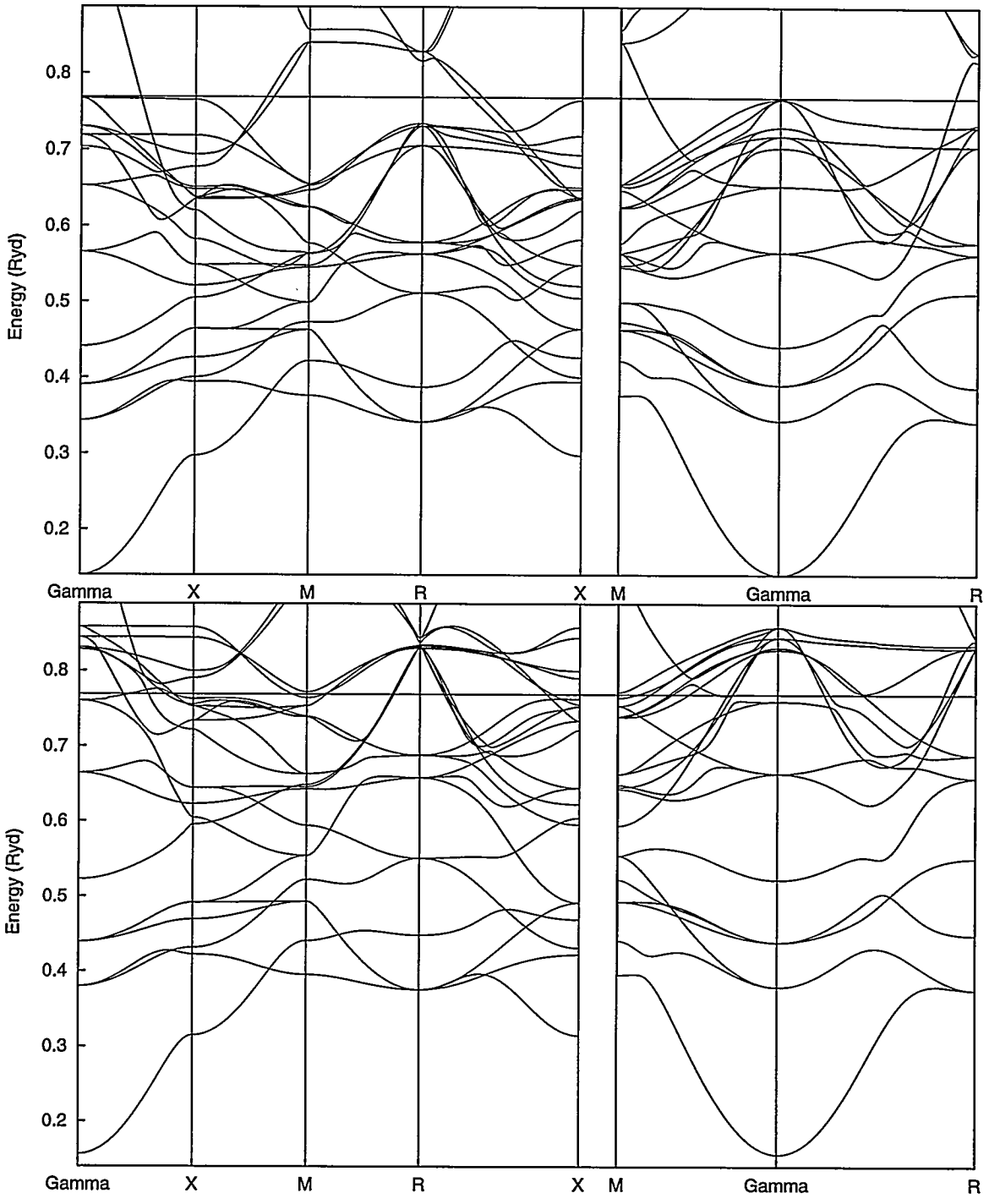

Figure 6.34 Spin-polarized band structures for ferromagnetic Co_3Pt along some symmetry lines. The Fermi level is shown at 0.769 Ryd. (A) For majority spin electrons; (B) for minority spin electrons.

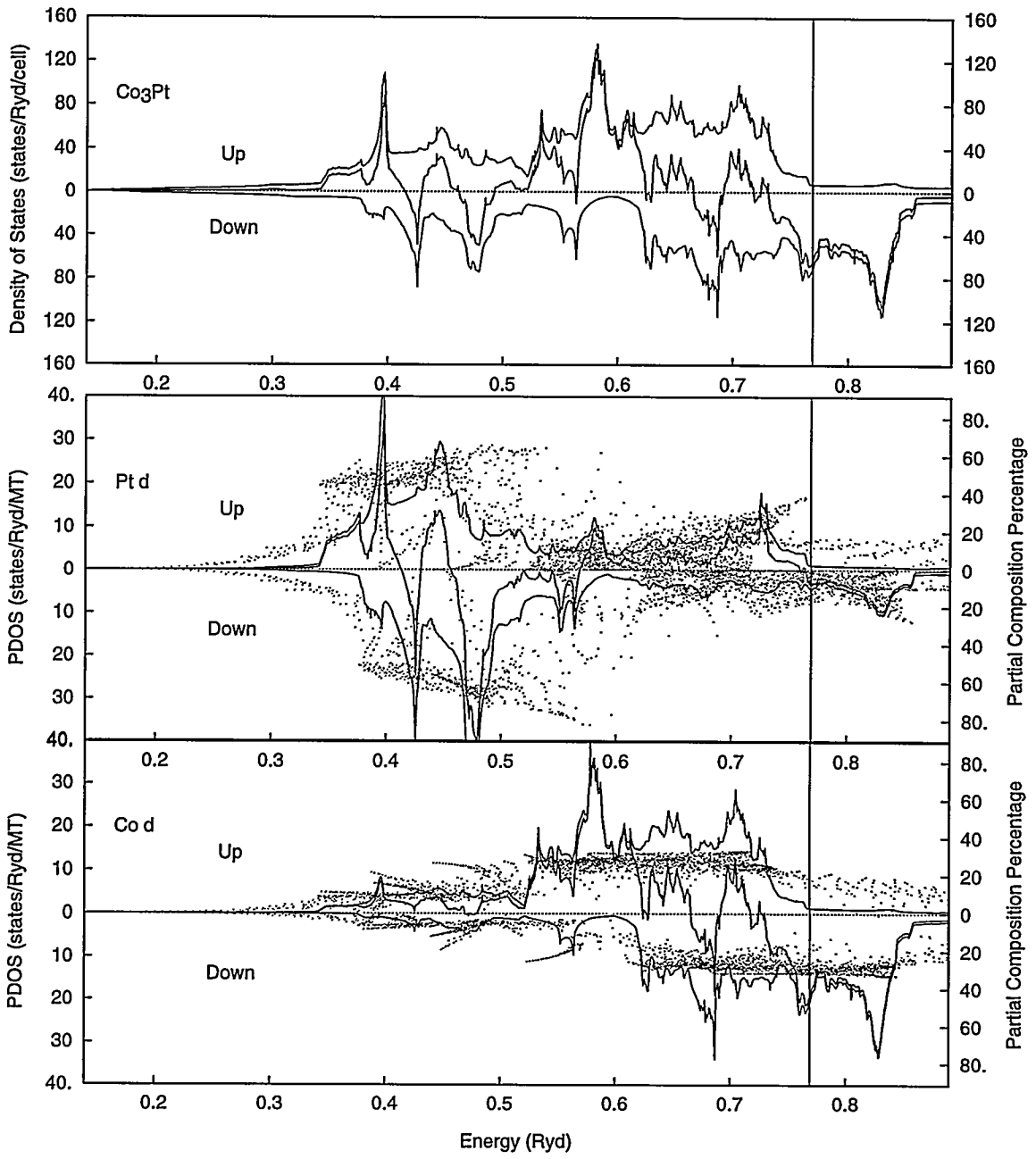

Figure 6.35 Total density of states per unit cell, partial densities of d states at muffin-tin sites, and the percentages of mixing (dots) between the d electronic states in forming the eigenstates at our 120 representative irreducible k points for Co_3Pt. The Fermi level E_F = 0.769 Ryd is shown by the vertical line.

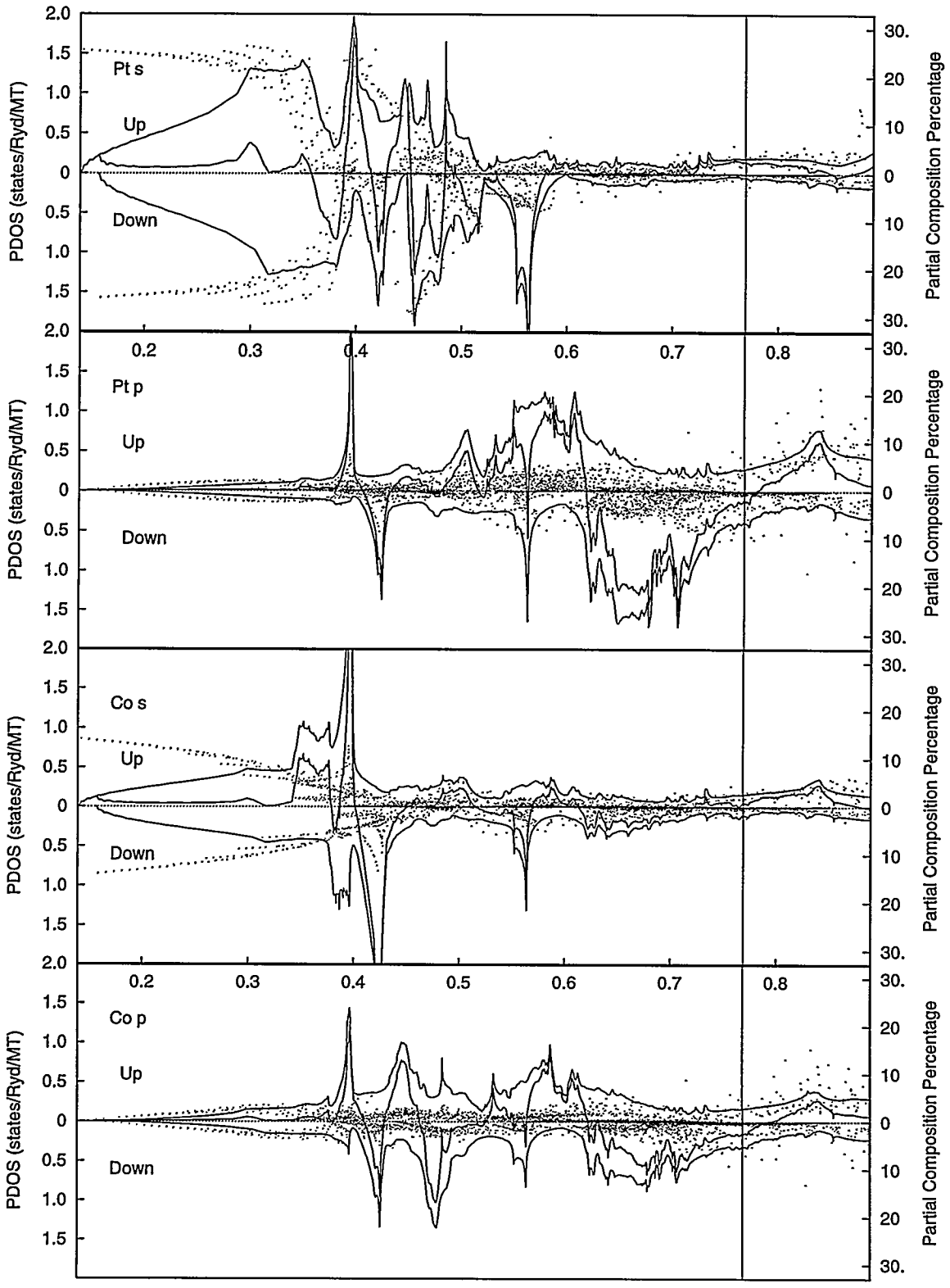

Figure 6.36 Partial densities for s and p states in Co_3Pt.

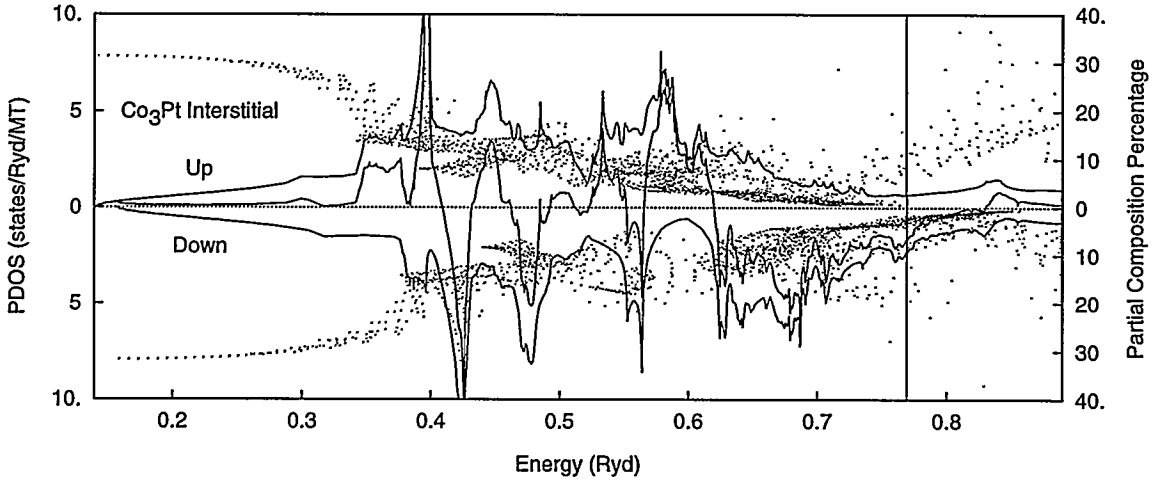

Figure 6.37 Partial densities for states from the interstitial region of Co_3Pt.

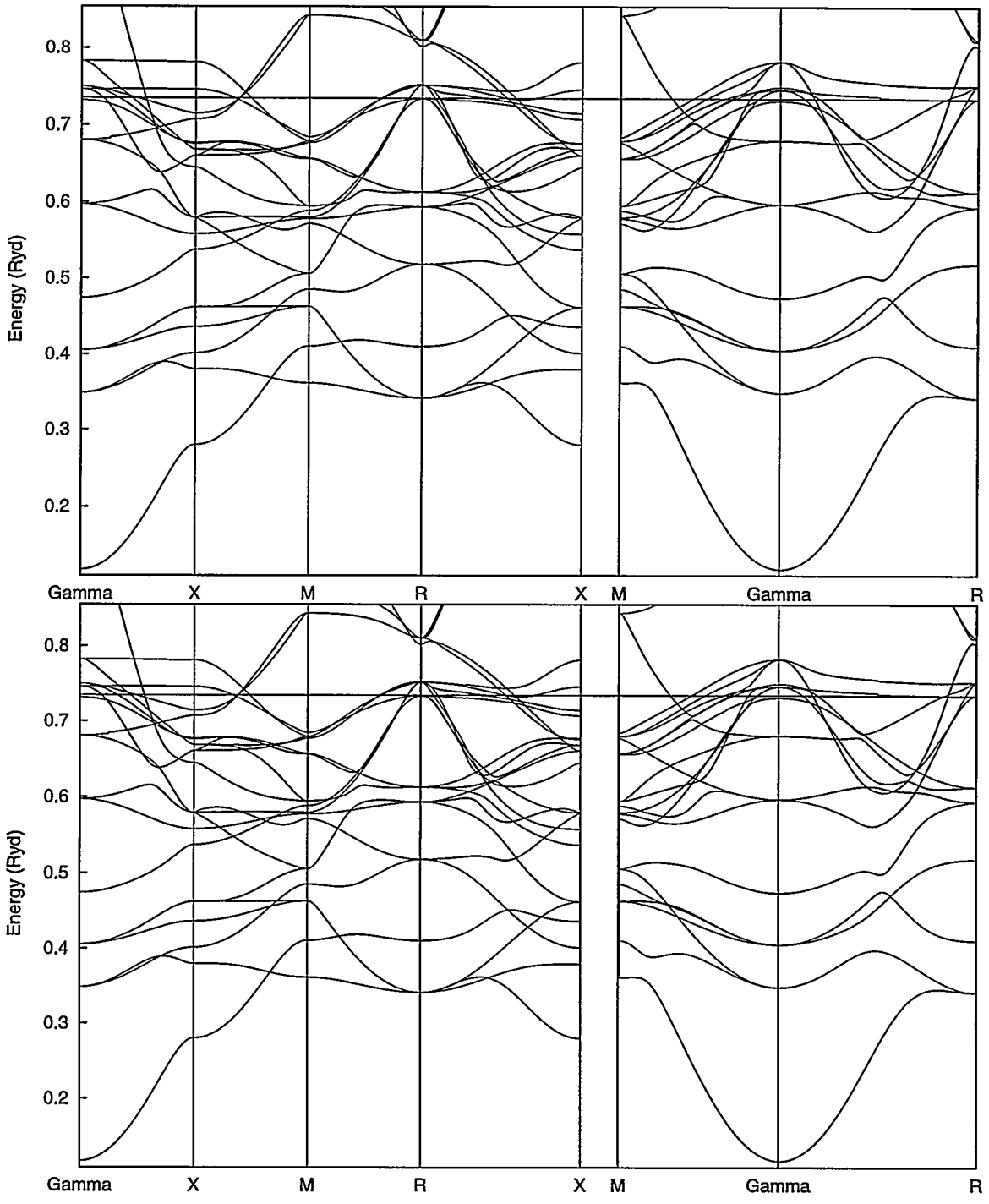

Figure 6.38 Spin-polarized band structures for ferromagnetic Ni_3Pt along some symmetry lines. The Fermi level is shown at 0.734 Ryd. (A) For majority spin electrons; (B) for minority spin electrons.

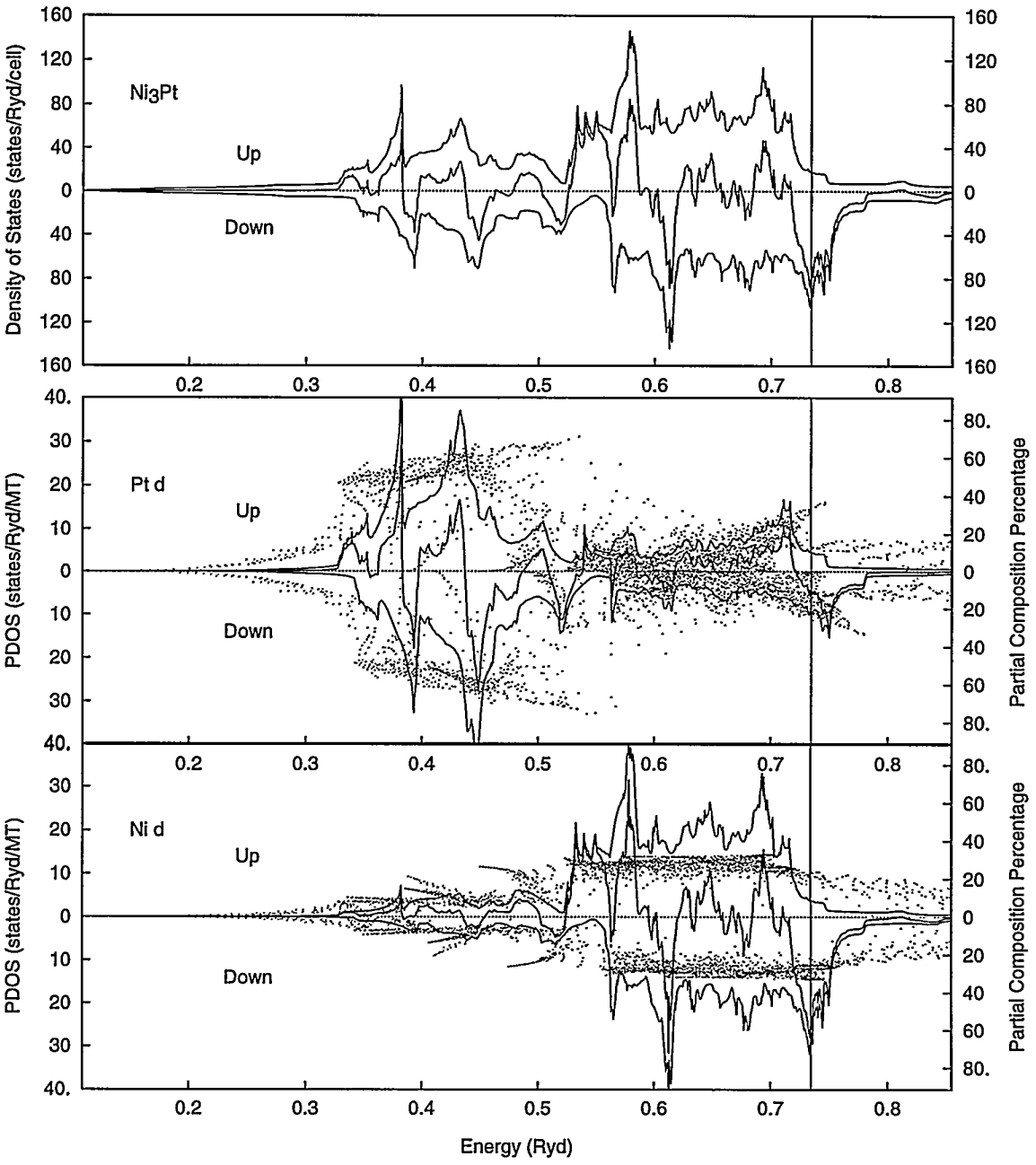

Figure 6.39 Total density of states per unit cell, partial densities of d states at muffin-tin sites, and the percentages of mixing (dots) between the d electronic states in forming the eigenstates at our 120 representative irreducible k points for Ni_3Pt. The Fermi level E_F = 0.734 Ryd is shown by the vertical line.

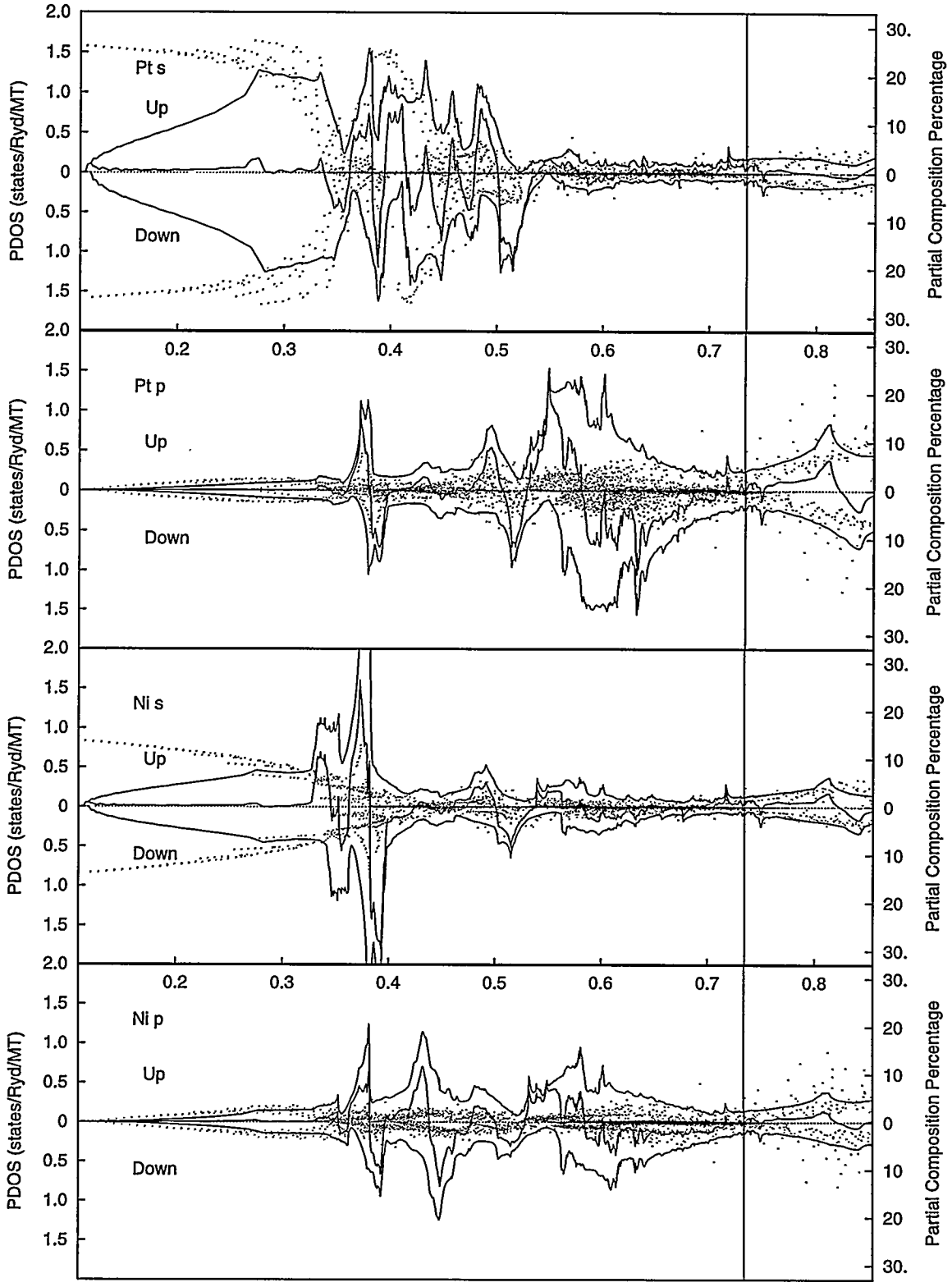

Figure 6.40 Partial densities for s and p states in Ni_3Pt.

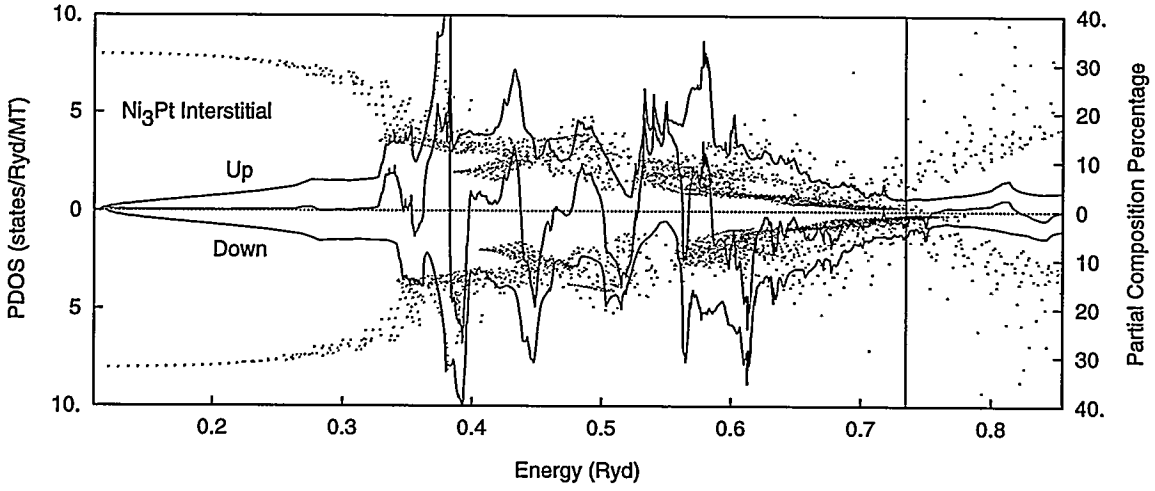

Figure 6.41 Partial densities for states from the interstitial region of Ni_3Pt.

between Fe and Pt. Around the Invar region (represented by Fe_5Ni_3, not as roughly by Fe_3Ni here), the partial pressures are comparable to those of Fe_3Pt, but the changes with composition are much less dramatic. Yet it should be emphasized that s and p partial pressure counterbalance the minority d electron pressure with their great magnitudes in a compositional range much wider than in Fe_3Pt. Both Invar systems have considerably large combined positive s and p pressures, counterbalancing negative pressures from the minority d electrons.

As we have seen before, both Invar Fe_3Pt, Fe_3Pd and Fe_3Ni systems distinguish themselves from the other chemically close alloys by the fact that they have great DOS densities for s and p electrons around the Fermi level. These electrons and the interstitial electrons, are the most sensitive to disturbances to the ground states for they are most extended in real space, and are likely transformed into d electrons upon thermal excitations, leading to the contraction of the system due to the above mentioned differences between the s and p pressure and d pressure. The high positive pressures from s-like and p-like electrons may be just due to the fact that s- and p-like electrons, which have highest Fermi kinetic energies, have relatively high densities near the Fermi level. More investigations should be made regarding this feature, though.

Conclusions and Perspectives

This work was undertaken mainly to determine if magnetic Compton scattering might provide some useful information concerning the temperature-dependent magnetic state of a well known Invar alloy,

Fe_3Pt, by analyzing its electronic properties at T = 0 K, especially the momentum distribution of spin electrons. Some other related materials are also studied to get some related information. The rather dramatic change in shape of the MCP between 305 K and 490 K where the "Invar mechanism" is presumably active, is qualitatively confirmed by the calculations, and needs a more systematic study of the progression of the MCPs starting at very low temperatures and extending into the paramagnetic region..

To get some referential information about Fe_3Pt, we have calculated band structures for Invar associated Fe_3Ni and Fe_3Pd, and then Co_3Pt and Ni_3Pt, which all have structurally the same crystal symmetry and are chemically related to Fe_3Pt. By comparison with the latter two materials, we found that all the three fcc Fe based alloys have significantly more s, p or interstitial electrons with energies just below E_F. Since it is the pressure from these electrons that primarily counterbalance the pressure from the binding d electrons, it would be interesting to learn how these most extended and sensitive electrons behave under thermal disturbances.

Naturally the theoretical MCP is dominated by the polarizing Fe d-orbitals. The dip of the MCP profiles at Pz = 0 is contributed significantly by the negatively polarized s-, p-like electrons all located near the Pt MT sphere boundaries, and by the negatively polarized interstitial electronic density found away from the Fe MT spheres. The contribution from the interstitial region between the muffin-tin spheres has a similar profile to that of the rather extended s- and p- like states. When obtaining the momentum density, the multiplication, of the smaller s and p and interstitial parts of the momentum wavefunction with the larger d parts gives an "interference" cross term, an oscillatory and rather extended contribution to the total MCP which differs from the dominant d-like contribution. While small, the s and p orbitals extend beyond a single site and "sample" the environment (short-range order) of the surrounding d-moments, so the s, p, and interference MCPs could be useful for investigating the changes of the magnetic state with temperature. The fcc Fe, and thus the fcc Fe based Invar Fe_3Pt, have complex magnetic states at finite temperatures because of the inherent insensitivity of their total energy to magnetic order. Therefore, we have further calculated the MCPs for Fe_3Fe and Fe_2FePt to search for the consequences of antiferromagnetic occurrences. A conclusion is that antiferromagnetism can enlarge the dip of the MCP. The discrepancy, between the experimental MCPs which are for finite temperatures and the calculated MCP which is for T = 0, hence can be partly due to local magnetic disordering. The antiferromagnetic studies show that the electrons become slightly more localized with the antiferromagnetism. More sophisticated methods should better deal with complex magnetic orderings, such as noncollinear spin orientations (Uhl, Sandratskii and Kübler 1994). To include temperature and

noncollinear magnetic moment directions into calculations for such models necessitates dealing with the loss of periodicity (very large supercells with hundreds of atoms are required, see Antropov, Katsnelson, Schilfgaarde and Harmon 1995). The new theoretical method, proposed to deal with such complex magnetic systems, has been implemented on parallel computers obtained some meaningful results (Harmon 1996). The method should permit calculations of temperature-dependent MCP in the future.

In conclusion, self-consistent band-structure calculations, using a spin-polarized, scalar, relativistic version of the FLAPW method, are used to analyze the results of a temperature-dependent MCS experiment on an ordered Fe_3Pt Invar alloy. The calculations have confirmed the presence of the dip at $P_z = 0$ and that the shape of the profile is sensitive to the magnetic state. Future experiments are planned in which the counting statistics and the energy/momentum resolution will be substantially increased, and the temperature range will be extended.

BIBLIOGRAPHY

[1] Abd–Elmeguid, M.M. and Micklitz, H., *Physica*, B 161 (1989) 17.

[2] Abd–Elmeguid, M.M. and Micklitz, H., *Phys. Rev.*, B 40 (1989) 7395.

[3] Abrahams, S. C., Guttman, L. and Kasper, J. S., *Phys. Rev.*, 127 (1962) 2052.

[4] Afagada, Z., *Augmented Plane Wave Method*, Oxford University Press: London, (1972).

[5] Andersen, O.K., Madsen, J. Poulsen, U.K., Jepsen, O. and Kellar, J., *Physica*, B 86-88 (1977) 249.

[6] Andersen, O.K., Jepsen, O. and Glötzel, D., *High Lights of Condensed Matter Theory*, eds. Bassani, F., Fumi, F. and Tosi, M.P., North-Holland: Amsterdam, (1985) 59.

[7] Antropov, V.P., Katsnelson, M.I., Schilfgaarde, M. van and Harmon, B.N., *Phys. Rev, Lett.*, 75 (1995) 729.

[8] Bagno, P., Jepsen, O. and Gunnarsson, O., *Phys. Rev.*, B 40 (1989) 1997.

[9] Balcar, E. and Lovesey, S. W., *Theory of magnetic neutron and photon scattering*, Clarendon Press: Oxford, (1989).

[10] Barbiellini, B., Moroni, E.G., and Jarlborg, T., *J. Phys.*, C2 (1990) 7597.

[11] Barth, U. von. and Hedin, L., *J. Phys.*, C 5 (1972) 1629.

[12] Barth, U. von., *The electronic Structure of Complex Systems*, eds. Phariseau, P. and Temmerman, W.M., Plenum Press: New York, (1982) 67.

[13] Bell, D. G., *Rev. Mod. Phys.*, 26, 3 (1954) 311.

[14] Berghout, C., *Z. Metallk*, 52 (1961) 179.

[15] de Bergevin, F. and Brunel, M., *Sturcture and Dynamics of Molecular Systems*, II, ed. Daudel, R. et al, Reidel Publishing Company: New York, (1986) 69.

[16] Blaha, P., Schwarz, K., Sorantin, P. and Trickey, S.B., *Computer Physics Communications*, 59 (1990) 399.

[17] Blume, M.J., *Appl. Phys.*, 57 (1985) 3618.

[18] Bonnenberg, D., Hempel, D.A. and Wijn, H.P.J., *Landolt-Börnstein Numerical Data and Functional Relationships in Science and Technology*, Group 3, vol. 19, pt. a, ed. Wijn, H.P.J., Springer-Verlag: Berlin, (1986) 149.

[19] Bradley, C.J. and Cracknell, A.P., *The Mathematical Theory of Symmetry in Solids*, Oxford University Press: London, (1972).

[20] Brown, P.J., Jassim, I.K., Neumann and Ziebeck, K.R.A., *Physica*, B161 (1989) 9.

[21] Buschow, K.H.J., van Engen, P.G. and Jongebreur, R., *J. Magn. Magn. Mater.*, 38 (1983) 1.

[22] Cadeville, M.C., Dahmani, C.E. and Kern, F., *J. Magn. Magn. Mater.*, 54-57 (1986) 1055.

[23] Cadeville, M.C. and Morán-López, J.L., *Phys. Rep.*, 153, 6 (1987) 331.

[24] Callaway, J., *Quantum Theory of the Solid State*, 2nd ed., Academic Press, Inc.: San Diego, (1991) 684.

[25] Caporaletti, O., Graham, G.M. and Sumiyama, K., *J. Magn. Magn. Mater.*, 10 (1979) 136.

[26] Caporaletti, O. and Gramham, G.M., *J. Magn. Magn. Mater.*, 22 (1980) 25.

[27] Carbone, C., Sohal, G.S., Kisker, E. and Wassermann, E.F., *J. Appl. Phys.*, 63 (1988) 3499.

[28] Chikazumi, S., *J. Magn. Magn. Mater.*, 15–18 (1980) 1130.

[29] Christensen, N.E. and Heine, V., *Phys. Rev.*, B32 (1985) 6145.

[30] Choi, E., Oh, S.J. and Choi, M., *Phys. Rev.*, B43 (1991) 6360.

[31] Collins, S.P., Cooper, M.J., Lovesey, S.W. and Laundy, D., *J. Phys.: Condens. Matter*, 2 (1990) 6439.

[32] Cooper, M.J., Laundy, D., Cardwell, D.A., Timms, D.N., Holt, R.S. and Clark, G., , *Phys. Rev.*, B34 (1986) 5984.

[33] Cooper, M.J., Collins, S.P., Timms, D.N., Brahmia, A., Kane, P.P., Holt, R.S. and Laundy, D., *Nature*, 333 (1988) 151.

[34] Cooper, M.J., Zukowski, E., Collins, S.P., Timms, D.N., Itoh, F. and Sakurai, H., *J. Phys.: Condens. Matter*, 4 (1992) L399.

[35] Cooper, M.J., Zukowski, E., Timms, D.N., Armstrong, R., Itoh, F., Tanaka, Y., Ito, M., Kawata, H. and Bateson, R., *Phys. Rev. Lett.*, 71, 7 (1993) 1095.

[36] Dreizler, R.M. and Providencia, J. da, *Density functional methods in physics*, Plenum Press: New York, (1985).

[37] *Landolt-Börnstein Numerical Data and Functional Relationships in Science and Technology*, Group 3, vol. 6, pt. a, ed. Eckerlin, P., Kandler, H. and Stegherr, Von A., Springer-Verlag: Berlin, (1986) 784.

[38] Entel, P., Hoffmann, E., Mohn, P., Schwarz, K. and Moruzzi, V.L., *Phys. Rev.*, B 47 (1993) 8706.

[39] Evarestov, R.A. and Smirnov, V.P., *Site Symmetry in Crystals*, Springer-Verlag: Berlin, (1993).

[40] Fischer, G. and Besnus, *Sol. Sta. Comm.*, 7 (1969) 527.

[41] Fujimori, H. and Saito, H., *J. Phys. Soc. Japan*, 20 (1964) 293.

[42] Fujimori, H. and Saito, H., *Physica*, B 119 (1983) 84.

[43] Geldcurt, D.J.W., *Density Functional Theory*, ed. Gross, E.K.U. and Dreizler, R.M., Plenum Press: New York, (1995) 33.

[44] Gonser, U., Krischel, K. and Nasu, S. *J. Magn. Magn. Mater.*, 15-18 (1980) 1145.

[45] Gradmann, U., Kummerie, W. and Tillmans, P., *Thin Solid Films*, 34 (1976) 249.

[46] Gradmann, U., and Isbert, H.O., *J. Magn. Magn. Mater.*, 15-18 (1980) 1109.

[47] Gradmann, U., *Handbook of Magnetic Materials*, Vol. 7, ed. Buschow, K.H.J., Elsevier Science Publishers B.V.: Amsterdam, (1993) 1.

[48] Gross, E.K.U. and Kurth, S., *Relativistic and Electron Correlation Effects in Molecules and Solids*, ed. Malli, G.L., Plenum Press: New York, (1994) 367.

[49] Guillaume, Ch. E., *Rend. Acad. Sci.*, 125 (1897) 235.

[50] Gunnarson, O. and Lundqvist, B.I., *Phys. Rev.*, B 13 (1976) 4274.

[51] Harmon, B.N., private communications, 1996.

[52] Harp, G.R., Weller, D., Rabedeau, T.A., Farrow, R.F.C. and Toney, M.F., *Phys. Rev. Lett.*, 71 (1993) 2493.

[53] Hasegawa, A., *J. Phys. Soc. Japan*, 54 (1985) 1477.

[54] Hathaway, K.B, Jansen, H.J.F. and Freeman, A.J., *Phys. Rev.*, B 31 (1985) 7603.

[55] Hausch, G., *J. Phys. Soc. Japan.*, 37 (1974) 819, 824.

[56] Hausch, G., *J. Magn. Magn. Mater.*, 92 (1990) 87.

[57] Hedin, L. and Lundqvist, B.I., *J. Phys.*, C 4 (1971) 2064.

[58] Hesse, J., Nülle, G. and Körner, H., *Sol. Sta. Comm.*, 46 (1983) 721.

[59] Hohenberg, P. and Kohn, W., *Phys. Rev.*, 136 B (1964) 864.

[60] Hu, C.D. and Langreth, D.C., *Phys. Rev.*, B 33 (1981) 943.

[61] Inden, G., *Mat. Res. Soc. Symp. Proc.*, 19 (1983) 175.

[62] Inui, T., Tanabe, Y. and Onodera, Y., *Group Theory and Its Applications in Physics*, Springer-Verlag: Berlin, (1990).

[63] Ishikawa, Y., Onodera, S. and Tajima, K., *J. Magn. Magn. Mater.*, 10 (1979) 183.

[64] Ito, Y., Sasaki, T. and Mizoguchi, T., *Sol. Sta. Comm.*, 15 (1974) 807.

[65] Ito, Y., Akimitsu, Matsui, M. and Chikazumi, *J. Magn. Magn. Mater.*, 10 (1979) 194.

[66] Janak, J. F. and Williams, A.R., *Phys. Rev.*, B14 (1976) 4199.

[67] Jansen, H.J.F., Hathaway, K.B. and Freeman, A.J., *Phys. Rev.*, B 30 (1979) 6177.

[68] Jansen, H.J.F. and Freeman A.J., *Phys. Rev.*, B 30 (1984) 561.

[69] Jones, R.O. and Gunnarsson, O., *Rev. Mod. Phys.*, 61 (1989) 689.

[70] Kalia, R.K. and Vashishta, P., *Phys. Rev.*, B17 (1978) 2655.

[71] Kashyap, A., Solanki, A. K., Nautiyal, T. and Auluck, S., *Phys. Rev.*, B 52 (1995) 13471.

[72] Kaufman, L., Cloughherty, E.V. and Weiss, R.J., *Acta Met.*, 11 (1961) 323.

[73] Kawald, U., Zemke, W., Bach, H., Pelzl J. and Saunders, G.A., *Physica*, B161 (1989) 72.

[74] Keune, W., Halbauer, R., Gonser, U., Lauer, J. and Williamson, D. L., *J. Appl. Phys.*, 48 (1977) 2976.

[75] Keune, W., Ezawa, T., Macedo, W. A. A., Glos, U., Schletz, K. P. and Kirschbaum, Z.Z., *Physica*, B 161 (1989) 269.

[76] Kisker, E., Wassermann, E. F. and Carbone, C., *Phys. Rev. Lett.*, 58 (1987) 1784.

[77] Kimura, H., Katsuki, A. and Shimizu, M, *J. Phys. Soc. Japan.*, 21 (1966) 307.

[78] Kittel, C., *Introduction to solid state physics*, 7th ed., New York: Wiley, (1996). 7th ed.

[79] Koelling, D. D. and Arbman, G. O., *J. Phys.*, F 5 (1975) 2041.

[80] Koelling, D. D. and Harmon, B. N., *J. Phys.*, C 10 (1977) 3107.

[81] Kohn, W. and Sham, L.J., *Phys. Rev.*, A140 (1965) 1133.

[82] Kohn, W. and Vashishta, P., *Theory of the Inhomogeneous Electron Gas*, ed. Lundqvist, S. and March, N.H., Plenum Press: New York, (1983) 79.

[83] Kohn, W., *Highlights of Condensed-matter Theory*, ed. Bassani, F., Fumi, F. and Tosi, M.P., North-Holland: Amsterdam (1985) 1.

[84] Kohn, W., *Density Functional Methods in Physics*, ed. Dreizler, R.M. and Providẽncia, J.d., Plenum Press: New York, (1985) 1.

[85] Kohn, W., *Density Functional Theory*, ed. Gross, E.K.U. and Dreizler, R.M., Plenum Press: New York, (1995) 3.

[86] Kootte, A., Haas, C. and Groot R.A. de, *J. Phys.: Condens. Matter*, 3 (1991) 1133.

[87] Krasko, g.L., *Phys. Rev.*, B36 (1987) 8565.

[88] Kryachko, E.S. and Ludẽna, E.V.,*Energy Density Functional Theory of Many-Electron Systems*, Kluwer Academic Publishers: Netherlands, (1990).

[89] Kubo, Y. and Asano, S., *Phys. Rev.*, B 42 (1990) 4431.

[90] Kurki–Suonio, K., *Israel Journal of Chemistry*, 16 (1977) 115.

[91] Kussmann, A., *Phys. Z.*, 38 (1937) 41.

[92] Kussmann, A. and Rittberg, G. V., *Z Metallkd*, 41 (1950) 470.

[93] Landau, L.D. and Lifshitz, E.M., *Quantum Electrodynamics*, 2nd Edition by Berestetskii, V.B., Lifshitz, E.M. and Piataevskii. Pergamon Press: Oxford, (1982) 354.

[94] Langreth, D.C., and Mehl, M.J., *Phys. Rev. Lett.*, 47 (1981) 446.

[95] Langreth, D.C., and Mehl, M.J., *Phys. Rev.*, B 28 (1983) 1809.

[96] Leung, T.C., Chan, C.T. and Harmon, B.N., *Phys. Rev.*, B 44 (1991) 2923.

[97] Levy, M., *Proc. Nat. Acad. Sci.*, U.S.A., A 76 (1979) 6062

[98] Levy, M., *Phys. Rev.*, A 26 (1982) 1200

[99] Levy, M. and Perdew, J.P., *Density Functional Methods in Physics*, ed. Dreizler, R.M. and Providẽncia, J.d., Plenum Press: New York, (1985) 11.

[100] Levy, M., *Density Functional Theory*, ed. Gross, E.K.U. and Dreizler, R.M., Plenum Press: New York, (1995) 11.

[101] Lipps, F. W. and Tolhoek, H. A., *Physica*, 20 (1954) 395.

[102] Lipps, F. W. and Tolhoek, H. A., *Physica*, 20 (1954) 85.

[103] Ludwig, W. and Falter, C., *Symmetries In Physics*, Springer-Verlag: Berlin, (1988).

[104] MacDonald, A. H., Pickett, W. E. and Koelling, D.D., *J. Phys. C: Solid Sta. Phys.*, 13 (1980) 2675.

[105] MacDonald, A. H. and Vosko, S.H., *J. Phys.*, C 12 (1979) 2977.

[106] *Landolt-Börnstein Numerical Data and Functional Relationships in Science and Technology*, Group 4, vol. 5, subvolume E, ed. Madelung, D., Springer-Verlag: Berlin, (1995) 194, 214, 216, 222.

[107] Mahan, G.D. and Subbaswamy, K.R., *Local Density Theory of Polarizability*, Plenum Press: New York, (1990).

[108] Maruyama, H., Matsuoka, F., Kobayashi, K. and Yamazaki, H. *J. Magn. Magn. Mater.*, 140-144 (1995) 43.

[109] Matsui, M., Shimizu, T., Yamada, H. and Adachi, K., *J. Magn. Magn. Mater.*, 15-18 (1980) 1201.

[110] Matsui, M., Adachi, K. and Asano, H., *Sci. Res. Inst. Tohoku Univ. Ser. A 29 Suppl.* (1) (1981) 61.

[111] Matsui, M., Shimizu, T., Yamada, H. and Adachi, K., *Physica*, B119 (1983) 84.

[112] Mattheiss, B.T., Peter, M., Williams, H.J., Clogston, A.M., Corenzwit, E. and Sherwood, R.C., *Phys. Rev. Lett.*, 5 (1960) 542.

[113] Mattheiss, L. F. and Hamann, D. R., *Phys. Rev.*, B 33 (1986) 823.

[114] Matveeva, N.M., *Intermetallic Compounds*, ed. Westbrook, J.H. and Fleischer, R.L., vol. 1 (John Wiley & Sons Ltd., England, 1995) 711.

[115] Menshikov, A.Z., Chamberod, A. and Roth, M., *Sol. Sta. Comm.*, 44 (1982) 243.

[116] Menshikov, A.Z., *Physica*, B 161 (1989) 1.

[117] Mills, D.M., *Phys. Rev.*, B 36 (1987) 6178.

[118] Miodownik, A.P., *J. Magn. Magn. Mater.*, 10 (1979) 126.

[119] Moriya, T. and Kawabata, *J. Phys. Soc. Japan*, 34 (1973) 639.

[120] Moroni, E. G. and Jarlborg, T., *Phys. Rev.*, B 41 (1990) 9600.

[121] Moruzzi, V.L., Janak, J.F. and Williams, A.R., *Calculated Electronic Properties of Metals*, Pergamon Press: New York, (1978).

[122] Moruzzi, V.L., Marcus, P.M. and Pattnaik, P.C., *Phys. Rev.*, B 37 (1988) 8003.

[123] Moruzzi, V.L. and Marcus, P.M., *Phys. Rev.*, B 38 (1988) 1613.

[124] Moruzzi, V.L. and Marcus, P.M., *J. Appl. Phys.*, 64 (1988) 5598.

[125] Moruzzi, V.L., *Physica*, B 161 (1989) 99

[126] Moruzzi, V.L., Marcus, P.M. and Kübler, J., *Phys. Rev.*, B39 (1989) 6957.

[127] Moruzzi, V.L., *Phys. Rev.*, B 41 (1990) 6939.

[128] Moruzzi, V.L. and Marcus, P.M., *Handbook of Magnetic Materials*, Vol. 7, ed. Buschow, K.H.J., Elsevier Science Publishers B.V.: Amsterdam, (1993) 97.

[129] Nakai, Y., Tomenu, I., Akimitsu and Ito, Y., *J. Phys. Soc. Japan*, 47 (1979) 1821.

[130] Nakamura, Y., Sumiyama, K. and Shiga, M., *Transition Metals*, Ed. Lee, M.J.G., Perz, J.M., Faucett, E., The Institute of Phys.: Bristol and London, (1978) 522.

[131] Nakamura, Y., Sumiyama, K. and Shiga, M., *J. Magn. Magn. Mater.*, 12 (1979) 127.

[132] Oomi, G. and Araki, H., *J. Magn. Magn. Mater.*, 140-144 (1995) 83.

[133] Onodera, S., Ishikawa, Y. and Tajima, K., *J. Appl. Phys.*, 50 (1981) 1513.

[134] Onodera, A., Tsunoda, Y., Kunitomi, N., Pringle, O.A., Nicklow, R.M. and Moon, R.M., *Phys. Rev.*, B50 (1994) 3532.

[135] Parra, R.E. and Cable, J.W., *Phys. Rev.*, B 21 (1980) 5494.

[136] Perdew, J.P. and Zunger, A., *Phys. Rev.*, B 23 (1981) 5048.

[137] Perdew, J.P. and Wang, Y., *Phys. Rev.*, B 33 (1986) 8800.

[138] Perdew, J.P., *Phys. Rev.*, B 33 (1986) 8822.

[139] Perdew, J.P., *Phys. Rev.*, B 34 (1986) 7407.

[140] Perdew, J.P., *Density Functional Theory of Molecules, Clusters and Solids*, ed. Ellis, D.E., Kluwer Academic Publishers: Netherlands, (1995) 47.

[141] Perdew, J.P., *Density Functional Theory*, ed. Gross, E.K.U. and Dreizler, R.M., Plenum Press: New York, (1995) 51.

[142] Pettifor, D.G., *J. Phys.*, F7 (1977) 613.

[143] Platzman, P.M. and Tzoar, N. *Phys. Rev.*, B 2 (1970) 3556.

[144] Podgórny, M., *Physica*, B 161 (1989) 110.

[145] Podgórny, M., *Acta Physica Polonica*, A 78 (1990) 941.

[146] Podgórny, M., *Phys. Rev.*, B 43 (1991) 11300.

[147] Podgórny, M., *Phys. Rev.*, B 46 (1992) 6293.

[148] Podgórny, M., Thon, M. and Wagner, D., *Magn. Magn. Mater.*, 104–107 (1992) 703.

[149] Predel, B., *Landölt-Börnstein New Series*, Group 4, volume 5, subvolume E, (Spinger-Verlag 1995) 215.

[150] Rajagopal, A. K. and Callaway J., *Phys. Rev.*, B7 (1973) 1912.

[151] Rajagopal, A.K., *J. Phys.*, C 11 (1978) L943.

[152] Rajagopal, A. K., *Adv. Chem. Phys.*, 41 (1979) 59.

[153] Ramana, M.V. and Rajagopal, A.K., *Adv. Chem. Phys.*, 54 (1983) 231.

[154] Sakai, N., Tersahima, O. and Sekizawa, H., *Nuclear Instruments and Methods in Physics Research*, 221 (1984) 419.

[155] Sakai, N., Shiotani, N., Ito, M., Itoh, F., Kawata, H., Amemiya, Y., Ando, M., Yamamoto, S. and Kitamura, H., *Rev. Sci. Instrum.*, 60(7) (1989) 1666.

[156] Salahub, D.R., Castro, M. and Proynov, E.I., *Relativistic and Electron Correlation Effects in Molecules and Solids*, ed. Malli, G.L., Plenum Press: New York, (1994) 411.

[157] Sanchez, J.M., Morán-López, J.L., Leroux, C. and Cadeville, M.C., *J. Phys. Cond. Mater.*, 1 (1989) 491.

[158] Sander, L.M., Shore, H.B. and Sham, L.J., *Phys. Rev. Lett.*, 31 (1973) 533.

[159] Shiga, M., Muraoka, Y. and Nakamura, Y., *J. Magn. Magn. Mater.* 10 (1979) 280.

[160] Shiga, M., *Materials Science and Technology*, ed. Cahn, R. W., Haasen, P. and Kramer, E. J., Vol.3B, VCH, Weinheim, (1994) 159.

[161] Shirane, G., Born, P. and Wicested, J.P, *Phys. Rev.*, B33 (1986) 1881.

[162] Sohmura, T., Oshima, R. and Fujita, F.E., *Scr. Metall.*, 14 (1980) 855.

[163] Sugiyama, M., Oshima, R. and Fujita, F.E., *Transactions of the Japan Institute of Metals*, 25(1984) 585.

[164] Sugiyama, M., Oshima, R. and Fujita, F.E., *Transactions of the Japan Institute of Metals*, 27 (1986) 719.

[165] Sumiyama, K., Shiga, M. and Nakamura, Y., *J. Phys. Soc. Japan*, 40, 4 (1976) 996.

[166] Sumiyama, K., Shiga, M., Kobayashi, Y., Nishi, K. and Nakamura, Y., *J. Phys.*, F 8 (1978) 1281.

[167] Sumiyama, K., Shiga, M., Morioka M. and Nakamura, Y., *J. Phys.*, F 9 (1979) 1665.

[168] Sumiyama, K., Shiga, M. and Nakamura, Y., *J. Phys. Soc. Japan*, 48 (1980) 1393.

[169] Sumiyama, K., Emoto, Y., Shiga, M. and Nakamura, Y., *J. Phys. Soc. Japan*, 50 (1981) 3296

[170] Suzuki, Y., Miyajima, H., Kido, G., Miura, N. and Chikazumi, S., *J. Phys. Soc. Japan.*, 50 (1981) 817.

[171] Tanaka, Y., Skai, N., Kubo, Y. and Kawata, H., *Phys. Rev. Lett.*, 70 (1993) 1537.

[172] Timms, D.N., Zukowski, E., Cooper, M.J., Laundy, D., Collins, S.P., Itoh, F., Sakurai, H., Iwazumi, T., Kawata, H., Ito, M., Sakai, N. and Tanaka, Y., *J. Phys. Soc. Japan*, 62 (1993) 1716.

[173] Tsunoda, Y., *J. Phys. Condens. Matter.*, 1 (1988) 10427

[174] Uemura, Y.J., Shirane, G., Steinsvoll, O and Wicksted, J., *Phys. Rev. Lett.*, 51 (1983) 2322.

[175] Uhl, M., Sandratskii, L. M. and Kübler, J., *J., Phys. Rev.*, B 50 (1994) 291

[176] Ullrich, H. and Hesse, J., J. Magn. Magn. Mat., 45 (1984) 315.

[177] Vosko, S.H., Wilk, L. and Nusair, M., *Can. J. Phys.*, 58 (1980) 1200.

[178] Wagner, D., *J. Phys. Condens. Matter*, 1 (1989) 4635.

[179] Wakoh, S. and Kubo, Y., *J. Magn. Magn. Mater.*, 5 (1977) 202.

[180] Wang, C.S., Klein, B.M. and Krakauer, H., *Phys. Rev. Lett.*, 54 (1985) 1852.

[181] Wassermann, E.F., *Phys. Scripta*, T25 (1989) 209.

[182] Wassermann, E.F., *Ferromagnetic Materials*, ed. Buschow, K.H.J. and Wohlfarth, E. P., Vol. 5 (Norht–Holland, Ameserdam, 1990), 236.

[183] Wassermann, E.F., *J. Magn. Magn. Mater.*, 90–91 (1990) 1260.

[184] Wassermann, E.F., *J. Magn. Magn. Mater.*, 100 (1991) 346.

[185] Weinert, M., *J. Math. Phys.*, 22(11) (1981) 2433.

[186] Weinert, M., Wimmer, E. and Freeman, A., *Phys. Rev.*, B26 (1982) 4571.

[187] Weiss, R. J., *Proc. Phys. Soc.*, 82 (1963) 281.

[188] Wigner, E. and Seitz F., *Phys. Rev.*, 46 (1934) 509.

[189] *Landolt-Börnstein Numerical Data and Functional Relationships in Science and Technology*, Group 3, vol. 19, subvolume I1, ed. Wijn, H.P.J., Springer-Verlag: Berlin, (1994) 195.

[190] Williams, B., *Compton Scattering*, McGraw-Hill: New York, (1977).

[191] Williams, A. R., Moruzzi, V. L. and Gelatt, C.D., Jr. and Kübler, J., *J. Magn. Magn. Mater.*, 31–34 (1983) 88.

[192] Williamson, D.L., Bukshspan, S. and Ingalls, R., *Phys. Rev.*, B 6 (1972) 4149.

[193] Window, B., *Philos. Mag*, 26 (1972) 681.

[194] Wright, J., *Philos. Mag.*, 24 (1971) 24.

[195] Yhanke, C.J., private communications, 1995.

[196] Ziebeck, K.R.A., Webster, P.J., Brown, P.J. and Capellmann, H. *J. Magn. Magn. Mater.*, 36 (1983) 151.

[197] Zukowski, E., Collins, S.P., Cooper, M.J., Timms, D.N., Sakurai, H., Kawata, H., Tanaka, Y. and Malinowski, A., *J. Phys.: Condens. Matter*, 5 (1993) 4077.